7 Continental rifts and rifted margins

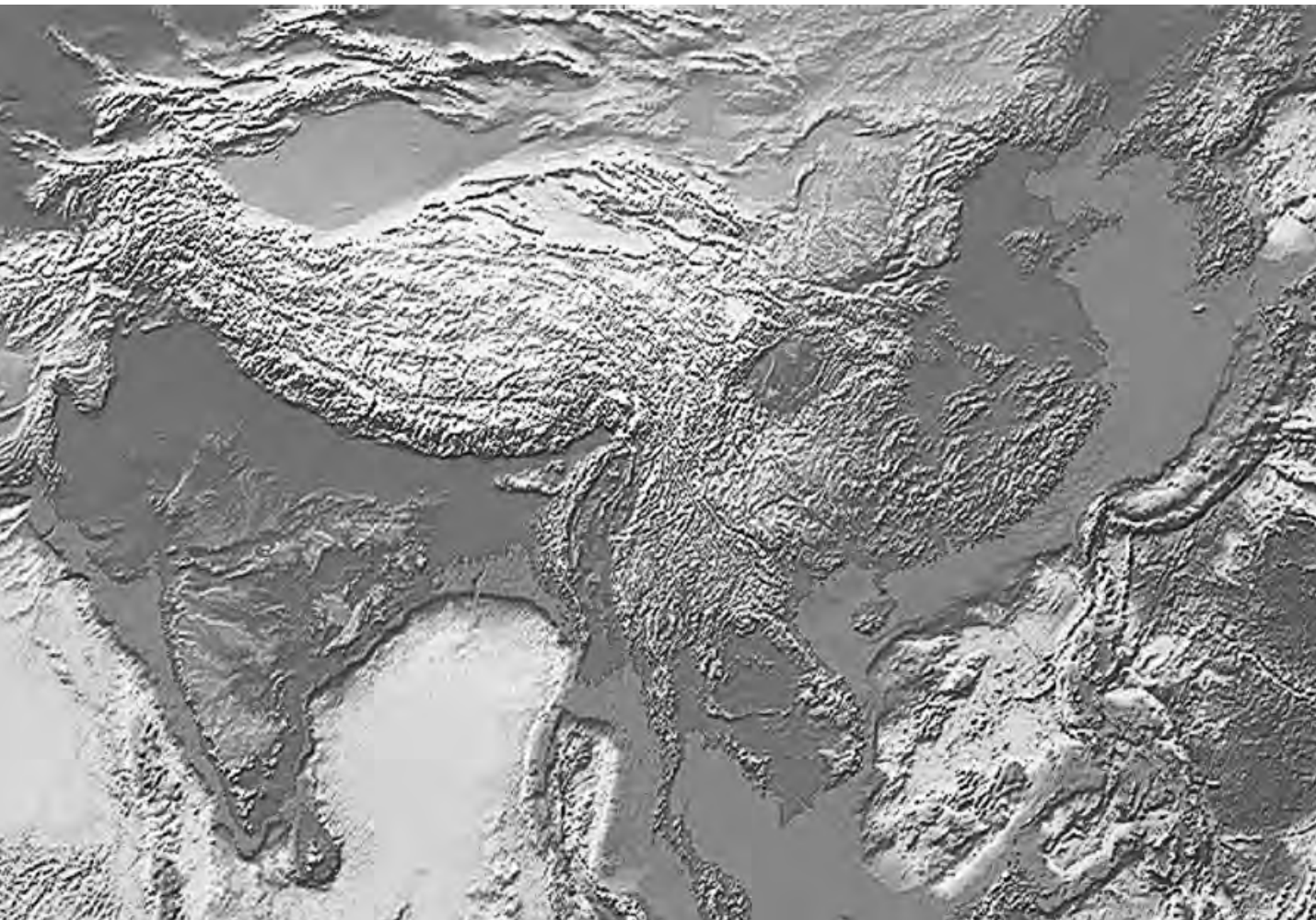

7.1 INTRODUCTION

Continental rifts are regions of extensional deformation where the entire thickness of the lithosphere has deformed under the influence of deviatoric tension. The term "rift" thus applies only to major lithospheric features and does not encompass the smaller-scale extensional structures that can form in association with virtually any type of deformation.

Rifts represent the initial stage of continental break-up where extension may lead to lithospheric rupture and the formation of a new ocean basin. If it succeeds to the point of rupture the continental rift eventually becomes inactive and a *passive* or rifted continental margin forms. These margins subside below sea level as a result of isostatic compensation of thinned continental crust and as the heat that was transferred to the plate from the asthenosphere during rifting dissipates. However, not all rifts succeed to the point where new ocean crust is generated. Failed rifts, or *aulacogens*, become inactive during some stage of their evolution. Examples of failed rifts include the Mesozoic Connecticut Valley in the northeastern United States and the North Sea Basin.

Studies of active rifts show that their internal structure, history, and dimensions are highly variable (Ruppel, 1995). Much of this variability can be explained by differences in the strength and rheology of the lithosphere (Section 2.10) at the time rifting initiates and by processes that influence these properties as rifting progresses (Section 7.6.1). Where the lithosphere is thick, cool, and strong, rifts tend to form narrow zones of localized strain less than 100 km wide (Section 7.2). The Baikal Rift, the East African Rift system, and the Rhine Graben are examples of this type of rift (Fig. 7.1). Where the lithosphere is thin, hot, and weak, rifts tend to form wide zones where strain is delocalized and distributed across zones several hundreds of kilometers wide (Section 7.3). Examples of this type of rift include the Basin and Range Province and the Aegean Sea. Both varieties of rift may be associated with volcanic activity (Section 7.4). Some rift segments, such as those in Kenya, Ethiopia, and Afar, are characterized by voluminous magmatism and the eruption of continental flood

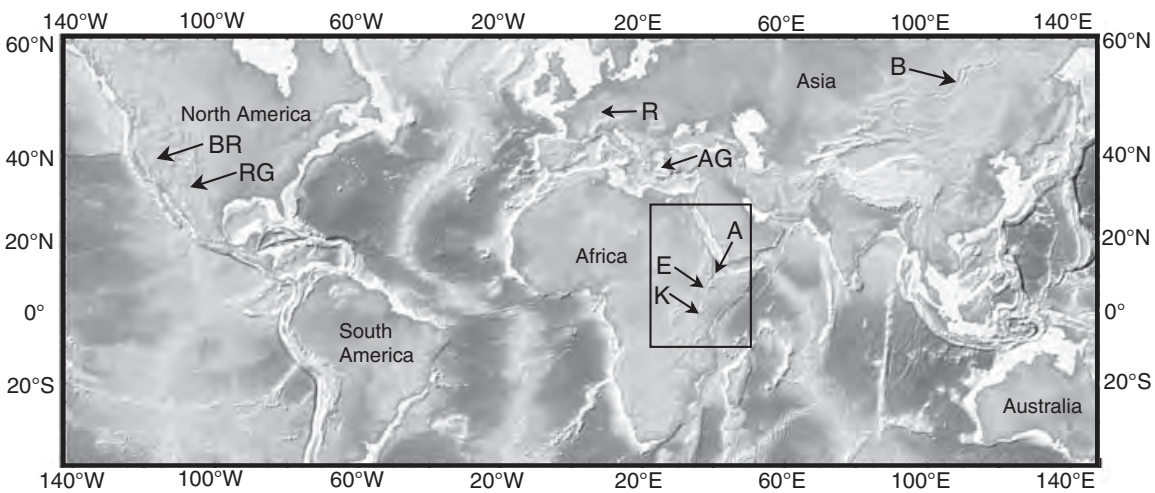

Figure 7.1 *Shaded relief map showing selected tectonically active rifts. Map constructed using digital seafloor topography of Smith & Sandwell, 1997, USGS Global 30 arc second elevation data (GTOPO30) for land areas (data available from USGS/EROS, Sioux Falls, SD, http://eros.usgs.gov/), and software provided by the Marine Geoscience Data System (http://www.marine-geo.org), Lamont-Doherty Earth Observatory, Columbia University. BR, Basin and Range; RG, Río Grande Rift; R, Rhine Graben; AG, Aegean Sea; B, Baikal Rift; E, Main Ethiopian Rift; A, Afar depression; K, Kenya Rift. Box shows location of Fig. 7.2.*

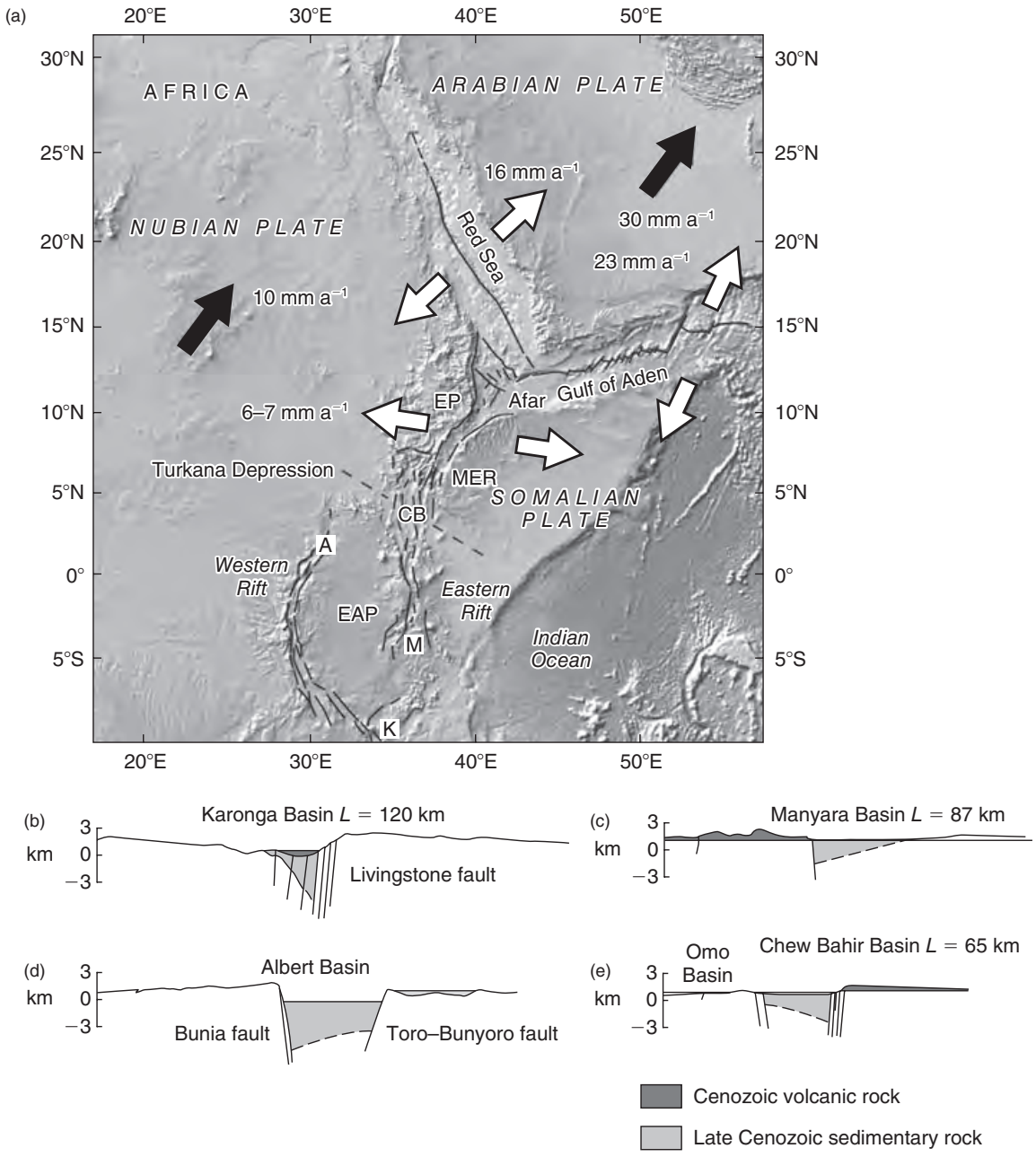

Figure 7.2 *(a) Shaded relief map and geodynamic setting of the East African Rift system constructed using digital topography data and software cited in Fig. 7.1. White arrows indicate relative plate velocities. Black arrows indicate absolute plate motion in a geodetic, no-net-rotation (NNR) framework (Section 5.4). (b–e) Cross-sections showing fault and half-graben morphology (after compilation of Ebinger* et al.*, 1999, with permission from the Royal Society of London). M, Manyara basin (from Foster* et al.*, 1997); K, Karonga basin (from van der Beek* et al.*, 1998); A, Albert basin (from Upcott* et al.*, 1996); CB, Chew Bahir basin (from Ebinger & Ibrahim, 1994); EAP, East African Plateau; EP, Ethiopian Plateau; MER, Main Ethiopian rift; L, the length of the border fault.*

basalts. Others, such as the Western branch of the East African Rift system (Fig. 7.2) and the Baikal Rift, are magma starved and characterized by very small volumes of volcanic rock.

In this chapter, several well-studied examples of rifts and rifted margins are used to illustrate how strain and magmatism are distributed as rifting proceeds to sea floor spreading. The examples also show how geoscientists combine different data types and use spatial and temporal variations in the patterns of rifting to piece together the tectonic evolution of these features.

7.2 GENERAL CHARACTERISTICS OF NARROW RIFTS

Some of the best-studied examples of tectonically active, narrow intracontinental rifts occur in East Africa (Fig. 7.2). Southwest of the Afar triple junction, the Nubian and Somalian plates are moving apart at a rate of approximately 6–7 mm a^{-1} (Fernandes *et al.*, 2004). This divergent plate motion results in extensional deformation that is localized into a series of discrete rift segments of variable age, including the Western Rift, the Eastern Rift, the Main Ethiopian Rift, and the Afar Depression. These segments display characteristics that are common to rifts that form in relatively strong, cool continental lithosphere. Key features include:

1 *Asymmetric rift basins flanked by normal faults.* Continental rifts are associated with the formation of sedimentary basins that are bounded by normal faults. Most tectonically active rift basins show an asymmetric *half graben* morphology where the majority of the strain is accommodated along border faults that bound the deep side of the basins (Fig. 7.2b–e). The polarity of these half grabens may change along the strike of the rift axis, resulting in a segmentation of the rift valley (Fig. 7.3a). In plan view, the border faults typically are the longest faults within each individual basin. Slip on these faults combined with flexural isostatic compensation of the lithosphere (Section 7.6.4) leads to uplift of the rift flanks, creating a characteristic asymmetric topographic profile. The lower relief side of the basin may be faulted and exhibits a monocline that dips toward the basin center. Deposition during slip on the bounding normal faults produces sedimentary and volcanic units that thicken towards the fault plane (Fig. 7.3b). The age of these *syn-rift* units, as well as units that pre-date rifting, provide control on the timing of normal faulting and volcanism. In plan view, displacements decrease toward the tips of border faults where they interact with other faults bounding adjacent basins. Within these *transfer zones* faults may accommodate differential horizontal (including strike-slip) and vertical displacements between adjacent basins.

2 *Shallow seismicity and regional tensional stresses.* Beneath the axis of most continental rifts earthquakes generally are confined to the uppermost 12–15 km of the crust, defining a *seismogenic layer* that is thin relative to other regions of the continents (Section 2.12). Away from the rift axis, earthquakes may occur to depths of 30 km or more. These patterns imply that rifting and thinning locally weaken the crust and affect its mechanical behavior (Section 7.6).

In Ethiopia, the record of seismicity from 1960 to 2005 (Fig. 7.4a) shows that the majority of large earthquakes occur between the Afar Depression and the Red Sea. Analyses of seismic moment release for this period shows that more than 50% of extension across the Main Ethiopian Rift is accommodated aseismically (Hofstetter & Beth, 2003). The earthquakes show combinations of normal, oblique and strike-slip motions. North of the Afar Depression, the horizontal component of most axes of minimum compressive stress strike to the north and northeast at high angles to the trend of the rift segments.

Keir *et al.* (2006) used nearly 2000 earthquakes to determine seismicity patterns within the northern Ethiopian Rift and its flanks

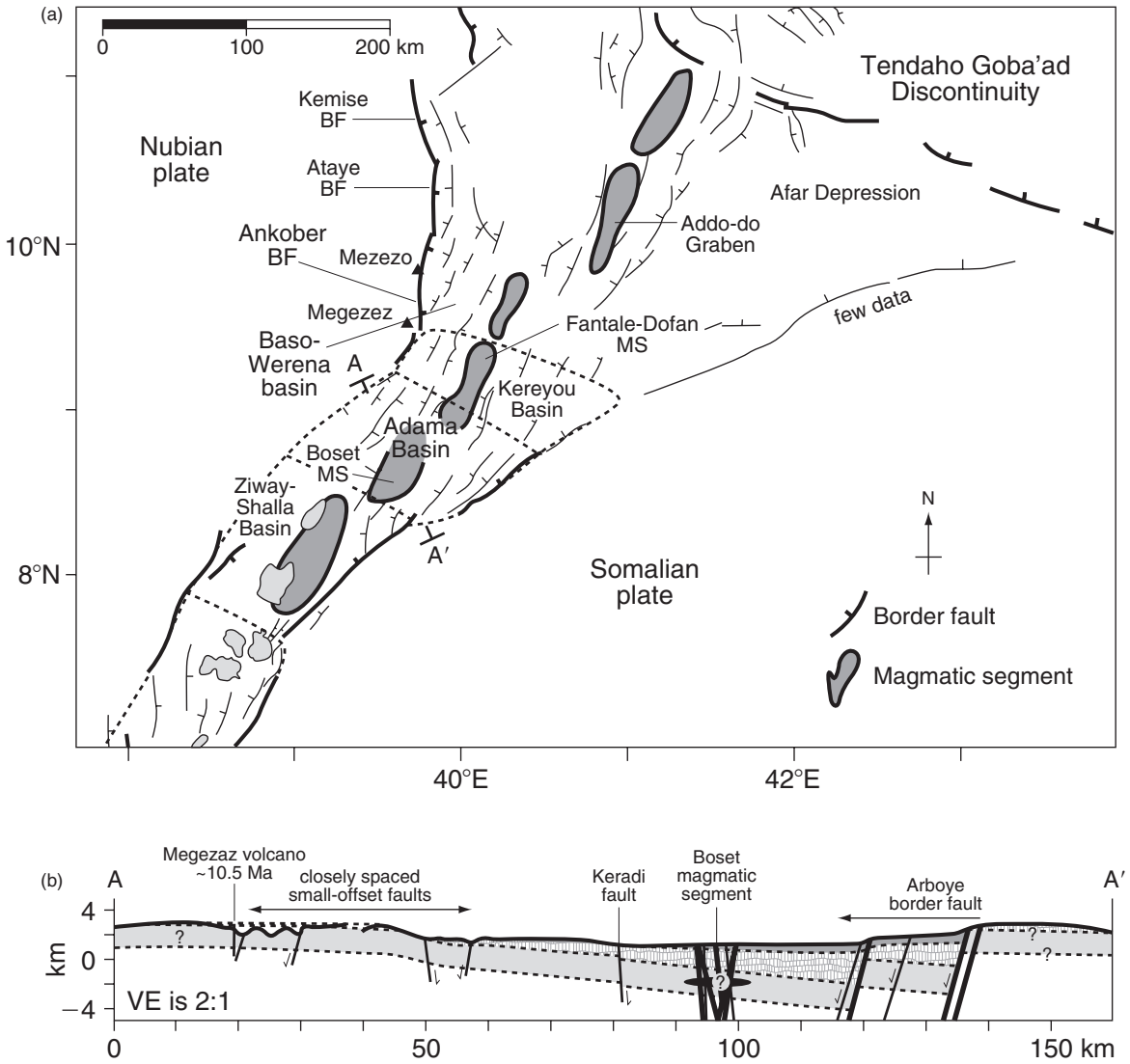

Figure 7.3 *(a) Major faults and segmentation pattern of the northern Main Ethiopian rift and (b) cross-section of Adama Rift Basin showing half graben morphology (images provided by C. Ebinger and modified from Wolfenden* et al.*, 2004, with permission from Elsevier). MS, magmatic segment; BF, border fault. In (b) note the wedge-shaped geometry of the syn-rift Miocene and younger ignimbrite and volcanic units (vertical lined pattern and upper shaded layer). Pre-rift Oligocene flood basalts (lowest shaded layer) show uniform thickness.*

(Fig. 7.4b). Inside the rift, earthquake clusters parallel faults and volcanic centers in a series of 20 km wide, right-stepping zones of magmatism (Fig. 7.4c). Up to 80% of the total extensional strain is localized within these magmatic segments (Bilham *et al.*, 1999; Ebinger & Casey, 2001). The largest earthquakes typically occur along or near major border faults, although the seismicity data indicate that the border faults are mostly aseismic. Earthquakes are concentrated around volcanoes and fissures at depths of

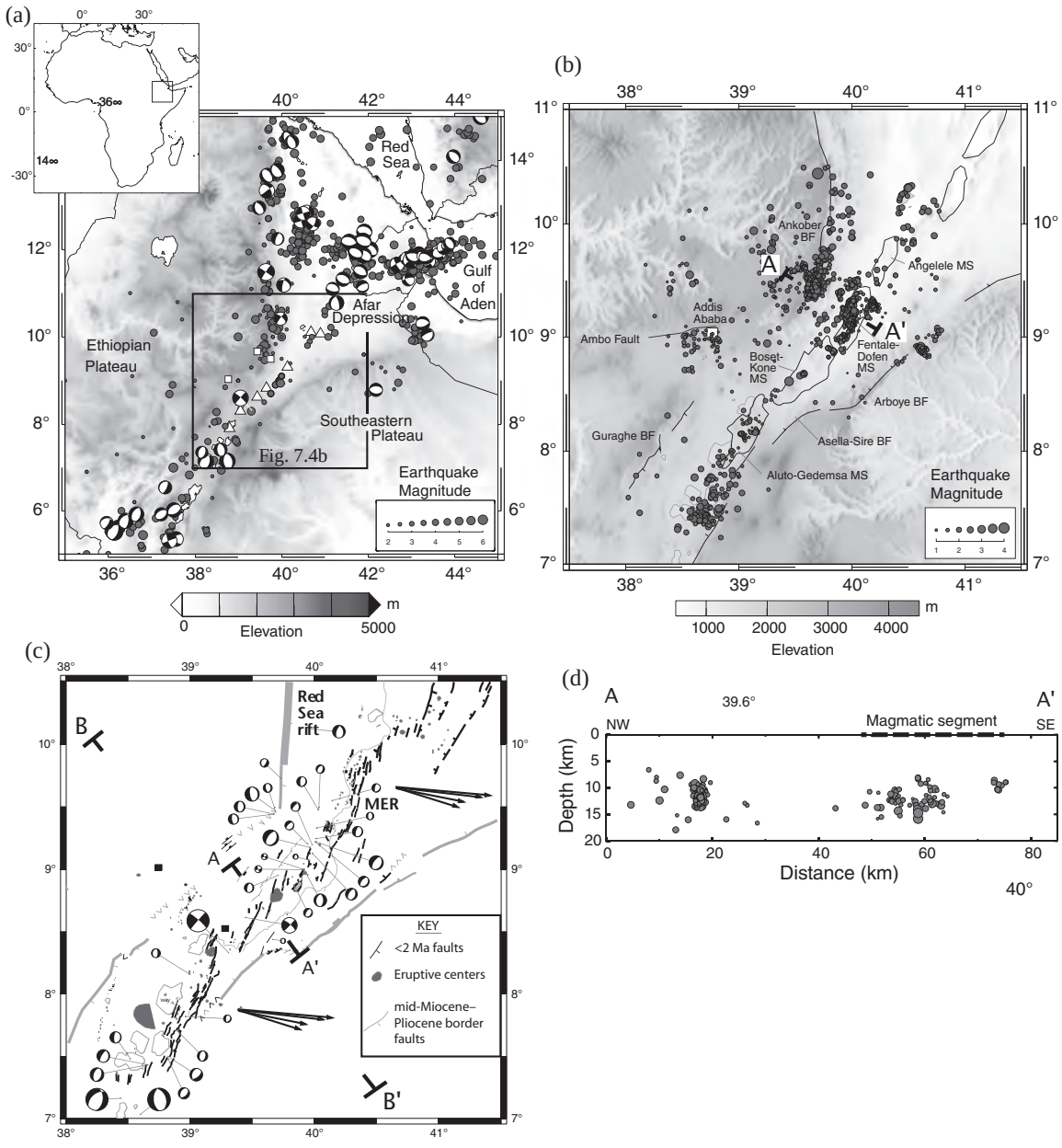

Figure 7.4 *(a) Seismicity and focal mechanisms of East Africa between 1960 and 2005. Late Cenozoic volcanoes shown by triangles. (b) Seismicity of rift segments in the northern Main Ethiopian Rift (MER) between October 2001 and January 2003. (c) Faults that cut <1.9 Ma lavas and late Cenozoic eruptive centers comprising magmatic segments (MS). Miocene border faults in rift basins also shown. Size of focal mechanism solutions indicates relative magnitude of earthquakes. Black arrows show approximate range of plate velocity vectors derived from geodetic data. (d) Earthquake depth distribution across profile A–A′ shown in (c). Cross-section B–B′ shown in Fig. 7.5 (images provided by D. Keir and modified from Keir* et al.*, 2006, by permission of the American Geophysical Union. Copyright © 2006 American Geophysical Union).*

less than 14 km (Fig. 7.4d), probably reflecting magma movement in dikes. In the rift flanks, seismic activity may reflect flexure of the crust (Section 7.6.4) as well as movement along faults. The orientation of the minimum compressive stress determined from earthquake focal mechanisms is approximately horizontal, parallel to an azimuth of 103°. This stress direction, like that in Afar, is consistent with determinations of extension directions derived from tension fractures in young <7000 year old lavas, geodetic measurements, and global plate kinematic data (Fig. 7.4c).

3 *Local crustal thinning modified by magmatic activity.* Geophysical data indicate that continental rifts are characterized by thinning of the crust beneath the rift axis. Crustal thicknesses, like the fault geometries in rift basins, are variable and may be asymmetric. Thick crust may occur beneath the rift flanks as a result of magmatic intrusions indicating that crustal thinning is mostly a local phenomenon (Mackenzie *et al.*, 2005; Tiberi *et al.*, 2005). Variations in crustal thickness may also reflect inherited (pre-rift) structural differences.

Mackenzie *et al.* (2005) used the results of controlled-source seismic refraction and seismic reflection studies to determine the crustal velocity structure beneath the Adama Rift Basin in the northern part of the Main Ethiopian Rift (Fig. 7.5a). Their velocity model shows an asymmetric crustal structure with maximum thinning occurring slightly west of the rift valley. A thin low velocity layer (3.3 km s^{-1}) occurs within the rift valley and thickens eastward from 1 to 2.5 km. A 2–5-km-thick sequence of intermediate velocity (4.5–5.5 km s^{-1}) sedimentary and volcanic rock lies below the low velocity layer and extends along the length of the profile. Normal crustal velocities (P_n = 6.0–6.8 km s^{-1}) occur to depths of 30–35 km except in a narrow 20–30 km wide region in the upper crust beneath the center of the rift valley where P_n velocities are 5–10% higher (>6.5 km s^{-1}) than those outside the rift (Fig. 7.5a). These differences probably reflect the presence of mafic intrusions associated with magmatic centers. A nearly continuous intracrustal reflector at 20–25 km depth and Moho depths of 30 km show crustal thinning beneath the rift axis. The western flank of the rift is underlain by a ~45 km thick crust and displays a ~15 km thick high velocity (7.4 km s^{-1}) lower crustal layer. This layer is absent from the eastern side, where the crust is some 35 km thick. Mackenzie *et al.* (2005) interpreted the high velocity lower crustal layer beneath the western flank as underplated material associated with pre-rift Oligocene flood basalts and, possibly, more recent magmatic activity. Variations in intracrustal seismic reflectivity also suggest the presence of igneous intrusions directly below the rift valley (Fig. 7.5b).

Gravity data provide additional evidence that the crustal structure of rift zones is permanently modified by magmatism that occurs both prior to and during rifting. In Ethiopia and Kenya, two long-wavelength (>1000 km) negative Bouguer gravity anomalies coincide with two major ~2 km high topographic uplifts: the Ethiopian Plateau and the Kenya Dome, which forms part of the East African Plateau (Figs 7.2, 7.6a). The highest parts of the Ethiopian Plateau are more than 3 km high. This great height results from the eruption of a large volume of continental flood basalts (Section 7.4) between 45 and 22 Ma, with the majority of volcanism coinciding with the opening of the Red Sea and Gulf of Aden at ~30 Ma (Wolfenden *et al.*, 2005). The negative gravity anomalies reflect the presence of anomalously low density upper mantle and elevated geotherms (Tessema & Antoine, 2004). In each zone, the rift valleys display short-wavelength positive Bouguer gravity anomalies (Fig. 7.6b) that reflect the presence of cooled, dense mafic intrusions (Tiberi *et al.*, 2005).

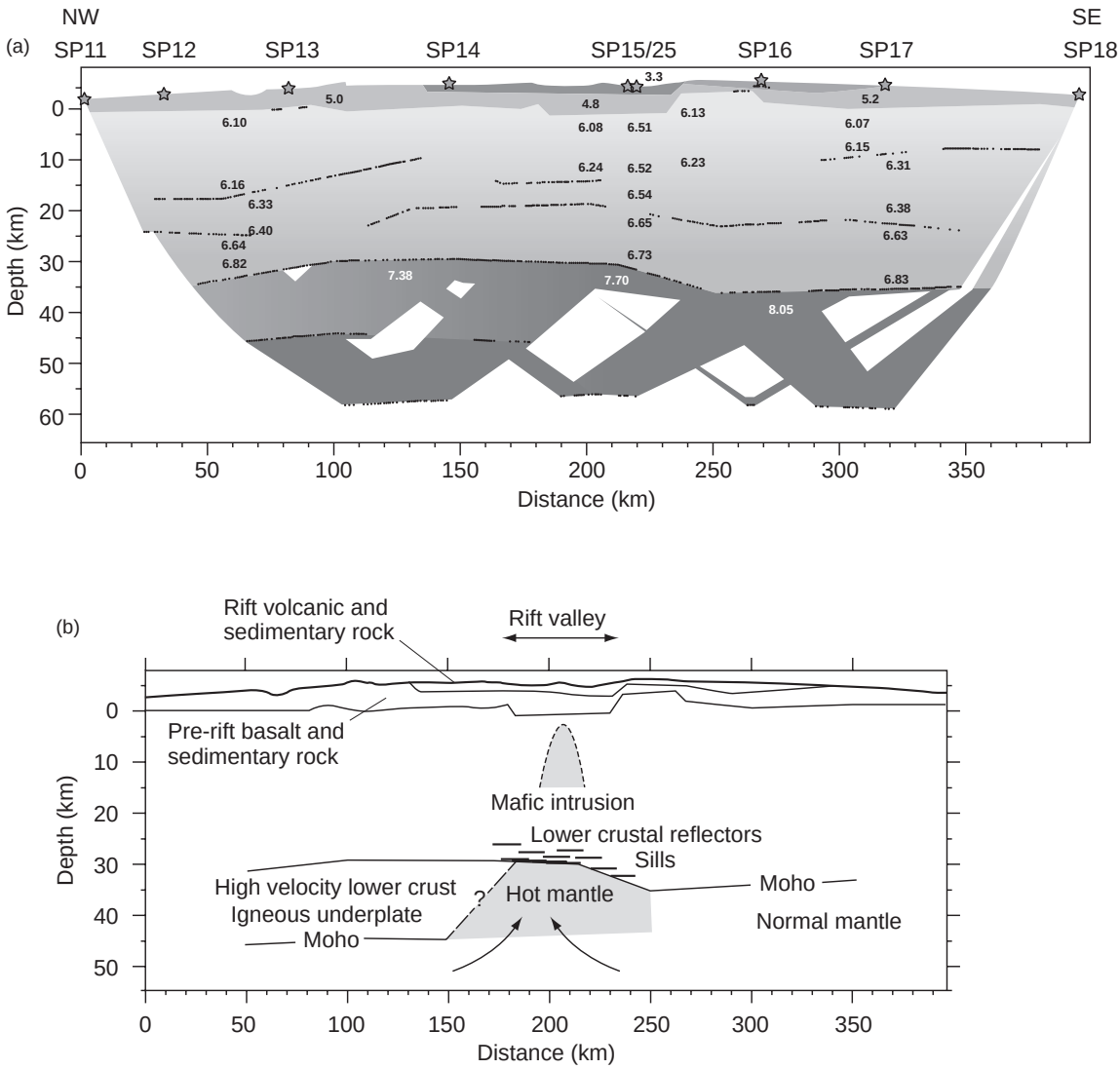

Figure 7.5 *(a) P-wave velocity model and (b) interpretation of the Main Ethiopian Rift (after Mackenzie* et al.*, 2005, with permission from Blackwell Publishing). Location of profile (B–B′) shown in Fig. 7.4c.*

4 *High heat flow and low velocity, low density upper mantle.* Heat flow measurements averaging 70–90 mW m^{-2} and low seismic velocities in many rift basins suggest temperature gradients (50–100°C km^{-1}) that are higher than those in the adjacent rift flanks and nearby cratons. Where the asthenosphere is anomalously hot, such as in East Africa, domal uplifts and pervasive volcanism result. Nevertheless, there is a large degree of variability in temperature and volcanic activity among rifts. The Baikal Rift, for example, is much cooler. This rift displays low regional heat flow of 40–60 mW m^{-2} (Lysack, 1992) and lacks volcanic activity.

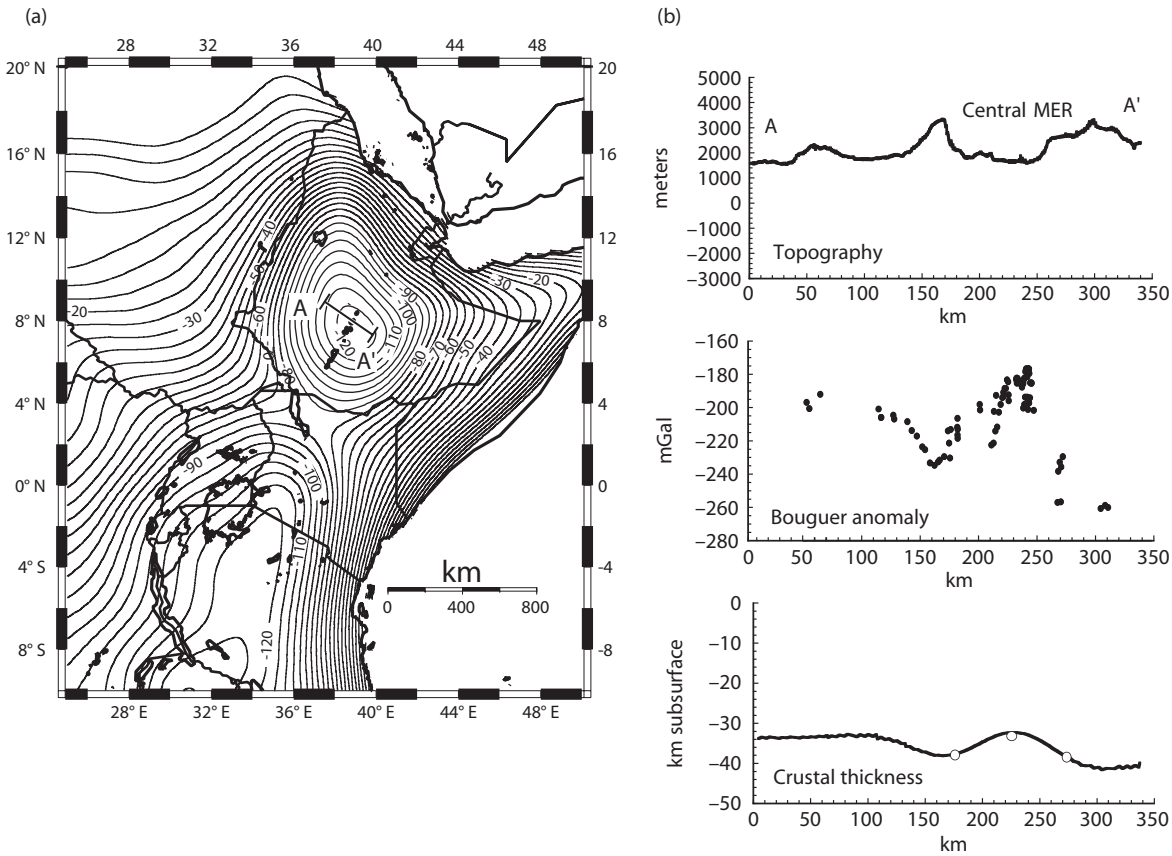

Figure 7.6 *(a) Map showing long-wavelength Bouguer gravity anomalies after removal of the short wavelength (image provided by A. Tessema and modified from Tessema & Antoine, 2004, with permission from Elsevier). (b) Profiles (A–A') of topography, short-wavelength Bouguer gravity anomaly, and crustal thickness estimates of the central Main Ethiopian Rift (MER) (images provided by C. Tiberi and modified from Tiberi* et al.*, 2005, with permission from Blackwell Publishing). Profile location shown in (a). Circles in crustal thickness profile indicate depths estimated from receiver function studies.*

In East Africa, relatively slow P_n wave velocities of 7.7 km s^{-1} in the upper mantle beneath the Adama Rift Basin in Ethiopia (Fig. 7.5a) suggest elevated temperatures (Mackenzie *et al.*, 2005). Elsewhere upper mantle P_n wave velocities are in the range 8.0–8.1 km s^{-1}, which is expected for stable areas with normal heat flow. Tomographic inversion of P- and S-wave data (Fig. 7.7a–c) indicate that the low velocity zone below the rift is tabular, approximately 75 km wide, and extends to depths of 200–250 km (Bastow *et al.*, 2005). The zone is segmented and offset away from the rift axis in the upper 100 km but becomes more central about the rift axis below this depth (Fig. 7.7c). In the more highly extended northern section of Ethiopian Rift (Fig. 7.7d), the low velocity anomaly broadens laterally below 100 km and may be connected to deeper low velocity structures beneath the Afar Depression (Section 7.4.3). This broadening of the low velocity zone is consistent with the propagation of the Main Ethiopian Rift, during Pliocene–Recent times, toward the older spreading centers of the Red Sea and Gulf of Aden.

In addition to the high temperatures, the low velocity zones beneath rifts may also reflect the

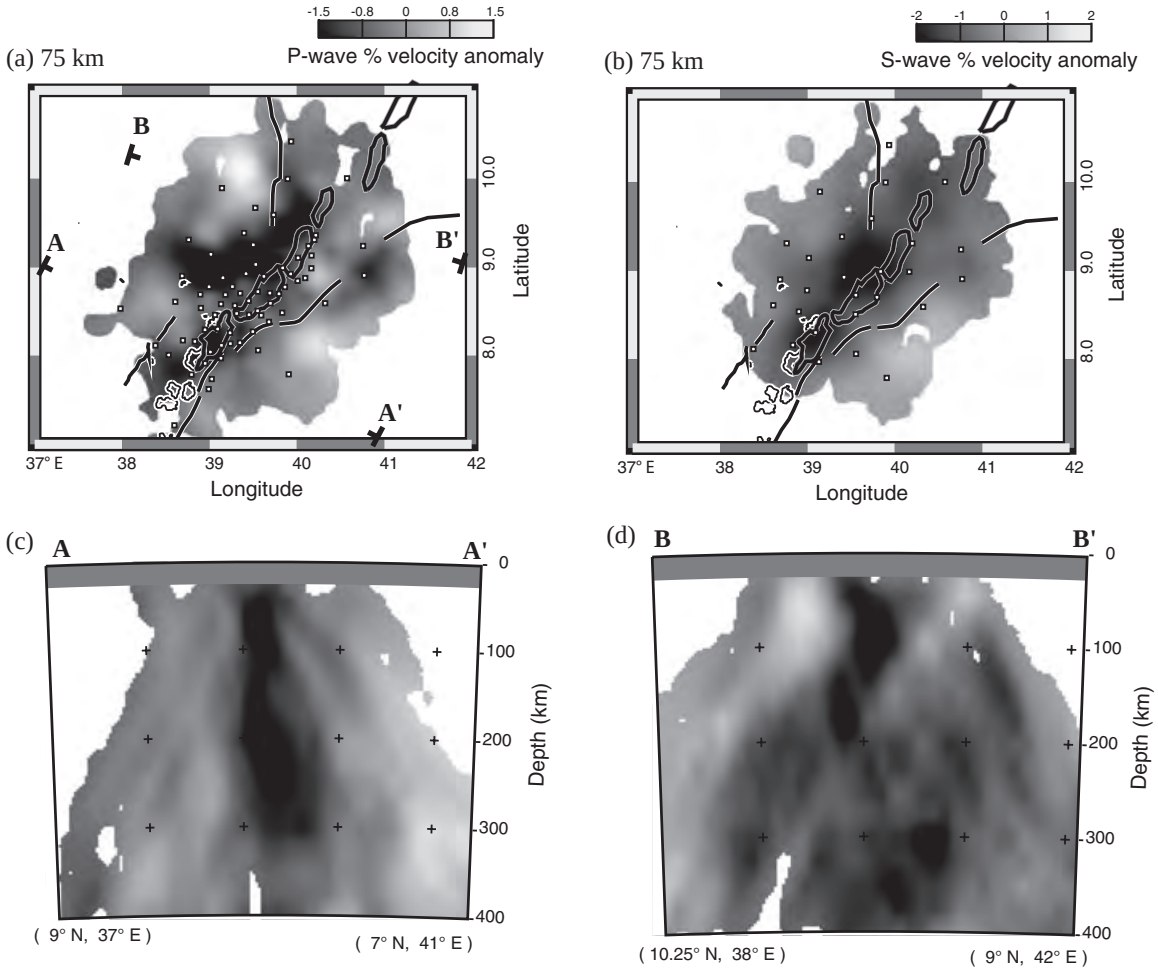

Figure 7.7 *Depth slices through (a) P-wave and (b) S-wave velocity models at 75 km depth in the Main Ethiopian Rift. (c,d) Vertical profiles through the P-wave velocity model (images provided by I. Bastow and modified from Bastow* et al.*, 2005, with permission from Blackwell Publishing). Heavy black lines in (a) and (b) are Pleistocene magmatic segments and mid-Miocene border faults (cf. Fig. 7.3). The locations of stations contributing to the tomographic inversions are shown with white squares in (a) and (b). Profile locations shown in (a). Velocity scales in (c) and (d) are same as in (a).*

presence of partial melt. Observations of shear wave splitting and delay times of teleseismic waves traveling beneath the Kenya Rift (Ayele *et al.*, 2004) and northern Ethiopian Rift (Kendall *et al.*, 2005) suggest the alignment of partial melt in steep dikes within the upper 70–90 km of the lithosphere or the lattice preferred orientation of olivine in the asthenosphere as hot material flows laterally into the rift zone. These observations indicate that the upper mantle underlying rifts is characterized by low velocity, low density and anomalously high temperature material.

7.3 GENERAL CHARACTERISTICS OF WIDE RIFTS

One of the most commonly cited examples of a wide intracontinental rift is the Basin and Range Province of western North America (Fig. 7.1). In this region, large extensional strains have accumulated across a zone ranging in width from 500 to 800 km (Fig. 7.8). In the central part of the province, some 250–300 km of horizontal extension measured at the surface has occurred since ~16 Ma (Snow & Wernicke, 2000). In eastern Nevada and western Utah alone the amount of total horizontal surface extension is approximately 120–150 km (Wernicke, 1992). These values, and the width of the zone over which the deformation occurs, greatly exceed those observed in narrow continental rifts (Section 7.2).

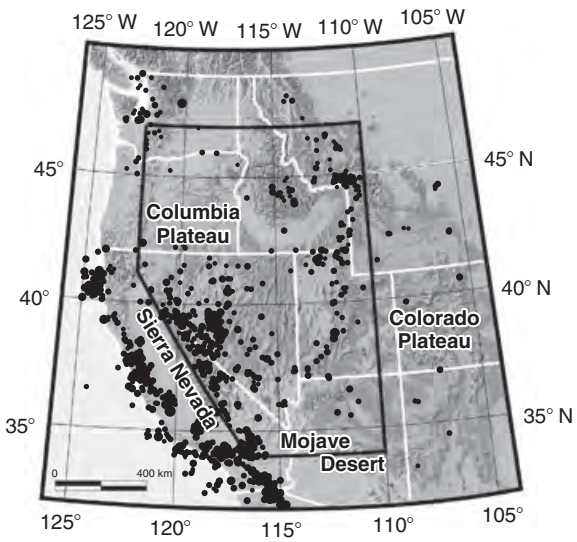

Figure 7.8 *Shaded relief map of the western United States showing topography and earthquakes with $M \geq 4.8$ in the northern and central sectors of the Basin and Range (image provided by A. Pancha and A. Barron and modified from Pancha* et al.*, 2006, with permission from the Seismological Society of America). Circle radius is proportional to magnitude. The area outlined with a bold polygon encloses all major earthquakes that are associated with deformation of the Basin and Range.*

The Basin and Range example thus shows that continental lithosphere may be highly extended without rupturing to form a new ocean basin. This pattern is characteristic of rifts that form in relatively thin, hot, and weak continental lithosphere. Here, the key features that distinguish wide rifts from their narrow rift counterparts are illustrated using the Basin and Range and the Aegean Sea provinces as examples:

1 *Broadly distributed deformation.* The Basin and Range Province is bounded on the west by the greater San Andreas Fault system and Sierra Nevada–Great Valley microplate and on the east by the Colorado Plateau (Figs 7.8, 7.9). Both the Sierra and the Plateau record comparatively low heat flow values (40–60 mW m^{-2}) and virtually no Cenozoic extensional deformation (Sass *et al.*, 1994; Bennett *et al.*, 2003). In between these two rigid blocks Cenozoic deformation has resulted in a broad zone of linear, north-trending mountain ranges of approximately uniform size and spacing across thousands of square kilometers. The mountain ranges are about 15–20 km wide, spaced approximately 30 km apart, and are elevated ~1.5 km above the adjacent sedimentary basins. Most are delimited on one side by a major range-bounding normal fault. Some strike-slip faulting also is present. In the northern part of the province (latitude 40°N) roughly 20–25 basin-range pairs occur across 750 km.

   The present day deformation field of the Basin and Range is revealed by patterns of seismicity (Figs 7.8, 7.10) and horizontal velocity estimates (Fig. 7.11) derived from continuous GPS data (Section 5.8) (Bennett *et al.*, 2003). The data show two prominent bands of high strain rate along the eastern side of the Sierra Nevada and the western side of the Colorado Plateau. These are the eastern California/central Nevada seismic belt and the Intermountain seismic belt, respectively (Fig. 7.9). Focal mechanisms (Fig. 7.10) indicate that the former accommodates both right lateral and normal displacements and the latter accommodates mostly normal motion.

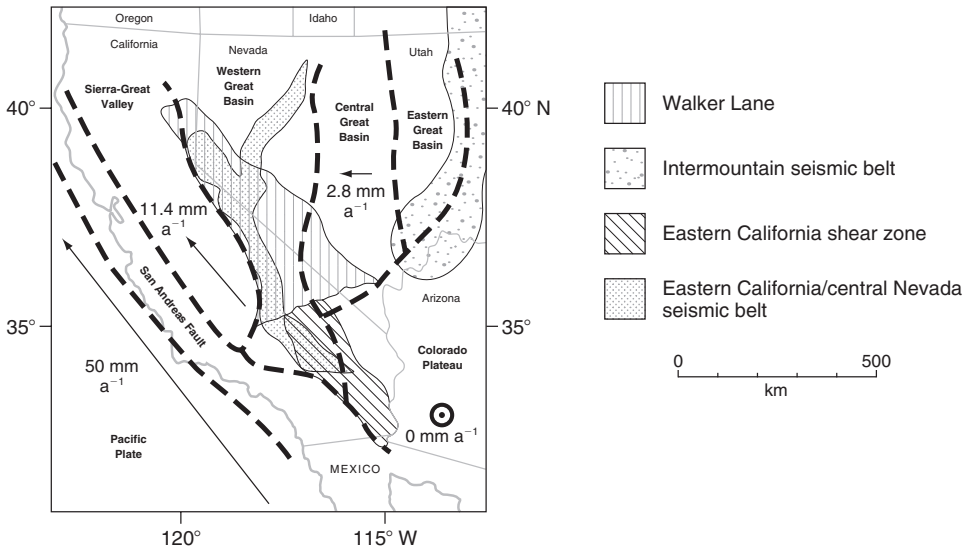

Figure 7.9 *Map showing the various tectonic provinces of the Basin and Range determined from geodetic and geologic data (modified from Bennett* et al.*, 2003, by permission of the American Geophysical Union. Copyright © 2003 American Geophysical Union). Rates given are relative to the North American plate.*

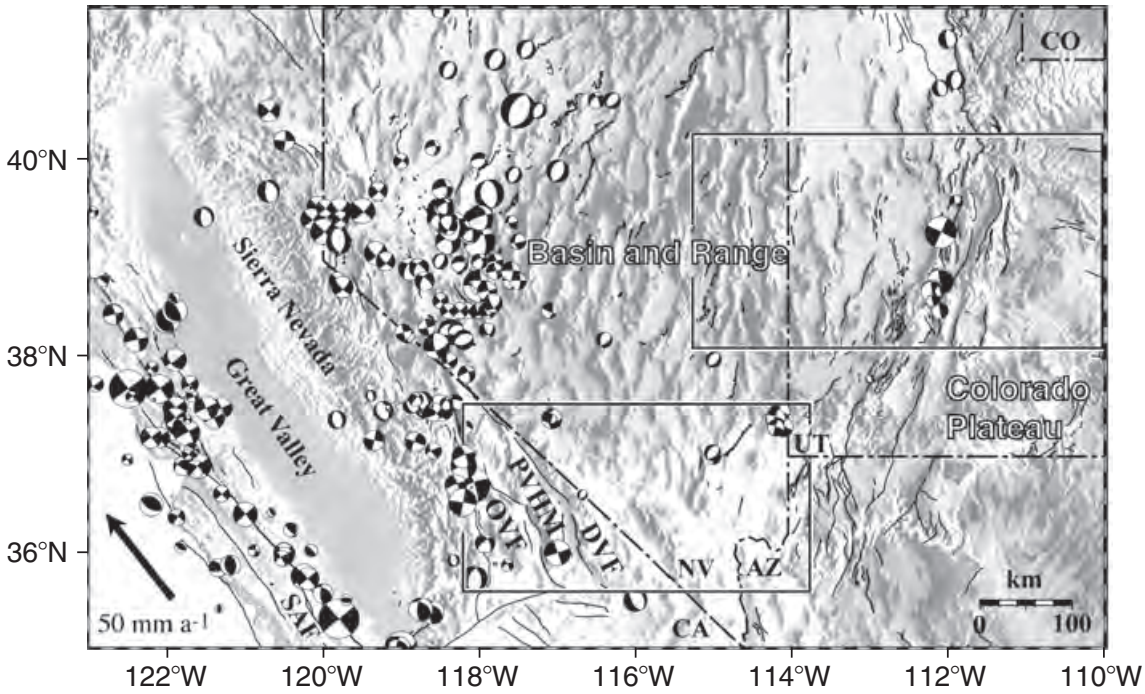

Figure 7.10 *Shaded relief map of the northern Basin and Range showing major faults and earthquake focal mechanisms (image provided by R. Bennett and modified from Bennett* et al.*, 2003, and Shen-Tu* et al.*, 1998, by permission of the American Geophysical Union. Copyright © 2003 and 1998 American Geophysical Union). SAF, San Andreas Fault. Northward translation of the Sierra Nevada–Great Valley microplate is accommodated by strike-slip motion on the Owens Valley (OVF), Panamint Valley–Hunter Mountain (PVHM), and Death Valley (DVF) fault zones. Black boxes show approximate area of Fig. 7.13 (lower box) and Fig. 7.14 (upper box).*

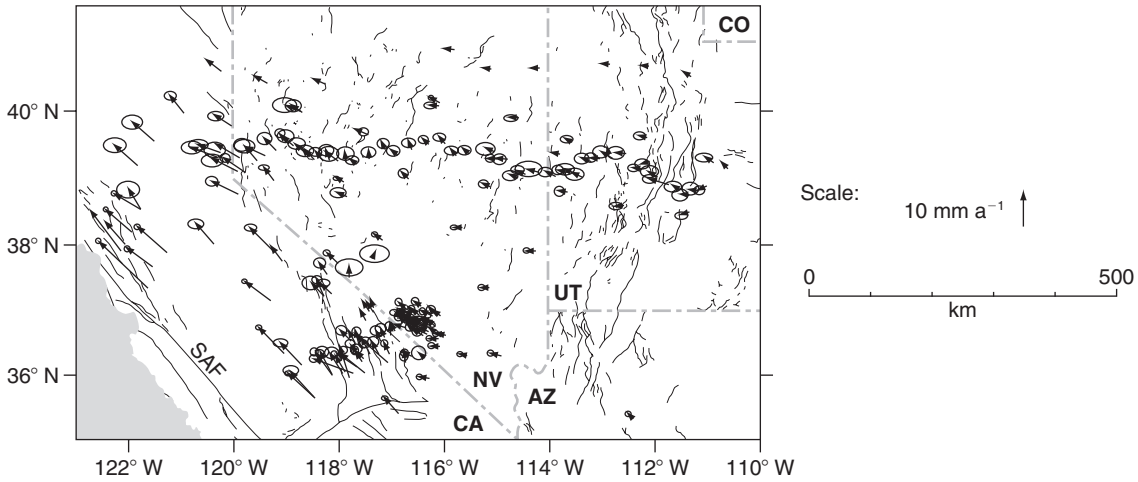

Figure 7.11 *GPS velocities of sites in the Sierra Nevada–Great Valley microplate, northern Basin and Range, and Colorado Plateau with respect to North America (image provided by R. Bennett and modified from Bennett* et al.*, 2003, by permission of the American Geophysical Union. Copyright © 2003 American Geophysical Union). Error ellipses represent the 95% confidence level. Velocity estimates were derived from continuous GPS data from GPS networks in and around the northern Basin and Range. SAF, San Andreas Fault.*

In the intervening area, deformation is diffusely distributed and, in some places, absent from the current velocity field. Three sub-provinces, designated the eastern, central and western Great basins, show distinctive patterns of strain (Fig. 7.9). Relative motion between the central Great Basin and Colorado Plateau occurs at a rate of 2.8 mm a^{-1} and is partly accommodated by diffuse east–west extension across the eastern Great Basin. Relative motion between the Sierra Nevada–Great Valley and the central Great Basin occurs at a rate of 9.3 mm a^{-1} toward N37°W and is accommodated by diffuse deformation across the western Great Basin (Section 8.5.2). The central Great Basin records little current internal deformation. Similar patterns of distributed deformation punctuated by zones of high strain rate occur in the extensional provinces of central Greece and the Aegean Sea (Goldsworthy *et al.*, 2002).

Two other zones of deformation in the Basin and Range have been defined on the basis of Middle Miocene–Recent geologic patterns. The Walker Lane (Fig. 7.9) displays mountain ranges of variable orientation and complex displacements involving normal faulting and both left lateral and right lateral strike-slip faulting. This belt overlaps with the Eastern California Shear Zone (Fig. 8.1 and Section 8.5.2) to the south. Hammond & Thatcher (2004) reasoned that the concentration of right lateral motion and extension within the western Basin and Range results from weak lithosphere in the Walker Lane. Linear gradients in gravitational potential energy and viscosity also may concentrate the deformation (Section 7.6.3). Together these data suggest that the broad region of the Basin and Range currently accommodates some 25% of the total strain budget between the Pacific and North American plates (Bennett *et al.*, 1999). The data also indicate that, at least currently, deformation in the Basin and Range involves a heterogeneous combination of normal and strike-slip displacements.

The depth distribution of microearthquakes also shows that the Basin and Range Province is characterized by a seismogenic layer that is thin relative to other regions of the continent. Approximately 98% of events occur at depths less than 15 km for all of

Utah (1962–1999) and 17 km for Nevada (1990–1999) (Pancha *et al.*, 2006). This thickness of the seismogenic layer is similar to that displayed by most other rifts, including those in East Africa, except that in the Basin and Range it characterizes thousands of square kilometers of crust. The pattern implies that high geothermal gradients and crustal thinning have locally weakened a very large area.

Because deformation is distributed over such a broad region, most of the major faults in the Basin and Range have recurrence times of several thousand years (Dixon *et al.*, 2003). In the northern part of the province, several hundred faults show evidence of slip since 130 ka, yet contemporary seismicity and large historical earthquakes are clustered on only a few of them. This observation raises the possibility that a significant portion of strain is accommodated by aseismic displacements. Niemi *et al.* (2004) investigated this possibility by combining geologic data from major faults with geodetic data in the eastern Great Basin. The results suggest that both data types define a ~350 km wide belt of east–west extension over the past 130 ka. Reconciling deformation patterns measured over different timescales is a major area of research in this and most other zones of active continental tectonics.

2 *Heterogeneous crustal thinning in previously thickened crust.* Wide rifts form in regions where extension occurs in thick, weak continental crust. In the Basin and Range and the Aegean Sea the thick crust results from a history of convergence and crustal shortening that predates rifting. Virtually the entire western margin of North America was subjected to a series of compressional orogenies during Mesozoic times (Allmendinger, 1992). These events thickened sedimentary sequences that once formed part of a Paleozoic passive margin. The ancient margin is marked now by an elongate belt of shallow marine sediments of Paleozoic and Proterozoic age that thicken to the west across the eastern Great Basin and are deformed by thrust faults and folds of the Mesozoic Sevier thrust belt (Fig. 7.12). This deformation created a thick pile of weak sedimentary rocks that has contributed to a delocalization of strain (Section 7.6.1) during Cenozoic extension (Sonder & Jones, 1999). Some estimates place parts of the province at a pre-rift crustal thickness of 50 km, similar to that of the unextended Colorado Plateau (Parsons *et al.*, 1996). Others have placed it at more than 50 km (Coney & Harms, 1984). This pre-extensional history is one of the most important factors that has contributed to a heterogeneous style of extensional deformation in the Basin and Range.

The uniformity in size and spacing of normal faults in the Basin and Range, and the apparent uniform thickness of the seismogenic layer, at first suggests that strain and crustal thinning, on average, might also be uniformly distributed across the province. However, this assertion is in conflict with the results of geologic and geophysical surveys. Gilbert & Sheehan (2004) found Moho depths ranging from 30 to 40 km beneath the eastern Basin and Range (Plate 7.1a), with the thinnest crust occurring in northern Nevada and Utah (Plate 7.1b) and thicknesses of 40 km in southern Nevada (Plate 7.1c) (Plate 7.1a–c between pp. 244 and 245). Louie *et al.* (2004) also found significant variations in Moho depths with the thinnest areas showing depths of only 19–23 km beneath the Walker Lane and northwest Nevada. This southward thickening of the crust coincides with variations in the pre-Cenozoic architecture of the lithosphere, including differences in age and pre-extensional thickness. Similar nonuniform variations in crustal thickness occur beneath the Aegean Sea (Zhu *et al.*, 2006). These results illustrate that crustal thinning in wide rifts is nonuniform and, like narrow rifts, is strongly influenced by the pre-existing structure of the lithosphere.

The nonuniformity of crustal thinning in the Basin and Range is expressed in patterns of faulting within the upper crust. The Death Valley region of eastern California contains some of the youngest examples of large-magnitude extension in the world adjacent to

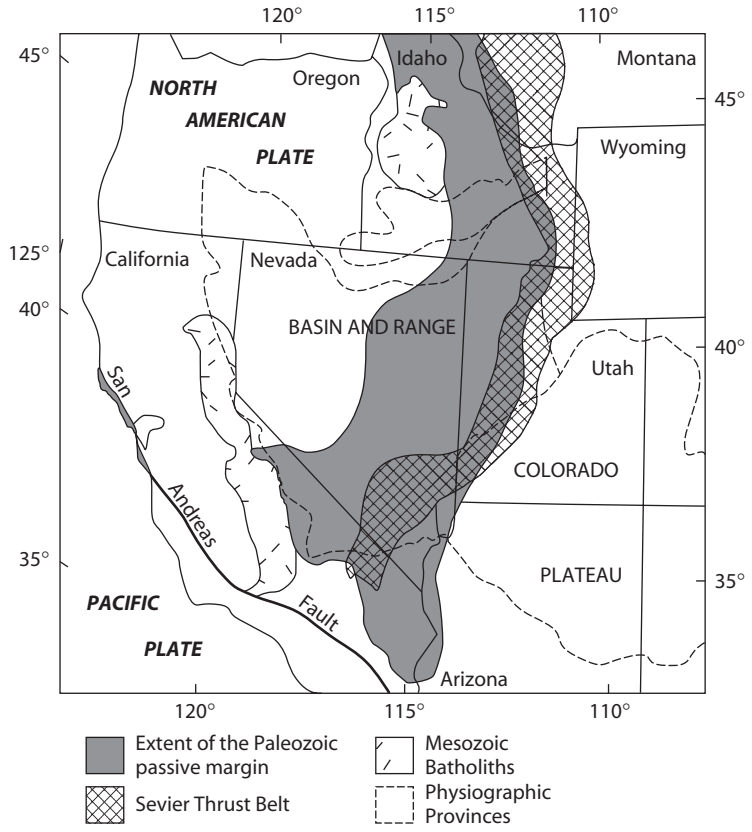

Figure 7.12 *Map of the western United States showing extent of Paleozoic passive margin sequences and the Sevier thrust belt (after Niemi* et al.*, 2004, with permission from Blackwell Publishing).*

areas that record virtually no upper crustal strain. East–west extension beginning about ~16 Ma has resulted in ~250 km of extension between the Sierras and the Colorado Plateau (Wernicke & Snow, 1998). The intervening region responded to this divergence by developing a patchwork of relatively unextended crustal blocks separated by regions strongly deformed by extension, strike-slip faulting, and contraction (Fig. 7.13a). The heterogeneous distribution of extension is illustrated in Fig. 7.13b, which shows estimates of the thickness of the pre-Miocene upper crust that remains after extension assuming an original thickness of 15 km. In some areas, such as the Funeral and Black mountains, the upper crust has been dissected and pulled apart to such a degree that pieces of the middle crust are exposed (Snow & Wernicke, 2000).

One of the most enigmatic characteristics of the Basin and Range Province involves local relationships between large-scale extension in the upper crust and the distribution of strain in the lower part of the crust. Some studies have shown that despite highly variable patterns of upper crustal strain, local crustal thickness appears to be surprisingly uniform (Gans, 1987; Hauser *et al.*, 1987; Jones & Phinney, 1998). This result implies that large strains have been compensated at depth by lateral flow in a weak lower crust, which acted to smooth out any Moho topography (Section 7.6.3). Park & Wernicke (2003) used magnetotelluric data to show that this lateral flow and flattening out of the Moho in the

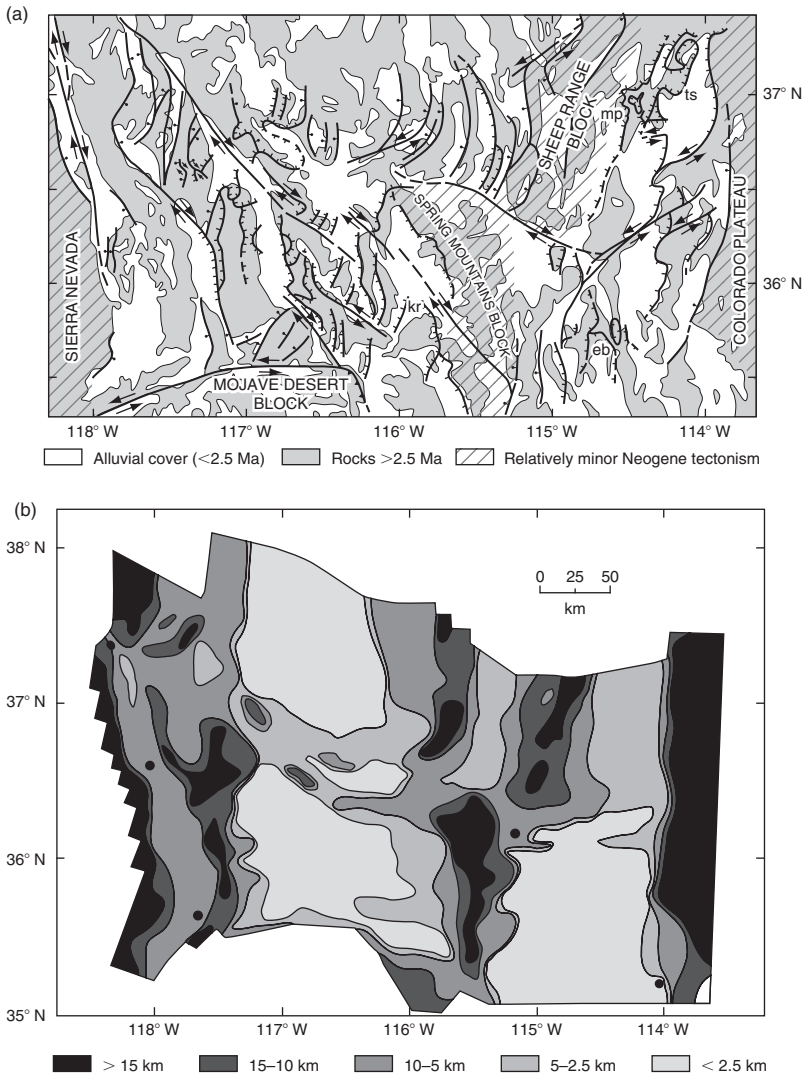

Figure 7.13 *Maps showing (a) major Cenozoic faults (heavy black lines) in the central Basin and Range Province and (b) the distribution of upper crustal thinning estimated by reconstructing Cenozoic extension using pre-extensional markers (images provided by B. Wernicke and modified from Snow & Wernicke, 2000. Copyright 2000 by* American Journal of Science*. Reproduced with permission of* American Journal of Science *in the format Textbook via Copyright* Clearance Center*). Symbols in (a) indicate strike-slip faults (arrows), high-angle normal faults (ball and bar symbols), low-angle normal faults (tick marks), and thrust faults (teeth). Large-magnitude detachment faults in metamorphic core complexes include the Eldorado-Black Mountains (eb), the Mormon Peak (mp), Tule Springs (ts), and the Kingston Range (kr) detachments. Contours in (b) represent the remaining thickness of a 15-km-thick pre-extensional Cenozoic upper crust, such that the lightly shaded areas represent the areas of greatest thinning. Black dots are points used in the reconstruction.*

Basin and Range probably occurred during the Miocene. By contrast, other regions, such as the Aegean Sea and the D'Entrecasteaux islands (Section 7.8.2), do not show this relationship, implying a more viscous lower crust that resists flow beneath highly extended areas.

3 *Thin mantle lithosphere and anomalously high heat flow.* Like most wide rifts, the Basin and Range is characterized by high surface heat flow, negative long-wavelength Bouguer gravity anomalies, and low crustal P_n and S_n velocities (Catchings & Mooney, 1991; Jones *et al.*, 1992; Zandt *et al.*, 1995; Chulick & Mooney, 2002). Regional topography in the Basin and Range also is unusually high with an average of 1.2 km above mean sea level. Low seismic velocities are discernible down to 300–400 km depth. Seismic tomographic models indicate that adiabatic mantle temperatures of 1300°C occur as shallow as 50 km under most of the province. For comparison, temperatures at 50–100 km in the cratonic mantle beneath the stable eastern part of North America are on average 500°C cooler than under the Basin and Range. All of these characteristics indicate a shallow asthenosphere and very thin, warm upper mantle (Goes & van der Lee, 2002).

Temperatures at 110 km depth inferred from seismic velocity models suggest the presence of small melt and fluid pockets in the shallow mantle beneath the Basin and Range (Goes & van der Lee, 2002). Warm, low-density subsolidus mantle also may contribute to the high average elevation and large-scale variations in topography of the region. Other factors contributing to the high elevations probably include isostatic effects caused by previously thickened continental crust and magmatic intrusions. However, a lack of correlation between crustal thickness variations and surface topography indicates that simple Airy isostasy is not at play and the high elevations across the southwestern United States must involve a mantle component (Gilbert & Sheehan, 2004).

Volcanic activity is abundant, including eruptions that occurred both before and during extension. This activity is compatible with evidence of high heat flow, elevated geotherms, and shallow asthenosphere. Pre-rift volcanism is mostly calc-alkaline in composition. Magmatism that accompanied extension is mostly basaltic. Basalts from Nevada have an isotopic signature suggesting that they were derived from sublithospheric mantle. This pattern matches evidence of mantle upwelling beneath the rift (Savage & Sheehan, 2000).

4 *Small- and large-magnitude normal faulting.* Large extensional strains and thinning of the crust in wide rifts is partly accommodated by slip on normal faults. Two contrasting patterns are evident. First, the deformation can involve distributed normal faulting where a large number of more or less regularly spaced normal faults each accommodate a relatively small amount (<10 km) of the total extension. Second, the strain may be highly localized onto a relatively small number of normal faults that accommodate large displacements of several tens of kilometers. Both patterns are common and may occur during different stages of rift evolution.

Many of the range-bounding normal faults in the Basin and Range record relatively small offsets. These structures appear similar to those that characterize narrow rift segments. Asymmetric half graben and footwall uplifts are separated by a dominant normal fault that accommodates the majority of the strain. The morphology of these features is governed by the elastic properties of the lithosphere (Section 7.6.4) and the effects of syn-rift sedimentation and erosion. The asymmetry of the half graben and the dips of the range-bounding faults also commonly change in adjacent basin-range pairs. Many of the tectonically active faults maintain steep dips (>45°) that may penetrate through the upper crust. However, unlike the border faults of East Africa, some of the range-bounding faults of the Basin and Range exhibit geometries that involve low-angle extensional detachment faults. A few of these low-angle normal faults accommodate very large displacements and penetrate tens of

kilometers into the middle and, possibly, the lower crust.

Extensional detachment faults are low-angle (<30°), commonly domed fault surfaces of large areal extent that accommodate displacements of 10–50 km (Axen, 2004). The footwalls of these faults may expose a thick (0.1–3 km) ductile shear zone that initially formed in the middle or lower crust and later evolved into a frictional (brittle) slip surface as it was unroofed during the extension (Wernicke, 1981). In the Basin and Range, these features characterize regions that have been thinned to such an extent (100–400% extension) that the upper crust has been completely pulled apart and metamorphic rocks that once resided in the middle and lower crust have been exhumed. These domed regions of deeply denuded crust and detachment faulting are the hallmarks of the Cordilleran extensional *metamorphic core complexes* (Crittenden *et al.*, 1980; Coney & Harms, 1984). Core complexes are relatively common in the Basin and Range (Figs 7.13, 7.14), although they are not unique to this province. Their ages are diverse with most forming during Late Oligocene–Middle Miocene time (Dickinson, 2002). Similar features occur in many other settings, including the southern Aegean Sea, in rifts that form above subduction zones, such as the D'Entrecasteaux Islands (Section 7.8.2), near oceanic spreading centers (Section 6.7), and in zones of extension within collisional orogens (Section 10.4.4).

Most authors view core complexes as characteristic of regions where weak crustal rheologies facilitate lateral flow in the deep crust and, in some cases, the mantle, causing upper crustal extension to localize into narrow zones (Sections 7.6.2, 7.6.5). Nevertheless, the mechanics of slip on low-angle normal faults is not well understood. Much of the uncertainty is centered on whether specific examples initially formed at low angles or were rotated from a steep orientation during deformation (Axen, 2004). The consensus is that both types probably occur (Section 7.8.2). Some low-angle, large-offset normal faults may evolve from high-angle faults by flexural rotation (Section 7.6.4). As the hanging wall is removed by slip on the fault, the footwall is mechanically unloaded and results in isostatic uplift and doming (Buck, 1988; Wernicke & Axen, 1988). The doming can rotate the normal fault to gentler dips and lead to the formation of new high-angle faults.

The variety of Cenozoic fault patterns that typify the Basin and Range is illustrated in Fig. 7.14, which shows a segment of the eastern Great Basin in Utah and eastern Nevada (Niemi *et al.*, 2004). The 350 km long Wasatch Fault Zone is composed of multiple segments with the largest displaying dips ranging from 35° to 70° to the west. Its subsurface geometry is not well constrained but it probably penetrates at least through the upper crust. The Sevier Desert Detachment Fault dips 12° to the west and can be traced continuously on seismic reflection profiles to a depth of at least 12–15 km (Fig. 7.14b). The range-bounding Spring Valley and Egan Range faults penetrate to at least 20 km depth and possibly through the entire 30 km thickness of the crust at angles of ~30°. The Snake Range Detachment also dips ~30° through most of the upper crust. Large-magnitude extension along the Snake Range (Miller *et al.*, 1999) and Sevier Desert (Stockli *et al.*, 2001) detachment faults began in Early Miocene time and Late Oligocene or Early Miocene time, respectively. In most areas, high-angle normal faults are superimposed on these older structures.

7.4 VOLCANIC ACTIVITY

7.4.1 Large igneous provinces

Many rifts and rifted margins (Section 7.7.1) are associated with the subaerial eruption of continental flood

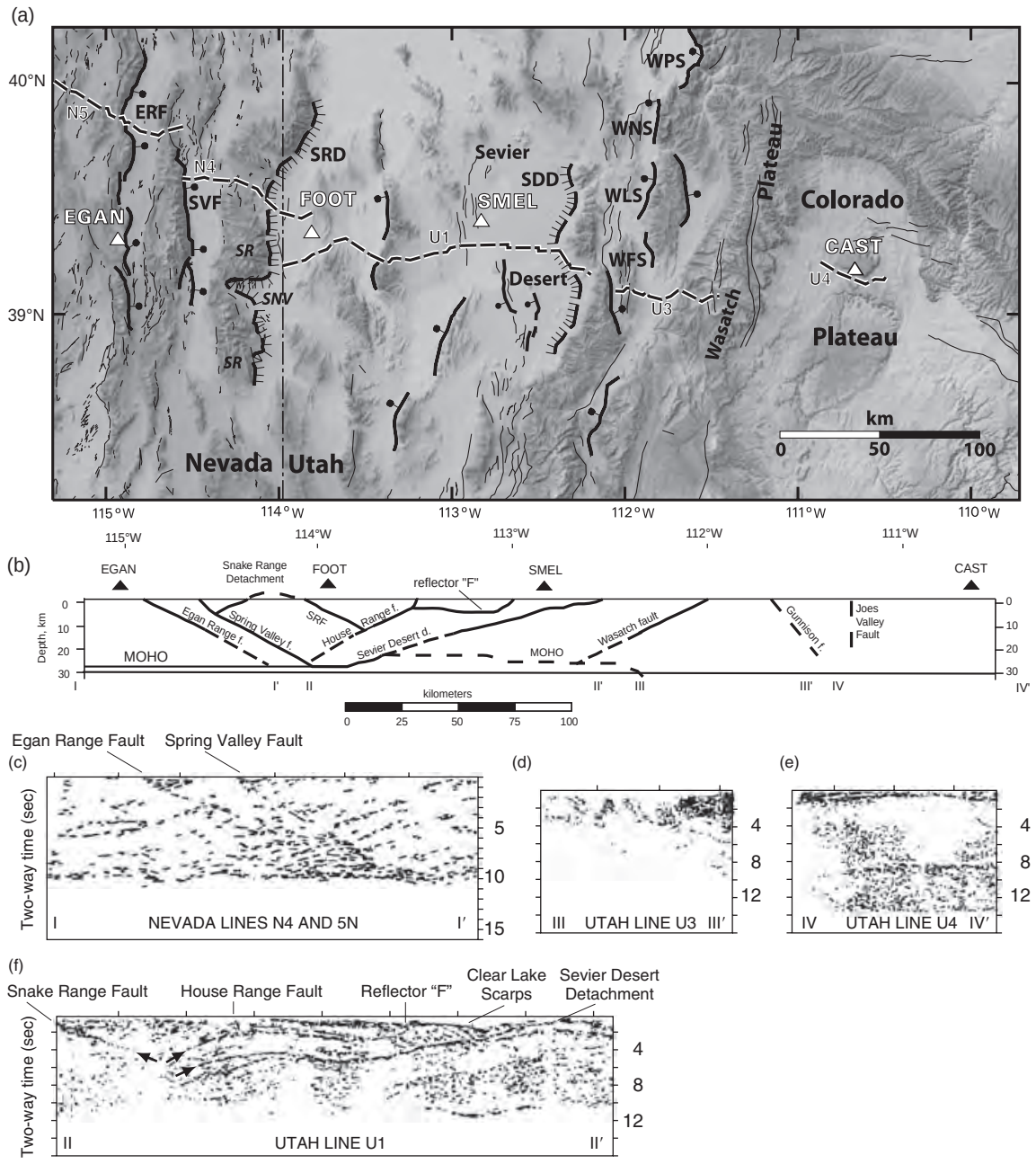

Figure 7.14 *(a) Shaded relief map of a part of the eastern Basin and Range showing range-bounding faults and locations of seismic reflection profiles (black dashed lines) and GPS sites (white triangles) (image provided by N. Niemi and modified from Niemi* et al.*, 2004, with permission from Blackwell Publishing). High-angle faults show ball and bar symbol in the hanging wall, low-angle faults show hachured pattern. Faults mentioned in the text include the Egan Range Fault (ERF), the Spring Valley Fault (SVF), the Sevier Desert Detachment (SDD), the Wasatch Fault Zone (WFS, WLS, WNS, WPS), and the Snake Range Detachment (SRD). Cross-section (b) constructed using seismic reflection data from (c) Hauser* et al.*, 1987 and (d) Allmendinger* et al.*, 1983 (with permission from the Geological Society of America). (e,f) Allmendinger* et al.*, 1986 (redrawn from Allmendinger* et al.*, 1986, by permission of the American Geophysical Union. Copyright © 1986 American Geophysical Union). SR, Snake Range Metamorphic Core Complex.*

basalts. These eruptions represent one major subcategory of a broad group of rocks known as *Large Igneous Provinces* (LIPs).

Large Igneous Provinces are massive crustal emplacements of mostly mafic extrusive and intrusive rock that originated from processes different from normal sea floor spreading. LIPs may cover areas of up to several million km^2 and occur in a wide range of settings. Within oceanic plates, LIPs form oceanic plateaux such as Kerguelen and Ontong Java (Fig. 7.15). This latter example occupies an area two-thirds that of Australia. The Siberian and Columbia River basalts are examples that have erupted in the interior of continental plates. In East Africa, the Ethiopian and Kenyan flood basalts are associated with active continental rifting and the Deccan Traps in India and the Karoo basalts in southern Africa were emplaced near rifted continental margins. This diversity indicates that not all LIPs are associated with zones of extension. Within rifts their eruption can occur synchronously with rifting or million of years prior to or after the onset of extension (Menzies *et al.*, 2002).

Estimation of the total volumes of lava in LIPs is complicated by erosion, dismemberment by sea floor spreading, and other tectonic processes that postdate their eruption. The Hawaiian Islands are well studied in this respect. Seismic data have shown that beneath the crust is a zone of rocks with a particularly high seismic velocity, which is probably derived from the same mantle source as the surface volcanic rocks. For Hawaii a basic relationship exists between velocity structure and the total volume of igneous rock (Coffin & Eldholm, 1994). This relationship has been applied to other LIPs to determine their volumes. For example, the Columbia River basalts are composed of 1.3 million km^3, whereas the Ontong Java Plateau is composed of at least 27 million km^3 of volcanic rock and possibly twice this amount (Section 5.5). These values are much higher than the continental flood basalts of East Africa. In Kenya the total volume of flood basalts has been

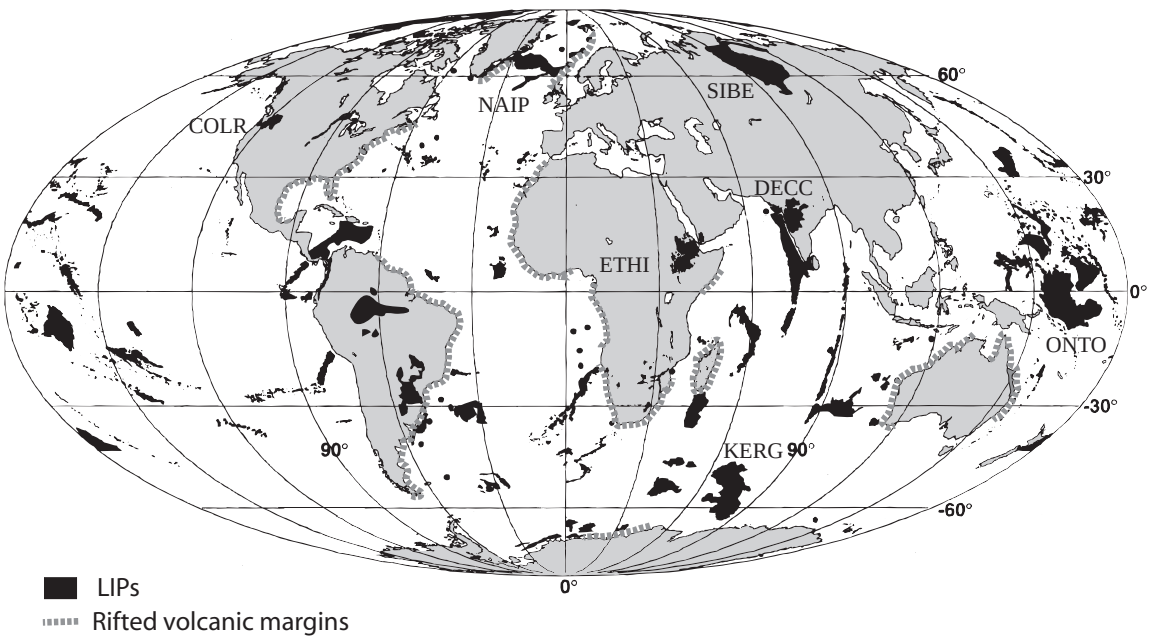

Figure 7.15 *Map showing global distribution of Large Igneous Provinces (modified from Coffin & Edholm, 1994, by permission of the American Geophysical Union. Copyright © 1994 American Geophysical Union). Rifted volcanic margins are from Menzies* et al. *(2002). Labeled LIPs: Ethiopian flood basalts (ETHI); Deccan traps (DECC); Siberian basalts (SIBE); Kerguelen plateau (KERG); Columbia River basalts (COLR); Ontong Java (ONTO); North Atlantic igneous province (NAIP).*

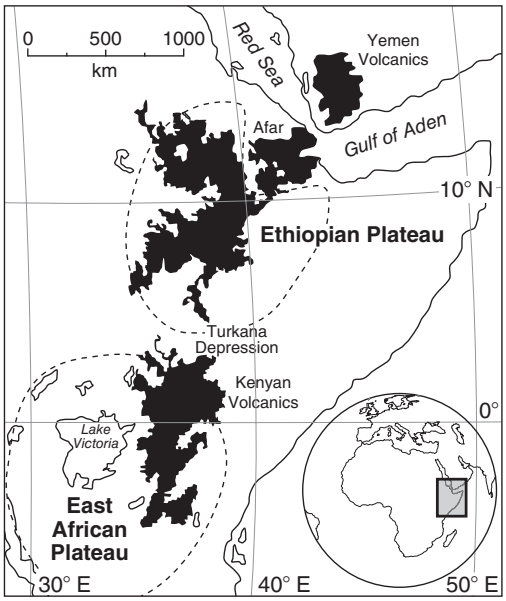

Figure 7.16 *Map showing the location of Cenozoic flood basalts of the Ethiopian Plateau and East African Plateau (Kenya Dome) (after Macdonald* et al.*, 2001, by permission of Oxford University Press).*

estimated at approximately 924,000 km^3 (Latin *et al.*, 1993). In Ethiopia (Fig. 7.16), layers of basaltic and felsic rock reach thickness of >2 km with a total volume estimated at 350,000 km^3 (Mohr & Zanettin, 1988). The eruption of such large volumes of mafic magma has severe environmental consequences, such as the formation of greenhouse gases, the generation of acid rain, and changes in sea level (Coffin & Eldholm, 1994; Ernst *et al.*, 2005). The eruptions also make significant contributions to crustal growth.

Some LIPs appear to form very quickly. For many continental flood volcanics, 70–80% of the basaltic rock erupted in less than 3 million years (Menzies *et al.*, 2002). Geochronologic studies have shown that the main flood event in Greenland (Tegner *et al.*, 1998), the Deccan Traps (Hofmann *et al.*, 2000), and the bulk of the Ethiopian Traps (Hofmann *et al.*, 1997) all erupted in less than one million years. Nevertheless, this latter example (Section 7.2) also shows that pulses of volcanism between 45 and 22 Ma contributed to the formation of the flood basalts in the Afar region. Submarine plateaux probably formed at similar rates, although less information is available from these types of LIPs. The North Atlantic Province and Ontong Java Plateau formed in less than 3 Ma and the Kerguelen Plateau in 4.5 Ma. Most of the volcanic activity occurred in short, violent episodes separated by long periods of relative quiescence. Estimates of the average rates of formation, which include the periods of quiescence, are 12–18 km^3 a^{-1} for the Ontong Java Plateau and 2–8 km^3 a^{-1} for the Deccan Traps. Ontong Java's rate of emplacement may have exceeded the contemporaneous global production rate of the entire mid-ocean ridge system (Coffin & Eldholm, 1994).

The outpouring of large volumes of mafic magma in such short periods of time requires a mantle source. This characteristic has encouraged interpretations involving deep mantle plumes (Sections 5.5, 12.10), although the existence and importance of these features are debated widely (Anderson & Natland, 2005). Mantle plumes may form large oceanic plateaux and some continental flood basalts also may be attributed to them. Beneath the Ethiopian Plateau and the Kenya Dome (in the East African Plateau), extensive volcanism and topographic uplift appear to be the consequences of anomalously hot asthenosphere (Venkataraman *et al.*, 2004). The isotopic characteristics of the volcanic rock and the large volume of mafic lava erupted over a short period of time (Hofmann *et al.*, 1997; Ebinger & Sleep, 1998) suggest that a plume or plumes below the uplifts tap deep undegassed mantle sources (Marty *et al.*, 1996; Furman *et al.*, 2004). As the deep plumes ascend they undergo decompression melting with the amount of melt depending on the ambient pressure (Section 7.4.2). Consequently, less melting is expected under thick continental lithosphere than under thick oceanic lithosphere. Nevertheless, the sources of magma that generated many LIPs are not well understood and it is likely that no single model explains them all. Ernst *et al.* (2005) review the many aspects of LIP research and models of their formation, including links to ore deposits (Section 13.2.2).

7.4.2 Petrogenesis of rift rocks

The geochemistry of mafic volcanic rocks extruded at continental rifts provides information on the sources and mechanisms of magma generation during rifting. Rift basalts typically are enriched in the alkalis (Na_2O, K_2O, CaO), large ion lithophile elements (LILE) such as K, Ba, Rb, Sr, Pb^{2+} and the light rare earths, and volatiles, in particular CO_2 and the halogens. Tholeiitic

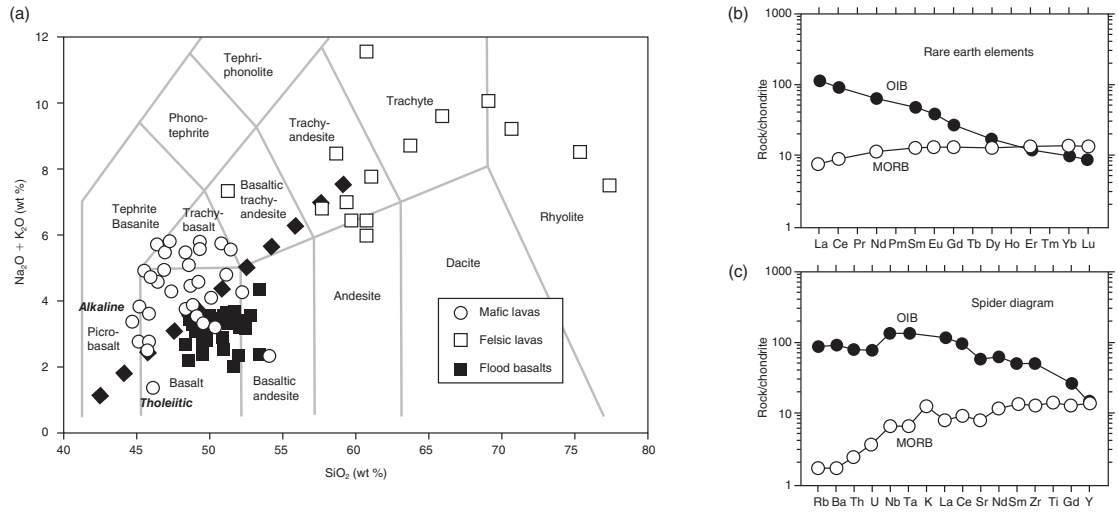

Figure 7.17 *(a) Total alkali-silica diagram showing the geochemical characteristics of lavas from Ethiopia (after Kieffer* et al.*, 2004, by permission of Oxford University Press). Dashed line separates alkaline from tholeiitic basalts. Rare earth element (b) and spider diagram (c) showing a typical alkaline oceanic island basalt (OIB) and a typical tholeiitic mid-ocean ridge basalt (MORB) (from Winter, John D.,* An Introduction to Igneous and Metamorphic Petrology*, 1st edition © 2001, p. 195. Reprinted by permission of Pearson Education, Inc., Upper Saddle River, NJ).*

flood basalts also are common and may be associated with silicic lavas, including rhyolite. Observations in East Africa indicate that a continuum of mafic rocks generally occurs, including alkaline, ultra-alkaline, tholeiitic, felsic, and transitional compositions (Fig. 7.17a). This diversity reflects both the compositional heterogeneity of mantle source regions and processes that affect the genesis and evolution of mafic magma.

There are three ways in which the mantle may melt to produce basaltic liquids beneath rifts. First, melting may be accomplished by heating the mantle above the normal geotherm (Fig. 7.18a). Perturbations in the geotherm could be related to the vertical transfer of heat by deep mantle plumes. It is probable, for example, that the volcanism and topographic uplift associated with the Ethiopian and East African plateaux reflect anomalously hot mantle. Investigations of P_n wave attenuation beneath the Eastern branch of the East African Rift suggest sublithospheric temperatures that are significantly higher than those in the ambient mantle (Venkataraman *et al.*, 2004). A second mechanism for melting the mantle is to lower the ambient pressure (Fig. 7.18b). The ascent of hot mantle during lithospheric stretching (Section 7.6.2) or the rise of a mantle plume causes a reduction in pressure that leads to decompression melting at a variety of depths, with the degree of melting depending on the rate of ascent, the geotherm, the composition of the mantle, and the availability of fluids. A third mechanism of melting involves the addition of volatiles, which has the effect of lowering the solidus temperature. All three of these mechanisms probably contribute to generation of basaltic melts beneath continental rifts.

Once formed, the composition of mafic magmas may be affected by *partial melting*. This process results in the separation of a liquid from a solid residue, which can produce a variety of melt compositions from a single mantle source. Primary mafic melts also tend to *fractionate*, whereby crystals are physically removed from melts over a wide range of crustal pressures, resulting in suites of compositionally distinctive rocks. Current models generally favor fractional crystallization of basaltic melts in shallow magma chambers as the dominant process that generates rhyolite.

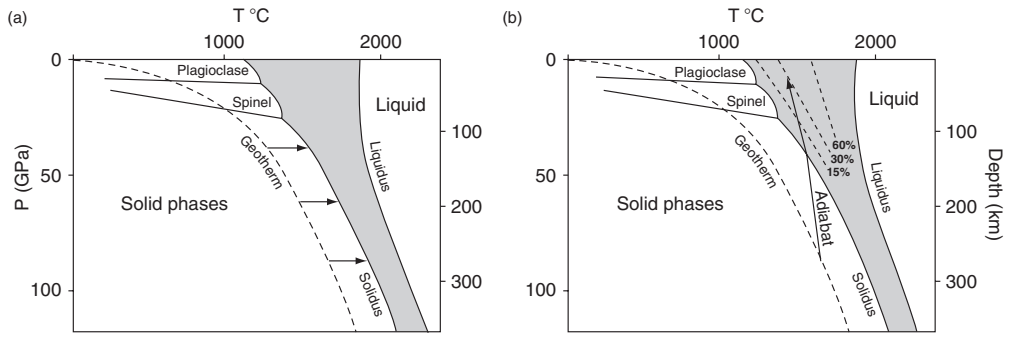

Figure 7.18 *(a) Melting by raising temperature. (b) Melting by decreasing pressure (from Winter, John D.,* An Introduction to Igneous and Metamorphic Petrology*, 1st edition © 2001, p. 195. Reprinted by permission of Pearson Education, Inc., Upper Saddle River, NJ). In (b) melting occurs when the adiabat enters the shaded melting zone. Percentages of melting are shown.*

Compositional variability also reflects the *assimilation* of crustal components and *magma mixing*. The bimodal basalt-rhyolite eruptions are thought to reflect combinations of mantle and silica-rich crustal melts.

A comparison of trace element concentrations and isotopic characteristics indicates that basalts generated in continental rifts are broadly similar to those of oceanic islands (Section 5.5). Both rock types preserve evidence of a mantle source enriched in incompatible trace elements, including the LILE, and show relatively high radiogenic strontium ($^{87}Sr/^{86}Sr$) and low neodymium ($^{143}Nd/^{144}Nd$) ratios. These patterns are quite different to those displayed by mid-ocean ridge basalts, which are depleted in incompatible trace elements (Fig. 7.17b,c) and display low strontium and high neodymium ratios. Trace elements are considered *incompatible* if they are concentrated into melts relative to solid phases. Since it is not possible to explain these differences in terms of the conditions of magma genesis and evolution, the mantle from which these magmas are derived must be heterogeneous. In general, the asthenosphere is recognized as depleted in incompatible elements, but opinions diverge over whether the enriched sources originate above or below the asthenosphere. Undepleted mantle plumes offer one plausible source of enriched mantle material. Enrichment also may result from the trapping of primitive undepleted asthenosphere at the base of the lithosphere or the diffusion of LILE-rich volatiles from the asthenosphere or deeper mantle into the lithosphere.

On the basis of trace element concentrations and isotopic characteristics, Macdonald *et al.* (2001) inferred that mafic magmas in the Eastern branch of the East African Rift system were derived from at least two mantle sources, one of sublithospheric origin similar to that which produces ocean island basalts and one within the subcontinental lithosphere. Contributions from the subcontinental mantle are indicated by xenoliths of lithospheric mantle preserved in lavas, distinctive rare earth element patterns, and by the mineralogy of basaltic rock. In southern Kenya, the presence of amphibole in some mafic lavas implies a magma source in the subcontinental lithosphere rather than the asthenosphere (le Roex *et al.*, 2001; Späth *et al.*, 2001). This conclusion is illustrated in Fig. 7.19 where the experimentally determined stability field of amphibole is shown together with a probable continental geotherm and adiabats corresponding to normal asthenospheric mantle and a 200°C hotter mantle plume. It is only in the comparatively cool lithospheric mantle that typical hydrous amphibole can exist. The additional requirement of garnet in the source, which is indicated by distinctive rare earth element patterns, constrains the depth of melting to 75–90 km. These and other studies show that the generation of lithospheric melts is common in rifts, especially during their early stages of development. They also indicate that the identification of melts derived from the subcontinental lithosphere provides a potentially useful tool for assessing changes in lithospheric thickness during rifting.

In addition to compositional variations related to source regions, many authors have inferred systematic relationships between basalt composition and the depth and amount of melting in the mantle beneath rifts

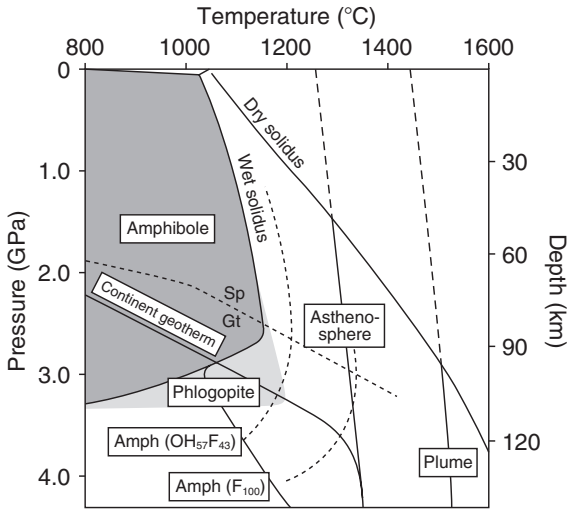

Figure 7.19 *Pressure–temperature diagram showing the stability field of amphibole (after le Roex* et al.*, 2001, Fig. 10. Copyright © 2001, with kind permission of Springer Science and Business Media). Amphibole is stable in the subcontinental mantle but not under conditions characteristic of the asthenospheric mantle or a mantle plume. Gt, garnet; Sp, spinel.*

(Macdonald *et al.*, 2001; Späth *et al.*, 2001). Tholeiitic basalts originate from relatively large amounts of melting at shallow mantle depths of 50 km or less. Transitional basalts are produced by less melting at intermediate depths and highly alkaline magmas originate at even greater depths (100–200 km) by relatively small amounts of melting. These relationships, and the general evolution of mafic magmas toward mid-oceanic ridge compositions as rifting progresses to sea floor spreading, imply a decrease in the depth of melting and a coincident increase in the amount of melting with time. In support of this generalization, tomographic images from East Africa show the presence of small melt fractions in relatively thick mantle lithosphere below juvenile rift segments, such as those in northern Tanzania and Kenya (Green *et al.*, 1991; Birt *et al.*, 1997). Larger melt fractions occur at shallower depths beneath more mature rift segments, such as those in northern Ethiopia and the Afar Depression (Bastow *et al.*, 2005). However, as discussed below, compositional trends in basaltic lavas erupted at continental rifts may not follow a simple progression, especially prior to lithospheric rupture.

Although there may be broad trends of decreasing alkalinity with time, defining systematic compositional trends in basalts is often difficult to achieve at the local and regional scales. For example, attempts to document a systematic decrease in the degree of lithospheric contamination as rifting progresses have proven elusive. Such a decrease might be expected if, as the lithosphere thins and eventually ruptures, melts from the sublithospheric mantle begin to penetrate the surface without significant interaction with lithosphere-derived melts. However, studies in Kenya and Ethiopia show no systematic temporal or spatial patterns in the degree of lithospheric contamination in rift basalts (Macdonald *et al.*, 2001). This indicates that rift models involving the progressive evolution of alkaline magmas toward more tholeiitic magmas during the transition to sea floor spreading are too simplistic. Instead, the data suggest that the full compositional range of mafic melts can coexist in continental rifts and that magma genesis may involve multiple sources at any stage of the rifting process. Tholeiites, for example, commonly are present during all stages of rifting and can precede the generation of alkaline and transitional basalts.

7.4.3 Mantle upwelling beneath rifts

The three-dimensional velocity structure of the upper mantle beneath rifts can be ascertained using teleseismic travel-time delays and seismic tomography. Davis & Slack (2002) modeled these types of data from beneath the Kenya Dome using two Gaussian surfaces that separate undulating layers of different velocities (Plate 7.2 between pp. 244 and 245). An upper layer (mesh surface) peaks at the Moho beneath the rift valley and has a velocity contrast of −6.8% relative to 8 km s^{-1} mantle. A lower layer (grayscale surface) peaks at about 70 km depth and has a −11.5% contrast extending to a depth of about 170 km. This model, which is in good agreement with the results of seismic refraction studies, shows a domal upper mantle structure with sides that dip away from the center of the Kenya Rift. The authors suggested that this structure results from the separation of upwelling asthenosphere into currents that impinge on the base of the lithosphere and form a low velocity, low density zone of melting between 70 and 170 km depth.

Park & Nyblade (2006) used teleseismic P-wave travel times to image the upper mantle beneath the

Eastern branch of the East African Rift system to depths of 500 km. They found a steep-sided, west-dipping low velocity anomaly that is similar to the one modeled by Davis & Slack (2002) above 160 km depth. Below this depth, the anomaly broadens to the west indicating a westerly dip. Similar structures have been imaged below Tanzania (Ritsema *et al.*, 1998; Weeraratne *et al.*, 2003) and parts of Ethiopia (Benoit *et al.*, 2006). Bastow *et al.* (2005) found that a tabular (75 km wide) low velocity zone below southern Ethiopia broadens at depths of >100 km beneath the more highly extended northern section of the rift (Fig. 7.7c,d). The anomalies are most pronounced at ~150 km depth. These broad, dipping structures are difficult to reconcile with models of a simple plume with a well-defined head and tail. Instead they appear to be more consistent with either multiple plumes or tomographic models (Plate 7.3 between pp. 244 and 245) where the hot asthenosphere connects to a broad zone of anomalously hot mantle beneath southern Africa.

In the deep mantle below South Africa, Ritsema *et al.* (1999) imaged a broad (4000 by 2000 km^2 area) low velocity zone extending upward from the core–mantle boundary and showed that it may have physical links to the low velocity zones in the upper mantle beneath East Africa (Plate 7.3 between pp. 244 and 245). The tilt of the deep velocity anomaly shows that the upwelling is not vertical. Between 670 and 1000–km depth the anomaly weakens, suggesting that it may be obstructed. These observations support the idea that anomalously hot asthenosphere beneath Africa is related in some way to this broad deep zone of upwelling known as the African superswell (Section 12.8.3). Nevertheless, a consensus on the location, depth extent and continuity of hot mantle material below the East African Rift system has yet to be reached (*cf.* Montelli *et al.*, 2004a).

A comparison of the mantle structure beneath rifts in different settings indicates that the size and strength of mantle upwellings are highly variable. Achauer & Masson (2002) showed that in relatively cool rifts, such as the Baikal Rift and the southern Rhine Graben, low velocity zones are only weakly negative (−2.5% relative to normal mantle P-wave velocities) and occur mostly above depths of 160 km. In these relatively cool settings, the low velocity zones in the uppermost mantle show no continuation to deeper levels (>160 km) and no broadening of an upwelling asthenosphere with depth below the rift. In still other settings, such as the Rio Grande rift, low velocity zones in the upper mantle may form parts of small-scale convection cells where upwelling occurs beneath the rift and downwelling beneath its margins (Gao *et al.*, 2004).

7.5 RIFT INITIATION

Continental rifting requires the existence of a horizontal deviatoric tensional stress that is sufficient to break the lithosphere. The deviatoric tension may be caused by stresses arising from a combination of sources, including: (i) plate motions; (ii) thermal buoyancy forces due to asthenospheric upwellings; (iii) tractions at the base of the lithosphere produced by convecting asthenosphere; and/or (iv) buoyancy (gravitational) forces created by variations in crustal thickness (Huismans *et al.*, 2001). These stresses may be inherited from a previous tectonic regime or they may develop during extension. Full rupture of the lithosphere leading to the formation of a new ocean basin only occurs if the available stresses exceed the strength of the entire lithosphere. For this reason lithospheric strength is one of the most important parameters that governs the formation and evolution of continental rifts and rifted margins.

The horizontal force required to rupture the entire lithosphere can be estimated by integrating yield stress with respect to depth. The integrated yield stress, or lithospheric strength, is highly sensitive to the geothermal gradient as well as to crustal composition and crustal thickness (Section 2.10.4). A consideration of these factors suggests that a force of 3×10^{13} N m^{-1} may be required to rupture lithosphere with a typical heat flow value of 50 mW m^{-2} (Buck *et al.*, 1999). In areas where lithosphere exhibits twice the heat flow, such as in the Basin and Range Province, it may take less than 10^{12} N m^{-1} (Kusznir & Park, 1987; Buck *et al.*, 1999). Several authors have estimated that the tectonic forces available for rifting are in the range $3–5 \times 10^{12}$ N m^{-1} (Forsyth & Uyeda, 1975; Solomon *et al.*, 1975). If correct, then only initially thin lithosphere or lithosphere with heat flow values greater than 65–70 mW m^{-2} is expected to undergo significant extension in the absence of any other weakening mechanism (Kusznir & Park, 1987). Elsewhere, magmatic intrusion or the addition of water may be required to sufficiently weaken the lithosphere to allow rifting to occur.

Another important factor that controls whether rifting occurs, is the mechanism that is available to

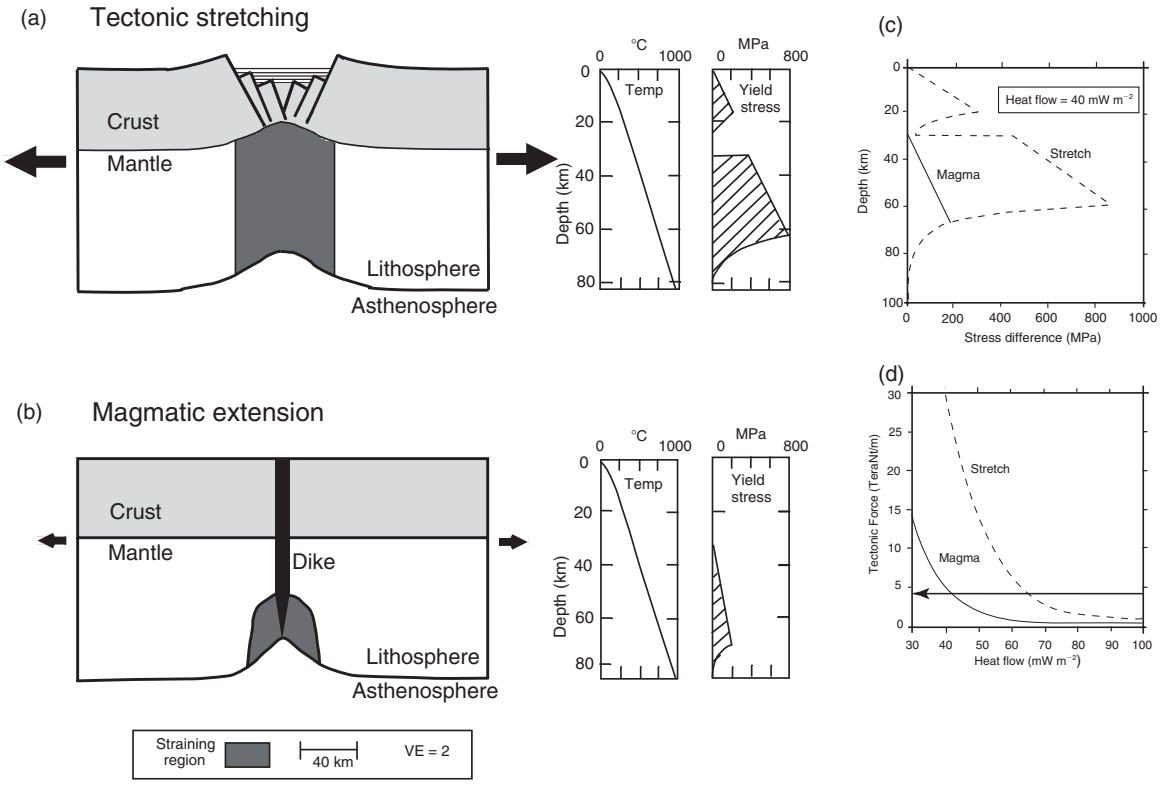

Figure 7.20 *Sketches showing the difference between extension of thick lithosphere without (a) and with (b) magmatic intrusion by diking. Temperature and yield stress curves for each case are show to the right of the sketches. VE, vertical exaggeration. (c) Example of yield stresses for strain rate $10^{-14}\,s^{-1}$ for 30-km-thick crust. Solid line, stress difference for magmatic rifting; dashed line, stress difference for lithospheric stretching. (d) Tectonic force for rifting with and without magma as a function of heat flow. The bold black line in (d) shows the estimated value of driving forces (from Buck, 2004. Copyright © 2004 from Columbia University Press. Reprinted with permission of the publisher).*

accommodate the extension. At any depth, deviatoric tension can cause yielding by faulting, ductile flow, or dike intrusion, depending on which of these processes requires the least amount of stress. For example, if a magma source is available, then the intrusion of basalt in the form of vertical dikes could permit the lithosphere to separate at much lower stress levels than is possible without the diking. This effect occurs because the yield stress that is required to allow basaltic dikes to accommodate extension mostly depends on the density difference between the lithosphere and the magma (Buck, 2004). By contrast, the yield stresses required to cause faulting or ductile flow depend upon many other factors that result in yield strengths that can be up to an order of magnitude greater than those required for lithospheric separation by diking (Fig. 7.20). High temperatures (>700°C) at the Moho, such as those that can result from the thermal relaxation of previously thickened continental crust, also may contribute to the tectonic forces required for rift initiation. For high Moho temperatures gravitational forces become increasingly important contributors to the stresses driving rifting.

Finally, the location and distribution of strain at the start of rifting may be influenced by the presence of pre-existing weaknesses in the lithosphere. Contrasts in lithospheric thickness or in the strength and temperature of the lithosphere may localize strain or control the orientations of rifts. This latter effect is illustrated by the change in orientation of the Eastern branch of

the East African Rift system where the rift axis meets the cool, thick lithospheric root of the Archean Tanzanian craton (Section 7.8.1). The Tanzanian example suggests that lateral heterogeneities at the lithosphere–asthenosphere boundary rather than shallow level structures in the crust are required to significantly alter rift geometry (Foster *et al.*, 1997).

7.6 STRAIN LOCALIZATION AND DELOCALIZATION PROCESSES

7.6.1 Introduction

The localization of strain into narrow zones during extension is achieved by processes that lead to a mechanical weakening of the lithosphere. Lithospheric weakening may be accomplished by the elevation of geotherms during lithospheric stretching, heating by intrusions, interactions between the lithosphere and the asthenosphere, and/or by various mechanisms that control the behavior of faults and shear zones during deformation. Working against these *strain softening* mechanisms are processes that promote the mechanical strengthening of the lithosphere. Lithospheric strengthening may be accomplished by the replacement of weak crust by strong upper mantle during crustal thinning and by the crustal thickness variations that result from extension. These and other *strain hardening* mechanisms promote the delocalization of strain during rifting. Competition among these mechanisms, and whether they result in a net weakening or a net strengthening of the lithosphere, controls the evolution of deformation patterns within rifts.

To determine how different combinations of lithospheric weakening and strengthening mechanisms control the response of the lithosphere to extension, geoscientists have developed physical models of rifting using different approaches. One approach, called *kinematic modeling*, involves using information on the geometry, displacements, and type of strain to make predictions about the evolution of rifts and rifted margins. Figures 7.4c, 7.10, and 7.11 illustrate the data types that frequently are used to generate these types of models. Among the most common kinematic examples are the *pure shear* (McKenzie, 1978), the *simple shear* (Wernicke, 1985), and the *crustal delamination* (Lister *et al.*, 1986) models of extension (Fig. 7.21). The predictions from these models are tested with observations of subsidence and uplift histories within rifts and rifted margins, and with information on the displacement patterns recorded by faults and shear zones. This approach has been used successfully to explain differences in the geometry of faulting and the history of extension among some rifts and rifted margins. However, one major limitation of kinematic modeling is that it does not address the underlying causes of these differences. By contrast, *mechanical models* employ information about the net strength of the lithosphere and how it changes during rifting to test how different physical processes affect rift evolution. This latter approach permits inhomogeneous strains and a quantitative evaluation of how changes to lithospheric strength and rheology influence rift behavior. The main physical processes involved in rifting and their effects on the evolution of the lithosphere are discussed in this section.

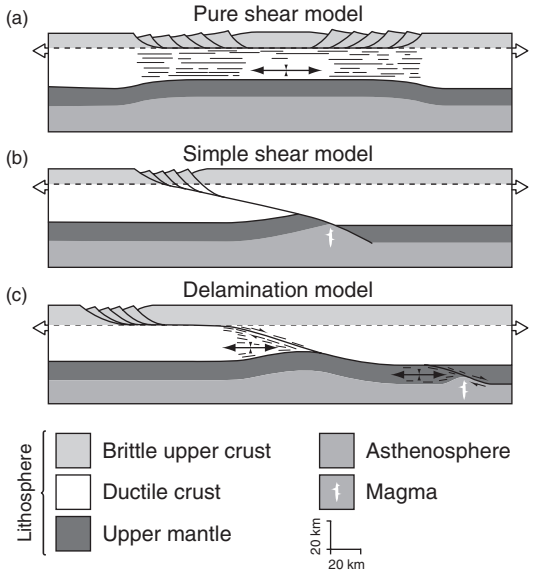

Figure 7.21 *Kinematic models of continental extension (after Lister* et al.*, 1986, with permission from the Geological Society of America).*

7.6.2 Lithospheric stretching

During horizontal extension, lithospheric stretching results in a vertical thinning of the crust and an increase in the geothermal gradient within the zone of thinning (McKenzie, 1978). These two changes in the physical properties of the extending zone affect lithospheric strength in contrasting ways. Crustal thinning or *necking* tends to strengthen the lithosphere because weak crustal material is replaced by strong mantle lithosphere as the latter moves upward in order to conserve mass. The upward movement of the mantle also may result in increased heat flow within the rift. This process, called *heat advection*, results in higher heat flow in the rift because the geotherms become compressed rather than through any addition of heat. The compressed geotherms tend to result in a net weakening of the lithosphere, whose integrated strength is highly sensitive to temperature (Section 2.10). However, the weakening effect of advection is opposed by the diffusion of heat away from the zone of thinning as hot material comes into contact with cooler material. If the rate of heat advection is faster than the rate of thermal diffusion and cooling then isotherms at the base of the crust are compressed, the geotherm beneath the rift valley increases, and the integrated strength of the lithosphere decreases. If thermal diffusion is faster, isotherms and crustal temperatures move toward their pre-rift configuration and lithospheric weakening is inhibited.

England (1983) and Kusznir & Park (1987) showed that the integrated strength of the lithosphere in rifts, and competition between cooling and heat advection mechanisms, is strongly influenced by the rate of extension. Fast strain rates ($10^{-13}\,s^{-1}$ or $10^{-14}\,s^{-1}$) result in larger increases in geothermal gradients than slow rates ($10^{-16}\,s^{-1}$) for the same amount of stretching. This effect suggests that high strain rates tend to localize strain because inefficient cooling keeps the thinning zone weak, allowing deformation to focus into a narrow zone. By contrast, low strain rates tend to delocalize strain because efficient cooling strengthens the lithosphere and causes the deformation to migrate away from the center of the rift into areas that are more easily deformable. The amount of net lithospheric weakening or strengthening that results from any given amount of stretching also depends on the initial strength of the lithosphere and on the total amount of extension. The total amount of thinning during extension usually is described by the stretching factor (β), which is the ratio of the initial and final thickness of the crust (McKenzie, 1978).

The thermal and mechanical effects of lithospheric stretching at different strain rates are illustrated in Fig. 7.22, which shows the results of two numerical experiments conducted by van Wijk & Cloetingh (2002). In these models, the lithosphere is divided into an upper crust, a lower crust, and a mantle lithosphere that have been assigned different rheological properties (Fig. 7.22a). Figures 7.22b–d show the thermal evolution of the lithosphere for uniform extension at a rate of $16\,mm\,a^{-1}$. At this relatively fast rate, heating by thermal advection outpaces thermal diffusion, resulting in increased temperatures below the rift and strain localization in the zone of thinning. As the crust thins, narrow rift basins form and deepen. Changes in stretching factors for the crust (β) and mantle (δ) are shown in Fig. 7.22e,f. The total strength of the lithosphere (Fig. 7.22g), obtained by integrating the stress field over the thickness of the lithosphere, gradually decreases with time due to stretching and the strong temperature dependence of the chosen rheologies. Eventually, at very large strains, the thermal anomaly associated with rifting is expected to dissipate. These and many other models of rift evolution that are based on the principles of lithospheric stretching approximate the subsidence patterns measured in some rifts and at some rifted continental margins (van Wijk & Cloetingh, 2002; Kusznir *et al.*, 2004) (Section 7.7.3).

The experiment shown in Fig. 7.22h–j shows the evolution of rift parameters during lithospheric stretching at the relatively slow rate of $6\,mm\,a^{-1}$. During the first 30 Ma, deformation localizes in the center of the rift where the lithosphere is initially weakened as isotherms and mantle material move upward. However, in contrast with the model shown in Fig. 7.22b–d, temperatures begin to decrease with time due to the efficiency of conductive cooling at slow strain rates. Mantle upwelling in the zone of initial thinning ceases and the lithosphere cools as temperatures on both sides of the central rift increase. At the same time, the locus of thinning shifts to both sides of the first rift basin, which does not thin further as stretching continues. The mantle thinning factor (Fig. 7.22l) illustrates this behavior. During the first 45 Ma, upwelling mantle causes δ to be larger in the central rift than its surroundings. After this time, δ decreases in the central rift as new upwelling zones develop on its sides. The total strength of the lithosphere (Fig. 7.22m) for this low strain rate model shows that the central rift is weakest until about 55 Ma.

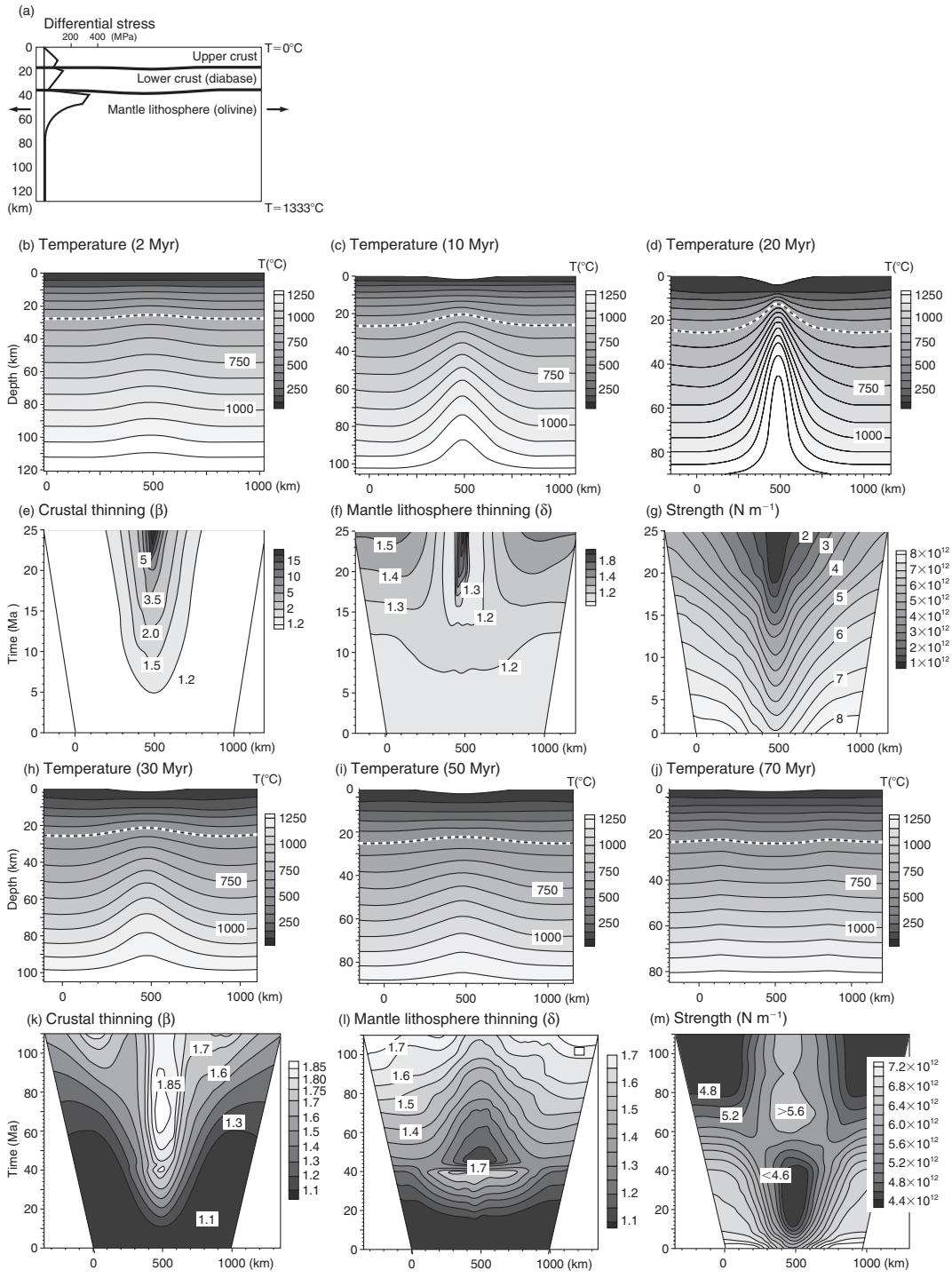

Figure 7.22 *(a) Three-layer lithospheric model where the base of the lithosphere is defined by the 1300°C isotherm at 120 km. Differential stress curves show a strong upper crust and upper mantle and a lower crust that weakens with depth. Thermal evolution of the lithosphere (b–d) during stretching for a horizontal extensional velocity of 16 mm a^{-1}. Evolution of lithospheric strength (g) and of thinning factors for the crust (e) and mantle (f) for a velocity of 16 mm a^{-1}. Thermal evolution of the lithosphere (h–j) during stretching for a velocity of 6 mm a^{-1}. Evolution of lithospheric strength (m) and of thinning factors for the crust (k) and mantle (l) for a velocity of 6 mm a^{-1} (image provided by J. van Wijk and modified from van Wijk & Cloetingh, 2002, with permission from Elsevier).*

After this time the weakest areas are found on both sides of the central rift basin. This model shows how the strong dependence of lithospheric strength on temperature causes strain delocalization and the formation of wide rifts composed of multiple rift basins at slow strain rates. The model predicts that continental break-up will not occur for sufficiently slow rift velocities.

7.6.3 Buoyancy forces and lower crustal flow

In addition to crustal thinning and the compression of geotherms (Section 7.6.2), lithospheric stretching results in two types of buoyancy forces that influence strain localization during rifting. First, lateral variations in temperature, and therefore density, between areas inside and outside the rift create a *thermal buoyancy* force that adds to those promoting horizontal extension (Fig. 7.23). This positive reinforcement tends to enhance those aspects of lithospheric stretching (Section 7.6.2) that promote the localization of strain. Second, a *crustal buoyancy* force is generated by local (Airy) isostatic effects as the crust thins and high density material is brought to shallow levels beneath the rift (Fleitout & Froidevaux, 1982). Because the crust is less dense than the underlying mantle, crustal thinning lowers surface elevations in the center of the rift (Fig. 7.23). This subsidence places the rift into compression, which opposes the forces driving extension. The opposing force makes it more difficult to continue deforming in the same locality, resulting in a delocalization of strain as the deformation migrates into areas that are more easily deformable (Buck, 1991).

Several processes may either reduce or enhance the effects of crustal buoyancy forces during lithospheric stretching. Buck (1991) and Hopper & Buck (1996) showed that where the crust is initially thin and cool, and the mantle lithosphere is relatively thick, the overall strength (the effective viscosity) of the lithosphere remains relatively high under conditions of constant strain rate (Fig. 7.24a). In this case, the effects of crustal buoyancy forces are reduced and the thermal effects of lithospheric necking are enhanced. Narrow rifts result because the changes in yield strength and thermal buoyancy forces that accompany lithospheric stretching dominate the force balance, causing extensional strains to remain localized in the region of necking. By contrast, where the crust is initially thick and hot, and the mantle lithosphere is relatively thin, the overall strength of the lithosphere remains relatively low. In this case, crustal buoyancy forces dominate because the amount of possible weakening due to lithospheric necking is relatively small, resulting in strain delocalization and the formation of wide zones of rifting (Fig. 7.24b) as the necking region migrates to areas that require less force to deform. These models illustrate how crustal thickness and the thermal state of the lithosphere at the start of rifting greatly influence the style of extension.

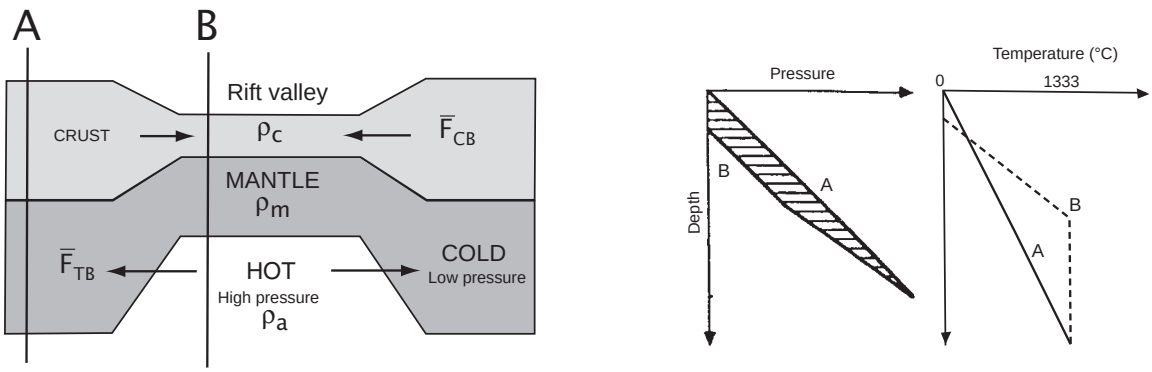

Figure 7.23 *Schematic diagram illustrating thermal and crustal buoyancy forces generated during rifting. A and B represent vertical profiles outside and inside the rift valley, respectively. Pressure and temperature as a function of depth for each profile are shown to the right of sketch (modified from Buck, 1991,by permission of the American Geophysical Union. Copyright © 1991 American Geophysical Union). Differences in profiles generate lateral buoyancy forces.*

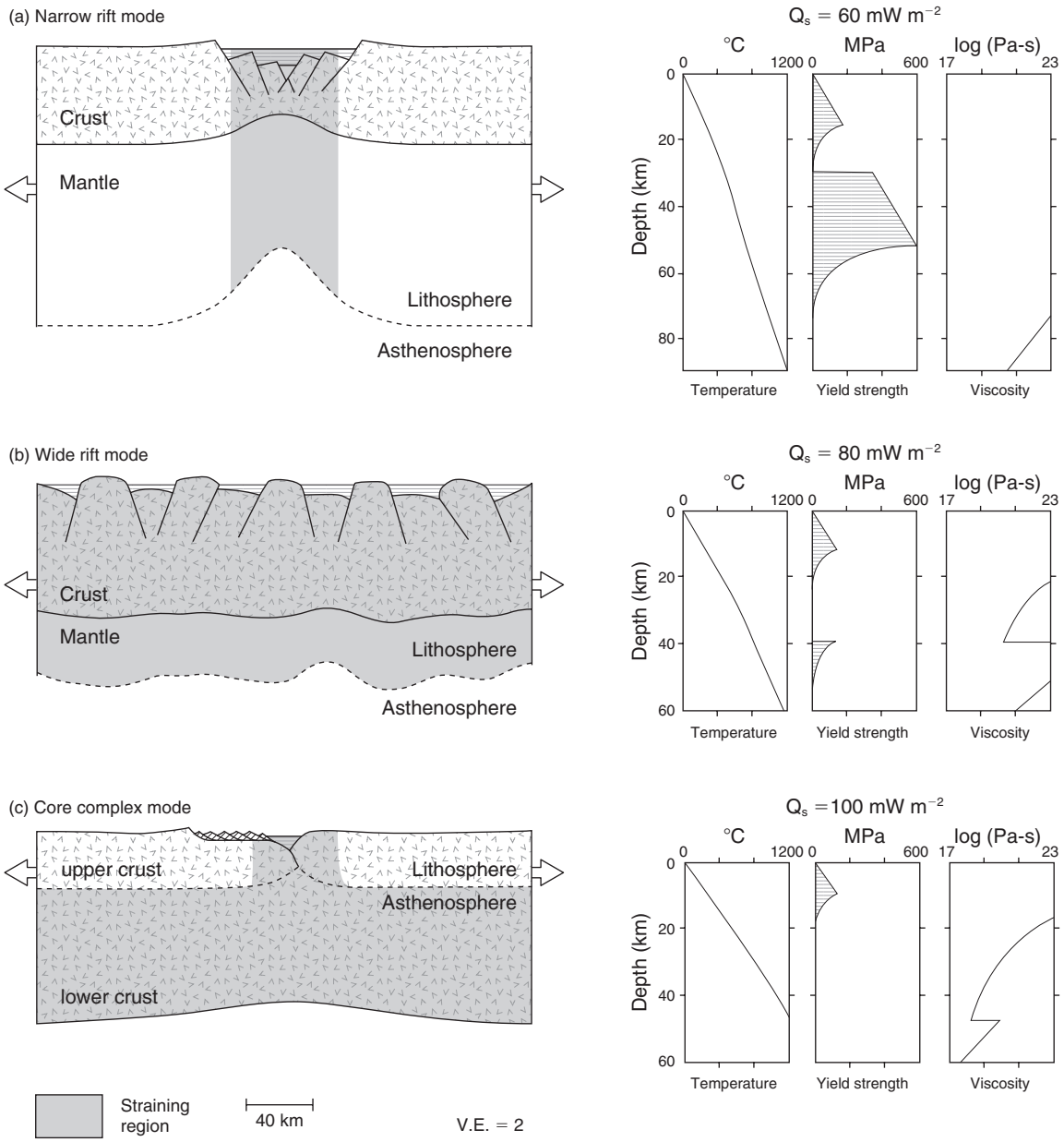

Figure 7.24 *Sketches of the lithosphere illustrating three modes of extension emphasizing the regions undergoing the greatest amount of extensional strain (modified from Buck, 1991, by permission of the American Geophysical Union. Copyright © 1991 American Geophysical Union). (a) Narrow mode, (b) wide mode, (c) core complex mode. Lithosphere is defined as areas with effective viscosities of $>10^{21}$ Pa s^{-1}. The plots to the right of each sketch show initial model geotherms, yield strengths (for a strain rate of 8×10^{-15} s^{-1}) and effective viscosities for a dry quartz crust overlying a dry olivine mantle. From top to bottom the crustal thicknesses are 30 km, 40 km, and 50 km. Q_s initial surface heat flow. (c) shows layers labeled at two scales: the upper crust and lower crust labels on the left side of diagram show a weak, deforming lower crust (shaded); the lithosphere and asthenosphere labels on the right side of diagram show a scale emphasizing that the zone of crustal thinning (shaded column) is localized into a relatively narrow zone of weak lithosphere.*

Models of continental extension that emphasize crustal buoyancy forces incorporate the effects of ductile flow in the lower crust. Buck (1991) and Hopper & Buck (1996) showed that the pressure difference between areas inside and outside a rift could cause the lower crust to flow into the zone of thinning if the crust is thick and hot. Efficient lateral flow in a thick, hot, and weak lower crust works against crustal buoyancy forces by relieving the stresses that arise from variations in crustal thickness. This effect may explain why the present depth of the Moho in some parts of the Basin and Range Province, and therefore crustal thickness, remains fairly uniform despite the variable amounts of extension observed in the upper crust (Section 7.3). In cases where low yield strengths and flow in the lower crust alleviate the effects of crustal buoyancy, the zone of crustal thinning can remain fixed as high strains build up near the surface. Buck (1991) and Hopper & Buck (1996) defined this latter style of deformation as core complex-mode extension (Fig. 7.24c). Studies of flow patterns in ancient lower crust exposed in metamorphic core complexes (e.g. Klepeis *et al.*, 2007) support this view.

The relative magnitudes of the thermal and crustal buoyancy forces may be affected by two other parameters: strain rate and strain magnitude. Davis & Kusznir (2002) showed that the strain delocalizing effects of the crustal buoyancy force are important at low strain rates, when thermal diffusion is relatively efficient (e.g. Fig. 7.22h–j), and after long (>30 Myr) periods of time. In addition, thermal buoyancy forces may dominate over crustal buoyancy forces immediately after rifting when strain magnitudes are relatively low. This latter effect occurs because variations in crustal thicknesses are relatively small at low stretching (β) factors. This study, and the work of Buck (1991) and Hopper & Buck (1996), suggests that shifts in the mode of extension are expected as continental rifts evolve through time and the balance of thermal and crustal forces within the lithosphere changes.

7.6.4 Lithospheric flexure

Border faults that bound asymmetric rift basins with uplifted flanks are among the most common features in continental rifts (Fig. 7.25). Some aspects of this characteristic morphology can be explained by the elastic response of the lithosphere to regional loads caused by normal faulting.

Plate flexure (Section 2.11.4) describes how the lithosphere responds to long-term (>10^5 years) geologic loads. By comparing the flexure in the vicinity of

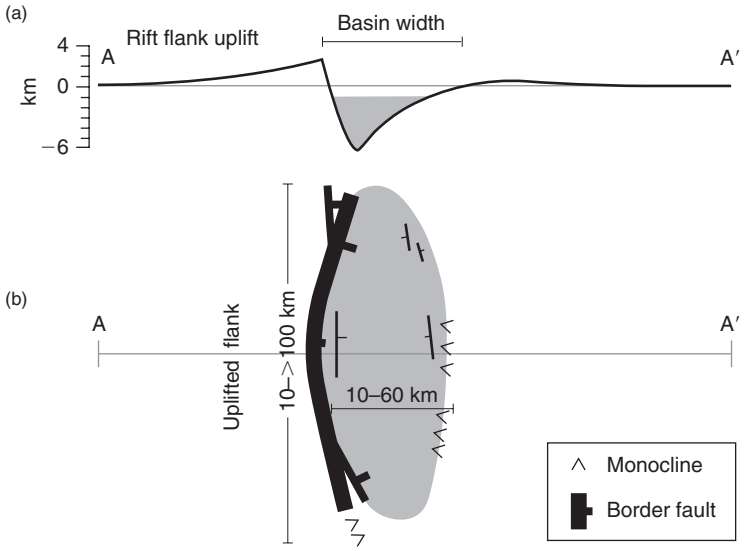

Figure 7.25 *Generalized form of an asymmetric rift basin showing border fault in (a) cross-section and (b) plan view (after Ebinger* et al.*, 1999, with permission from the Royal Society of London). Line of section (A–A′) shown in (b). Shading in (b) shows areas of depression.*

different types of load it has been possible to estimate the effective long-term elastic thickness (T_e) of continental lithosphere (Section 2.12) using forward models of topography and gravity anomaly profiles (Weissel & Karner, 1989; Petit & Ebinger, 2000). The value of T_e in many rifts, such as the Basin and Range, is low (4 km) due to the weakening effects of high geothermal gradients. However, in other rifts, including those in East Africa and in the Baikal Rift, the value of T_e exceeds 30 km in lithosphere that is relatively strong (Ebinger *et al.*, 1999). The physical meaning of T_e, and its relationship to the thickness (T_s) of the seismogenic layer, is the subject of much discussion. Rheological considerations based on data from experimental rock mechanics suggest that T_e reflects the integrated brittle, elastic, and ductile strength of the lithosphere. It, therefore, is expected to differ from the seismogenic layer thickness, which is indicative of the depth to which short term (periods of years) anelastic deformation occurs as unstable frictional sliding (Watts & Burov, 2003). For these reasons, T_e typically is larger than T_s in stable continental cratons and in many continental rifts.

The deflection of the crust by slip on normal faults generates several types of vertical loads. A mechanical unloading of the footwall occurs as crustal material in the overlying hanging wall is displaced downward and the crust is thinned. This process creates a buoyancy force that promotes surface uplift. Loading of the hanging wall may occur as sediment and volcanic material are deposited into the rift basin. These loads combine with those that are generated during lithospheric stretching (Section 7.6.2). Loads promoting surface uplift are generated by increases in the geothermal gradient beneath a rift, which leads to density contrasts. Loads promoting subsidence may be generated by the replacement of thinned crust by dense upper mantle and by conductive cooling of the lithosphere if thermal diffusion outpaces heating.

Weissel & Karner (1989) showed that flexural isostatic compensation (Section 2.11.4) following the mechanical unloading of the lithosphere by normal faulting and crustal thinning leads to uplift of the rift flanks. The width and height of the uplift depend upon the strength of the elastic lithosphere and, to a lesser extent, on the stretching factor (β) and the density of the basin infill. Other factors may moderate the degree and pattern of the uplift, including the effects of erosion, variations in depth of lithospheric necking (van der Beek & Cloetingh, 1992; van der Beek, 1997) and, possibly, small-scale convection in the underlying mantle (Steckler, 1985). Ebinger *et al.* (1999) showed that increases in the both T_e and T_s in several rift basins in East Africa and elsewhere systematically correspond to increases in the length of border faults and rift basin width. As the border faults grow in size, small faults form to accommodate the monoclinal bending of the plate into the depression created by slip on the border fault (Fig. 7.25). The radius of curvature of this bend is a measure of flexural rigidity. Strong plates result in a narrow deformation zone with long, wide basins and long border faults that penetrate deeper into the crust. Weak plates result in a very broad zone of deformation with many short, narrow basins and border faults that do not penetrate very deeply. These studies suggest that the rheology and flexural rigidity of the upper part of the lithosphere control several primary features of rift structure and morphology, especially during the first few million years of rifting. They also suggest that the crust and upper mantle may retain considerable strength in extension (Petit & Ebinger, 2000).

Lithospheric flexure also plays an important role during the formation of large-magnitude normal faults (Section 7.3). Large displacements on both high- and low-angle fault surfaces cause isostatic uplift of the footwall as extension proceeds, resulting in dome-shaped fault surfaces (Buck *et al.*, 1988; Axen & Bartley, 1997; Lavier *et al.*, 1999; Lavier & Manatschal, 2006). Lavier & Manatschal (2006) showed that listric fault surfaces whose dip angle decreases with depth (i.e. concave upward faults) are unable to accommodate displacements large enough (>10 km) to unroof the deep crust. By contrast, low-angle normal faults whose dips increase with depth (i.e. concave downward faults) may unroof the deep crust efficiently and over short periods of time if faulting is accompanied by a thinning of the middle crust and by the formation of serpentinite in the lower crust and upper mantle. The thinning and serpentinization weaken the crust and minimize the force required to bend the lithosphere upward during faulting, allowing large magnitudes of slip.

7.6.5 Strain-induced weakening

Although differences in the effective elastic thickness and flexural strength of the lithosphere (Section 7.6.4) may explain variations in the length of border faults and the width of rift basins, they have been much less

successful at explaining another major source of variability in rifts: the degree of strain localization in faults and shear zones. In some settings normal faulting is widely distributed across large areas where many faults accommodate a relatively small percentage of the total extension (Section 7.3). However, in other areas or at different times, extension may be highly localized on relatively few faults that accommodate a large percentage of the total extension. Two approaches have been used to explain the causes of this variability. The first incorporates the effects of a strain-induced weakening of rocks that occurs during the formation of faults and shear zones. A second approach, discussed in Section 7.6.6, shows how vertical contrasts in the rheology of crustal layers affect the localization and delocalization of strain during extension.

In order for a normal fault to continue to slip as the crust is extended it must remain weaker than the surrounding rock. As discussed in Section 7.6.4, the deflection of the crust by faulting changes the stress field surrounding the fault. Assuming elastic behavior, Forsyth (1992) showed that these changes depend on the dip of the fault, the amount of offset on the fault, and the inherent shear strength or *cohesion* of the faulted material. He argued that the changes in stresses by normal faulting increase the yield strength of the layer and inhibit continued slip on the fault. For example, slip on high-angle faults create surface topography more efficiently than low-angle faults, so more work is required for large amounts of slip on the former than on the latter. These processes cause an old fault to be replaced with a new one, leading to a delocalization of strain. Buck (1993) showed that if the crust is not elastic but can be described with a finite yield stress (elastic-plastic), then the amount of slip on an individual fault for a given cohesion depends on the thickness of the elastic-plastic layer. In this model the viscosity of the elastic-plastic layer is adjusted so that it adheres to the Mohr–Coulomb criterion for brittle deformation (Section 2.10.2). For a brittle layer thickness of >10 km and a reasonably low value of cohesion a fault may slip only a short distance (a maximum of several kilometers) before a new one replaces it. If the brittle layer is very thin, then the offset magnitude can increase because the increase in yield strength resulting from changes in the stress field due to slip is small.

Although layer thickness and its inherent shear strength play an important role in controlling fault patterns, a key process that causes strain localization and may lead to the formation of very large offset (tens of kilometers) faults is a reduction in the cohesion of the faulted material. During extension, cohesion can be reduced by a number of factors, including increased fluid pressure (Sibson, 1990), the formation of fault gouge, frictional heating (Montési & Zuber, 2002), mineral transformations (Bos & Spiers, 2002), and decreases in strain rate (Section 2.10). Lavier *et al.* (2000) used simple two-layer models to show that the formation of a large-offset normal fault depends on two parameters: the thickness of the brittle layer and the rate at which the cohesion of the layer is reduced during faulting (Plate 7.4a,b between pp. 244 and 245). The models include an upper layer of uniform thickness overlying a ductile layer having very little viscosity. In the ductile layer the yield stress is strain-rate- and temperature-dependent following dislocation creep flow laws (Section 2.10.3). In the upper layer brittle deformation is modeled using an elastic-plastic rheology. The results show that where the brittle layer is especially thick (>22 km) extension always leads to multiple normal faults (Plate 7.4c between pp. 244 and 245). In this case the width of the zone of faulting is equivalent to the thickness of the brittle layer. However, for small brittle layer thicknesses (<22 km), the fault pattern depends on how fast cohesion is reduced during deformation (Plate 7.4d,e between pp. 244 and 245). To obtain a single large-offset fault, the rate of weakening must be high enough to overcome the resistance to continued slip on the fault that results from flexural bending.

These studies provide some insight into how layer thickness and the loss of cohesion during faulting control the distribution of strain, its symmetry, and the formation of large-offset faults. However, at the scale of rifts, other processes also impact fault patterns. In ductile shear zones changes in mineral grain size may promote a switch from dislocation creep to grain-size-sensitive diffusion creep (Section 2.10.3), which can reduce the yield strengths of layers in the crust and mantle. In addition, the rate at which a viscous material flows has an important effect on the overall strength of the material. The faster it flows, the larger the stresses that are generated by the flow and the stronger the material becomes. This latter process may counter the effects of cohesion loss during faulting and could result in a net strengthening of the lithosphere by increasing the depth of the brittle–ductile transition (Section 2.10.4). At the scale of the lithosphere, it therefore becomes necessary to examine the interplay among the various weakening mechanisms in both brittle and ductile layers in order to reproduce deformation patterns in rifts.

Huismans & Beaumont (2003, 2007) extended the work of Lavier *et al.* (2000) by investigating the effects of strain-induced weakening in both brittle (frictional-plastic) and ductile (viscous) regimes on deformation patterns in rifts at the scale of the lithosphere and over time periods of millions of years. This study showed that strain softening in the crust and mantle can produce large-offset shear zones and controls the overall symmetry of the deformation. Figure 7.26a shows a simple three-layer lithosphere where brittle deformation is modeled by using a frictional-plastic rheology that, as in most physical experiments, is adjusted so that it adheres to the Mohr–Coulomb failure criterion. Ductile deformation is modeled using a thermally activated power law rheology. During each experiment, ambient conditions control whether the deformation is frictional-plastic (brittle) or viscous (ductile). Viscous flow occurs when the state of stress falls below the frictional-plastic yield point. Variations in the choice of crustal rheology also allow an investigation of cases where the crust is either coupled or decoupled to the mantle lithosphere. Coupled models involve deformation that is totally within the frictional-plastic regime. Decoupled models involve a moderately weak viscous lower crust. Strain-induced weakening is specified by linear changes in the effective angle of internal friction (Section 2.10.2) for frictional-plastic deformation and in the effective viscosity for viscous deformation. The deformation is seeded using a small plastic weak region.

A reference model (Fig. 7.26b,c) shows how a symmetric style of extensional deformation results when strain softening is absent. An early phase of deformation is controlled by two conjugate frictional-plastic shear zones (S1A/B) that are analogous to faults and two forced shear zones in the mantle (T1A/B). During a subsequent phase of deformation, second generation shear zones develop and strain in the mantle occurs as focused pure shear necking beneath the rift axis. Figures 7.26d and e show the results of another model where frictional-plastic (brittle) strain softening occurs and the resulting deformation is asymmetric. An initial stage is very similar to the early stages of the reference model, but at later times strain softening focuses deformation into one of the conjugate faults (S1B). The asymmetry is caused by a positive feedback between increasing strain and the strength reduction that results from a decreased angle of internal friction (Section 2.10.2). Large displacements on the S2A and T1B shear zones cut out a portion of the lower crust (LC) at point C (Fig. 7.26, insert) and begin to exhume the lower plate. By 40 Ma, a symmetric necking of the lower lithosphere and continued motion on the asymmetric shear zones results in the vertical transport of point P until mantle lithosphere is exposed. The model shown in Fig.7.26f and g combines both frictional-plastic and viscous weakening mechanisms. The early evolution is similar to that shown in Fig. 7.26d, except that S1B continues into the ductile mantle. The two softening mechanisms combine to make deformation asymmetric at all levels of the lithosphere where displacements are mostly focused onto one shear zone. These models show how a softening of the dominant rheology in either frictional-plastic or viscous layers influences deformation patterns in rifts through a positive feedback between weakening and increased strain.

The effect of strain-dependent weakening on fault asymmetry also is highly sensitive to rift velocity. This sensitivity is illustrated in the models shown in Fig. 7.27. The first model (Fig. 7.27a) is identical to that shown in Fig. 7.26d and e except that the velocity is decreased by a factor of five to $0.6\,\mathrm{mm\,a^{-1}}$. Reducing the velocity has the effect of maintaining the thickness of the frictional-plastic layer, which results in deformation that is more strongly controlled by the frictional regime than that shown in Fig. 7.26e. The overall geometry matches a lithospheric-scale simple shear model (cf. Fig. 7.21b) in which the lower plate has been progressively uplifted and exhumed beneath a through-going ductile shear zone that remains the single major weakness during rifting. By contrast, a velocity that is increased to $100\,\mathrm{mm\,a^{-1}}$ (Fig. 7.27b) results in deformation that is more strongly controlled by viscous flow at the base of the frictional layer than that in the model involving slow velocities. However, at high velocities the strain softening does not develop in part because of the high viscous stresses that result from high strain rates. The model shows no strong preference for strain localization on one of the frictional fault zones. The deformation remains symmetrical as the ductile mantle undergoes narrow pure shear necking. These results suggest that increasing or decreasing rift velocities can either promote or inhibit the formation of large asymmetric structures because varying the rate changes the dominant rheology of the deforming layers.

These experiments illustrate the sensitivity of deformation patterns to strain-induced weakening mechanisms during faulting and ductile flow. The results suggest that extension is most likely to be asymmetric in models that include frictional-plastic fault zone weakening mechanisms, a relatively strong lower crust, and slow rifting velocities. However, before attempting to

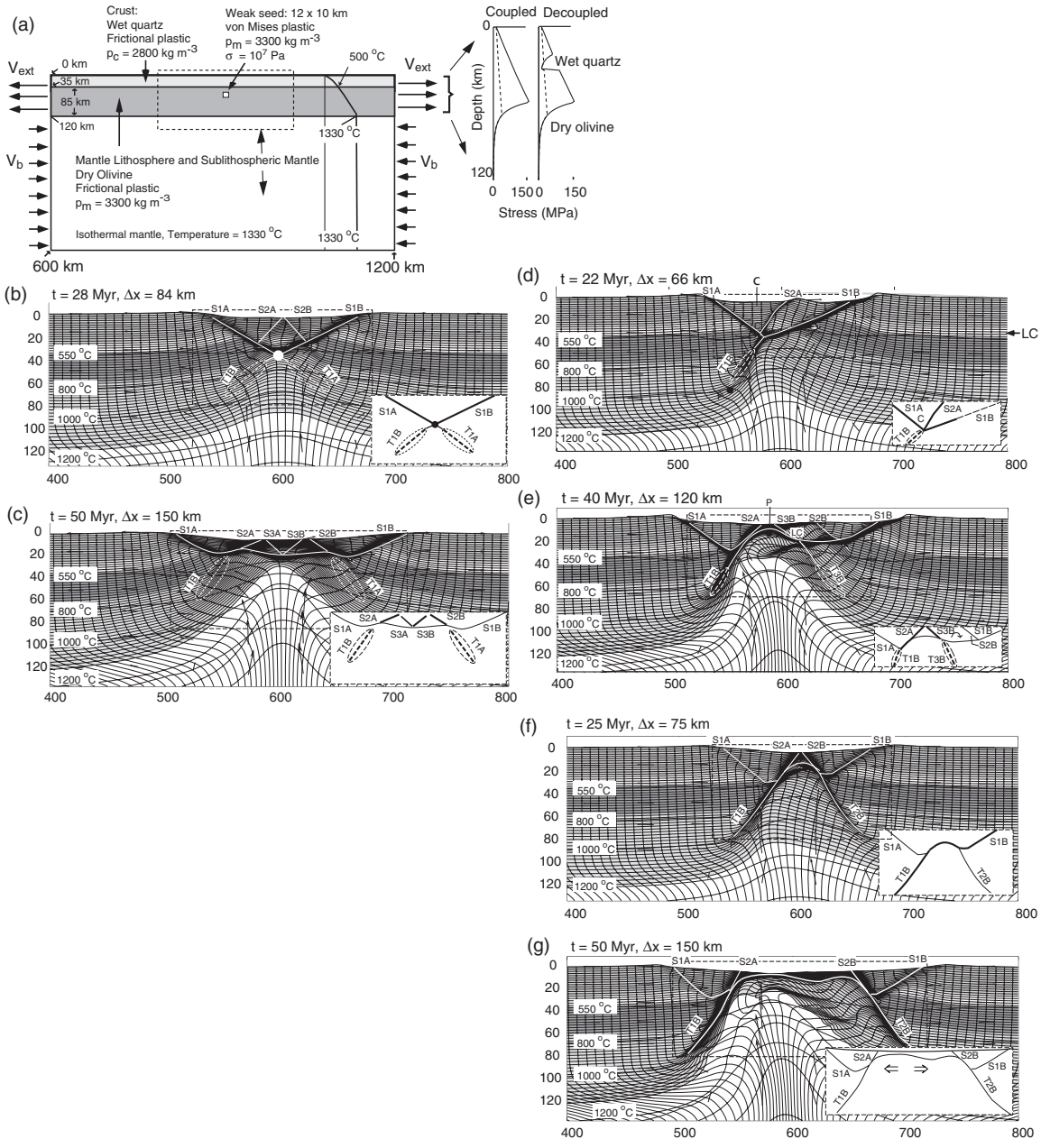

Figure 7.26 *(a) Model geometry showing temperature structure of the crust, mantle lithosphere and sublithospheric mantle (images provided by R. Huismans and modified from Huismans & Beaumont, 2003, by permission of the American Geophysical Union. Copyright © 2003 American Geophysical Union). Initial (solid lines) and strain softened (dashed lines) strength envelopes are shown for an imposed horizontal extensional velocity of $V_{ext} = 3\,mm\,a^{-1}$, with V_b chosen to achieve mass balance. Decoupling between crust and mantle is modeled using a wet quartzite rheology for the lower crust. (b,c) Reference model of extension when strain softening is absent. Models of extension involving (d,e) frictional-plastic (brittle) strain softening and (f,g) both frictional-plastic and viscous weakening mechanisms. Models in (b–g) show a subdivision of the crust and mantle into an upper and lower crust, strong frictional upper mantle lithosphere, ductile lower lithosphere, and ductile sublithospheric mantle. Scaling of quartz viscosity makes the three upper layers frictional-plastic in all models shown. t, time elapsed in millions of years; Δx, amount of horizontal extension. Vertical and horizontal scales are in kilometers. $V_{ext} = 3\,mm\,a^{-1}$ for every model.*

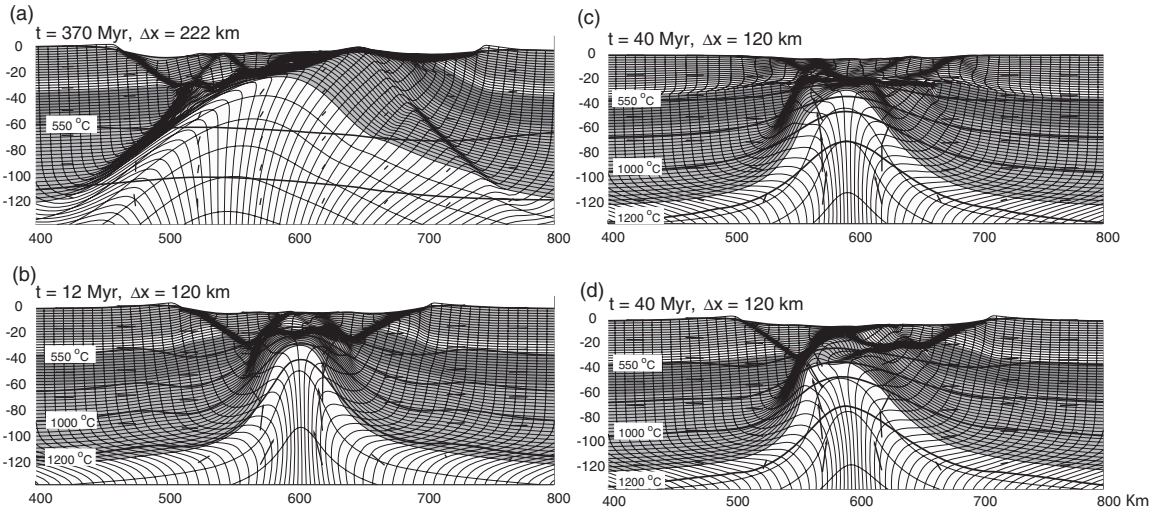

Figure 7.27 *Models of extension involving frictional-plastic (brittle) strain softening at (a) low extensional velocities ($V_{ext} = 0.6\,mm\,a^{-1}$) and (b) high extensional velocities ($V_{ext} = 100\,mm\,a^{-1}$). Models also show rift sensitivity to (c) a weak and (d) a strong middle and lower crust at $V_{ext} = 3\,mm\,a^{-1}$ (images provided by R. Huismans and modified from Huismans & Beaumont, 2007, with permission from the Geological Society of London). t, time elapsed in millions of years; Δx amount of horizontal extension. Vertical and horizontal scales are in kilometers.*

apply these results to specific natural settings, it is important to realize that the effects of strain-induced weakening can be suppressed by other mechanisms that affect the rheology of the lithosphere. For example, a comparison of two models, one incorporating a weak lower crust (Fig. 7.27c) and the other a strong lower crust (Fig. 7.27d), illustrates how a weak crust can diminish crustal asymmetry. This suppression occurs because conjugate frictional shears that develop during rifting sole out in the weak ductile lower crust where they propagate laterally beneath the rift flanks. As rifting progresses, viscous flow in a weak lower crust results in a nearly symmetric ductile necking of the lower lithosphere. These examples show that the degree of rift asymmetry depends not only on strain softening mechanisms and rifting velocities, but also on the strength of the lower crust.

7.6.6 Rheological stratification of the lithosphere

In most quantitative models of continental rifting, the lithosphere is assumed to consist of multiple layers that are characterized by different rheologies. (Section 2.10.4). This vertical stratification agrees well with the results from both geophysical investigations of continental lithosphere and with the results of laboratory experiments that reveal the different behaviors of crust and mantle rocks over a range of physical conditions. In the upper part of the lithosphere strain is accommodated by faulting when stress exceeds the frictional resistance to motion on fault planes. In the ductile layers, strain is described using temperature-dependent power law rheologies that relate stress and strain-rate during flow (Section 2.10.3). Using these relationships, experimentally derived friction and flow laws for crustal and mantle rocks can be incorporated into models of rifting. This approach has allowed investigators to study the effects of a rheological stratification of the lithosphere on strain localization and delocalization processes during extension, including the development of large-offset normal faults (Sections 7.3, 7.6.4). The sensitivity of strain patterns to the choice of crustal rheology for different initial conditions are illustrated below using three different physical models of continental rifting.

Behn *et al.* (2002) explored how the choice of crustal rheology affects the distribution of strain within the lithosphere during extension using a simple two-layer

model composed of an upper crustal layer and a lower mantle layer (Fig. 7.28a). These authors incorporated a strain-rate softening rheology to model brittle behavior and the development of fault-like shear zones. Ductile deformation was modeled using temperature-dependent flow laws that describe dislocation creep in the crust and mantle. Variations in the strength (effective viscosity) of the crust at any given temperature and strain rate are defined by material parameters that are derived from rock physics experiments. The use of several flow laws for rocks with different mineralogies and water contents allowed the authors to classify the rheologies as either weak, intermediate, or strong. Variations in crustal thickness and thermal structure were added to a series of models to examine the interplay among these parameters and the different rheologies. The results show that when crustal thickness is small, so that no ductile layer develops in the lower crust, deformation occurs mostly in the mantle and the width of the rift is controlled primarily by the vertical geothermal gradient (Fig. 7.28b,f). By contrast, when the crustal thickness is large the stress accumulation in the upper crust becomes much greater than the stress accumulation in the upper mantle (Fig. 7.28c,d). In these cases the deformation becomes crust-dominated and the width of the rift is a function of both crustal rheology and the vertical geothermal gradient (Fig. 7.28e,f).

Figure 7.28e illustrates the effects of the strong, intermediate and weak crustal rheologies on rift morphology (half-width). The models predict the same rift half-width for mantle-dominated deformation. However, the transition between mantle- and crust-dominated deformation begins at a slightly larger crustal thickness for the strong rheology than for the intermediate or weak rheologies. In addition, the strong crustal rheology results in a rift half-width for the crust-dominated regime that is ~1.5 times greater than the value predicted by the intermediate rheology and ~4 times greater than that predicted by the weak rheology. Figure 7.28f summarizes the combined effects of crustal thickness, crustal rheology, and a vertical geothermal gradient on rift half-width. These results illustrate that the evolution of strain patterns during lithospheric stretching is highly sensitive to the choice of crustal rheology, especially in situations where the crust is relatively thick.

A similar sensitivity to crustal rheology was observed by Wijns *et al.* (2005). These authors used a simple two-layer crustal model where a plastic yield law controlled brittle behavior below a certain temperature and the choice of temperature gradient controlled the transition from a brittle upper crust into a ductile lower crust. This formulation and a 20-km-thick upper crust lying above a 40-km-thick lower crust allowed them to investigate how a mechanically stratified crust influenced fault spacing and the distribution of strain during extension. They found that the ratio of the integrated strength of the upper and lower crust governs the degree of strain localization on fault zones. When this ratio is small, such that the lower crust is relatively strong, extension results in widely distributed, densely spaced faults with a limited amount of slip on each fault. By contrast, a large strength ratio between the upper and lower crust, such that the lower crust is very weak, causes extension to localize onto relatively few faults that accommodate large displacements. In this latter case, the large-offset faults dissect the upper crust and exhume the lower crust, leading to the formation of metamorphic core complexes (Section 7.3). Wijns *et al.* (2005) also concluded that secondary factors, such as fault zone weakening and the relative thicknesses of the upper and lower crust (Section 7.6.5), determine the exact value of the critical ratio that controls the transition between localized and delocalized extension.

The results of Wijns *et al.* (2005), like those obtained by Behn *et al.* (2002), suggest that a weak lower crust promotes the localization of strain into narrow zones composed of relatively few faults. This localizing behavior reflects the ability of a weak lower crust to flow and transfer stress into the upper crust, which may control the number of fault zones that are allowed to develop. This interpretation is consistent with field studies of deformation and rheology contrasts in ancient lower crust exposed in metamorphic core complexes (e.g. Klepeis *et al.* 2007). It is also consistent with the results of Montési & Zuber (2003), who showed that for a brittle layer with strain localizing properties overlying a viscous layer, the viscosity of the ductile layer controls fault spacing. In addition, a weak lower crust allows fault blocks in the upper crust to rotate, which can facilitate the dissection and dismemberment of the upper crust by faulting.

Lastly, a third numerical model of rifting illustrates how the interplay among strain-induced weakening, layer thickness, and rheological contrasts can influence deformation patterns in a four-layer model of the lithosphere. Nagel & Buck (2004) constructed a model that consisted of a 12-km-thick brittle upper crust, a relatively strong 10-km-thick lower crust, a thin (3 km) weak mid-crustal layer, and a 45-km-thick upper mantle (Fig. 7.29a). The model incorporates temperature-dependent power law rheologies that determine viscous behavior in the crust and mantle. The mantle and upper and

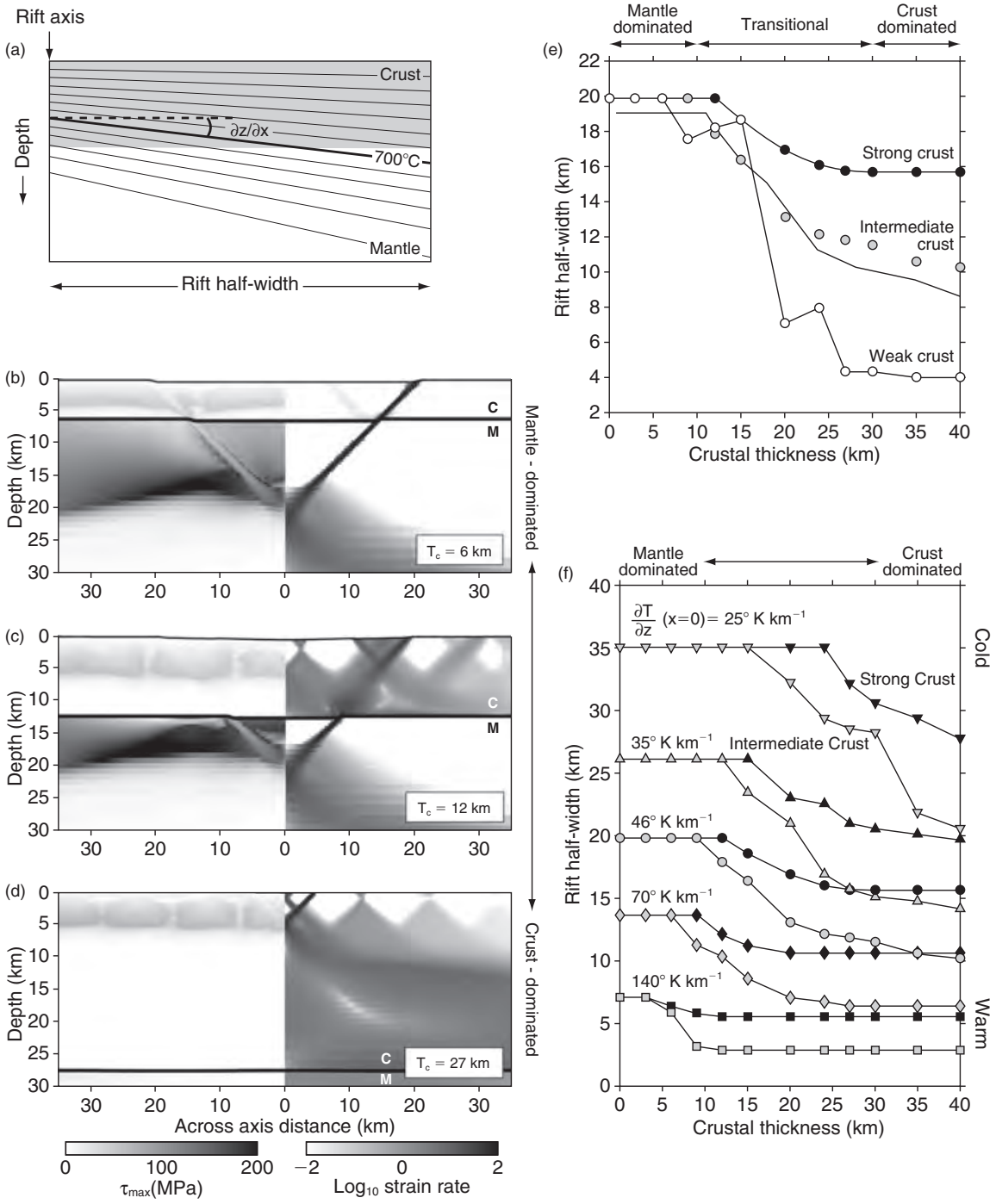

Figure 7.28 *(a) Model setup for numerical simulations of lithospheric stretching. The transition from mantle- to crust-dominated deformation is illustrated by (b), (c), and (d), which show the deformation grid after 1% total strain for a crustal thickness (T_c) of 6, 12 and 27 km, respectively. Grayscale indicates the magnitude of shear stress on left and normalized strain-rate on right. C and M mark the base of the crust and top of the mantle, respectively. (e) Effect of crustal thickness on predicted rift half-width. (f) Effect of vertical geothermal gradient on predicted rift half-width (images provided by M. Behn and modified from Behn* et al.*, 2002, with permission from Elsevier). Each point in (e) and (f) represents an experiment. Black, strong; gray, intermediate; and white, weak rheology.*

lower crust also follow the Mohr–Coulomb failure criterion and cohesion loss during faulting is included. The model also incorporates a predefined bell-shaped thermal perturbation at its center that serves to localize deformation at the beginning of extension. The horizontal thermal gradient created by this perturbation, and the predetermined vertical stratification, control the mechanical behavior of the lithosphere during rifting.

As extension begins, the upper mantle and lower crust undergo localized necking in the hot, weak center of the rift. Deformation in the upper crust begins as a single graben forms above the area of necking in the lower crust and mantle and subsequently evolves into an array of parallel inward dipping normal faults. The faults root down into the weak mid-crustal layer where distributed strain in the upper crust is transferred into the necking area in the strong lower parts of the model (Fig. 7.29b,c).

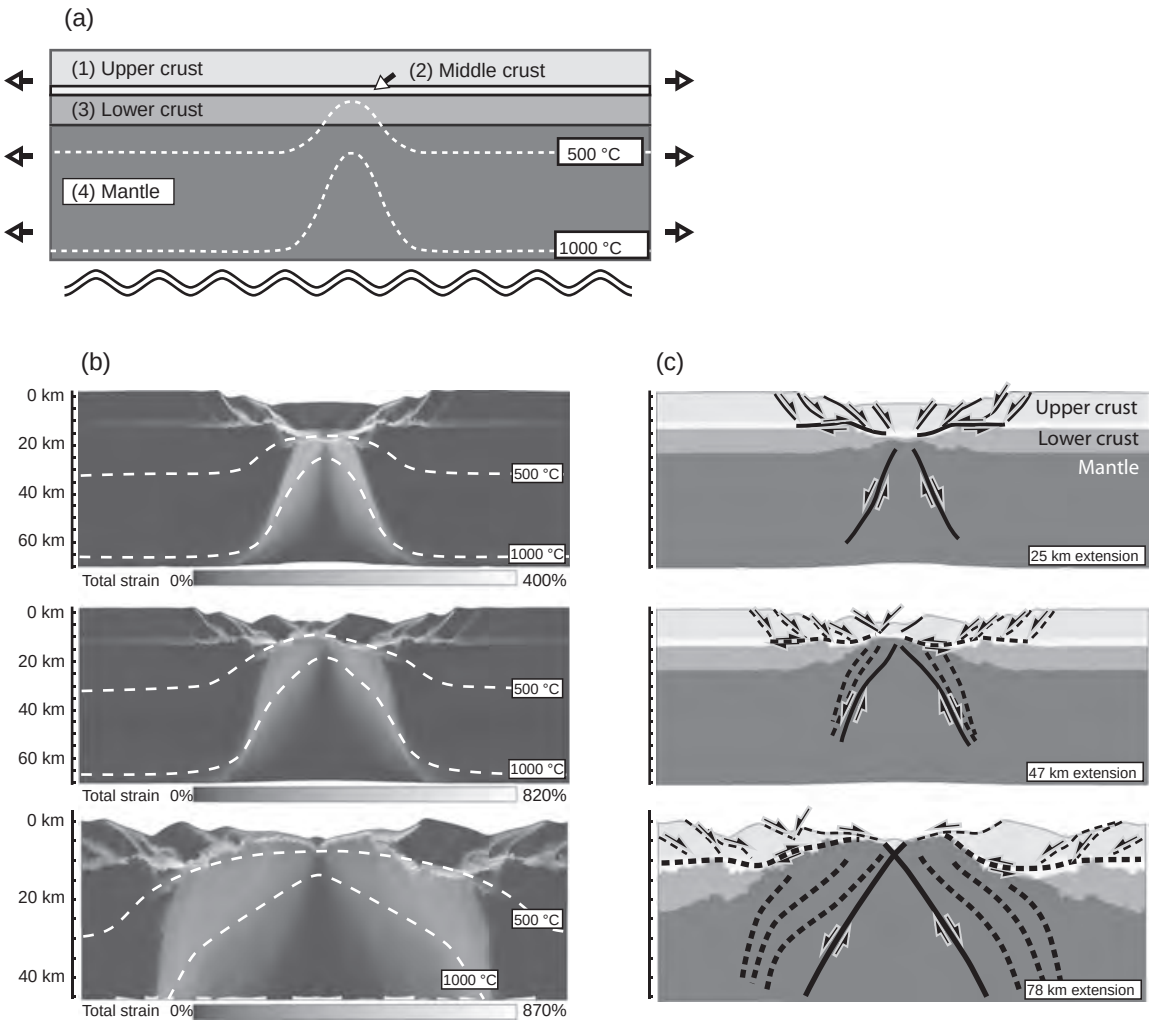

Figure 7.29 *Model of symmetric rifting (images provided by T. Nagel and modified from Nagel & Buck, 2004, with permission from the Geological Society of America). (a) Model setup. (b) Total strain and (c) distribution of upper, middle and lower crust and mantle after 25, 47 and 78 km of extension. Solid black lines, active zones of deformation; dashed lines, inactive zones; thin black lines, brittle faults; thick black lines, ductile shear zones.*

After ~25 km of extension, the lower crust pulls apart and displacements on the normal faults lead the collapse and dismemberment of the upper crust at the margins of the rift. Mantle material wells upward into the zone of thinning where the collapsing upper crust is placed in direct contact with mantle rocks. After 40 km of extension, the array of normal faults is abandoned and upper crustal deformation is concentrated in the center of the rift. Finally, after ~75 km, new ocean lithosphere is generated, leaving behind two tectonically quiet passive margins. This, and the other physical models described in this section, show how combinations of competing processes that either weaken or strengthen the crust can be used to explain much of the variability in deformation patterns observed in rifts.

7.6.7 Magma-assisted rifting

Most quantitative treatments of continental rifting focus on the effects of variations in lithospheric conditions. This emphasis reflects both the success of these models at explaining many aspects of rifting and the relative ease at which geoscientists can constrain the physical properties of the lithosphere compared to those of the asthenosphere. Nevertheless, it is evident that interactions between the asthenosphere and the lithosphere form crucial components of rift systems (Ebinger, 2005). One of the most important aspects of these interactions involves magmatism (Section 7.4), which weakens the lithosphere and causes strain localization.

Among its possible effects, mafic magmatism may allow rifting to initiate in regions of relatively cold or thick continental lithosphere (Section 7.5). In addition to its weakening effects, the availability of a significant source of basaltic magma influences the thickness, temperature, density, and composition of the lithosphere. The presence of hot, partially molten material beneath a rift valley produces density contrasts that result in thermal buoyancy forces (Section 7.6.3). As the two sides of the rift separate, magma also may accrete to the base of the crust where it increases in density as it cools and may lead to local crustal thickening (Section 7.2, Fig. 7.5). These processes can create bending forces within the lithosphere as the plate responds to the changing load, and affect the manner in which strain is accommodated during rifting. The changes may be recorded in patterns of uplift and subsidence across rifts and rifted margins.

Buck (2004) developed a simple two-dimensional thermal model to illustrate how rifting and magma intrusion can weaken the lithosphere and influence subsidence and uplift patterns. The emplacement of large quantities of basalt in a rift can accommodate extension without crustal thinning. This process has been observed in the mature rift segments of northern Ethiopia (Section 7.8.1) where strain accommodation by faulting has been greatly reduced as magmatism increased (Wolfenden *et al.*, 2005). If enough material intrudes, the crustal thickening that can result from magmatism can lessen the amount of subsidence in the rift and may even lead to regional uplift. This effect is illustrated in Fig. 7.30, which shows the average isostatic elevation through time for magma-assisted rifting compared to a typical subsidence curve for lithospheric stretching due to thermal relaxation (McKenzie, 1978). The uplift or subsidence result from changes in density related to the combined effects of crustal thinning, basalt intrusion and temperature differences integrated over a 100 km wide rift to a depth of 150 km. Buck (2004) suggested that this process might explain why some continental margins, such as those off the east coast of Canada (Royden & Keen, 1980), show less initial tectonic subsidence related to crustal thinning compared to the

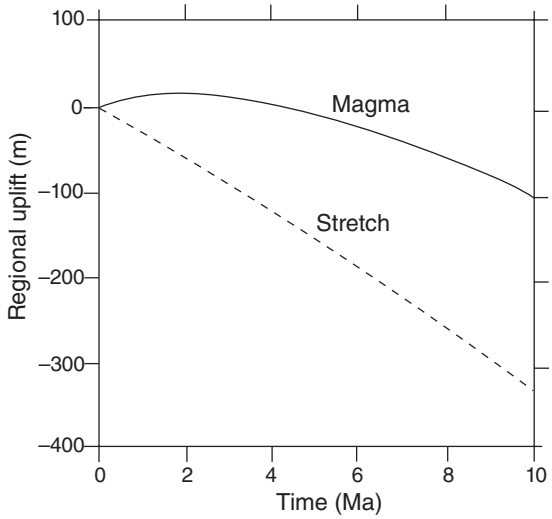

Figure 7.30 *Comparison of the predicted average regional isostatic elevation changes for magma-assisted rifting (solid line) and pure shear necking (dashed line) (from Buck, 2004. Copyright © 2004 from Columbia University Press. Reprinted with permission of the publishers).*

long-term (tens of millions of years) subsidence induced by cooling.

Two other problems of rift evolution that also might be resolved by incorporating the effects of magmatism and/or flow of the asthenosphere include the extra subsidence observed at some rifted margins and the lack of magma that characterize nonvolcanic margins (Buck, 2004). These effects are discussed in the context of the evolution of rifted continental margins in Section 7.7.3.

7.7 RIFTED CONTINENTAL MARGINS

7.7.1 Volcanic margins

Rifted volcanic margins are defined by the occurrence of the following three components: Large Igneous Provinces (Section 7.4.1) composed of thick flood basalts and silicic volcanic sequences, high velocity (V_p > 7 km s^{-1}) lower crust in the continent–ocean transition zone, and thick sequences of volcanic and sedimentary strata that give rise to *seaward-dipping reflectors* on seismic reflection profiles (Mutter *et al.*, 1982). The majority of rifted continental margins appear to be volcanic, with some notable exceptions represented by the margins of the Goban Spur, western Iberia, eastern China, South Australia, and the Newfoundland Basin–Labrador Sea. Relationships evident in the Red Sea and southern Greenland suggest that a continuum probably exists between volcanic and nonvolcanic margins.

The high velocity lower crust at volcanic margins occurs between stretched continental crust and normal thickness oceanic crust (Figs 7.31, 7.32). Although these layers have never been sampled directly, the high P_n wave velocities suggest that they are composed of thick accumulations of gabbro that intruded the lower crust during continental rifting. The intrusion of this material helps to dissipate the thermal anomaly in the mantle that is associated with continental rifting.

The Lofoten–Vesterålen continental margin off Norway (Figs 7.31, 7.32) illustrates the crustal structure of a volcanic margin that has experienced moderate extension (Tsikalas *et al.*, 2005). The ocean–continent transition zone between the shelf edge and the Lofoten basin is 50–150 km wide, includes an abrupt lateral gradient in crustal thinning, and is covered by layers of volcanic material that display shallow seaward dipping reflectors (Fig. 7.32a). The 50–150 km width of this zone is typical of many rifted margins, although in some cases where there is extreme thinning the zone may be several hundred kilometers wide. Crustal relief in this region is related to faulted blocks that delineate uplifted highs. In the Lofoten example, the continent–ocean boundary occurs landward of magnetic anomaly 24B (53–56 Ma) and normal ocean crust occurs seaward of magnetic anomaly 23 (Fig. 7.31b). Crustal thinning is indicated by variations in Moho depth. The Moho reaches a maximum depth of 26 km beneath the continental shelf and 11–12 km beneath the Lofoten basin. Along profile A–A′ a region of 12–16 km thick crust within the ocean–continent transition zone coincides with a body in the lower crust characterized by a high lower crustal velocity (7.2 km s^{-1}) (Fig. 7.32a,c). This body thins to the north along the margin, where it eventually disappears, and thickens to the south, where at one point it has a thickness of 9 km (Fig. 7.31c). Oceanic layers display velocities of 4.5–5.2 km s^{-1}, sediments show velocities of ≤2.45 km s^{-1}. These seismic velocities combined with gravity models (Fig. 7.32b) provide information on the nature of the material within the margin (Fig. 7.32c).

In most volcanic margins the wedges of seaward-dipping reflectors occur above or seaward of the high velocity lower crust in the continent–ocean transition zone. Direct sampling of these sequences indicates that they are composed of a mixture of volcanic flows, volcaniclastic deposits, and nonvolcanic sedimentary rock that include both subaerial and submarine types of deposits. Planke *et al.* (2000) identified six units that are commonly associated with these features (Fig. 7.33): (i) an outer wedge of seaward-dipping reflectors; (ii) an outer high; (iii) an inner wedge of seaward-dipping reflectors; (iv) landward flows; (v) lava deltas; and (vi) inner flows. The wedge-like shape of the reflector packages is interpreted to reflect the infilling of rapidly subsiding basement rock. The outer reflectors tend to be smaller and weaker than the inner variety. The outer high is a mounded, commonly flat-topped feature that may be up to 1.5 km high and 15–20 km wide. In some places this may be a volcano or a pile of erupted basalt. Landward flows are subaerially erupted flood basalts that display little to no sediment layers between the flows. The inner flows are sheet-like bodies located

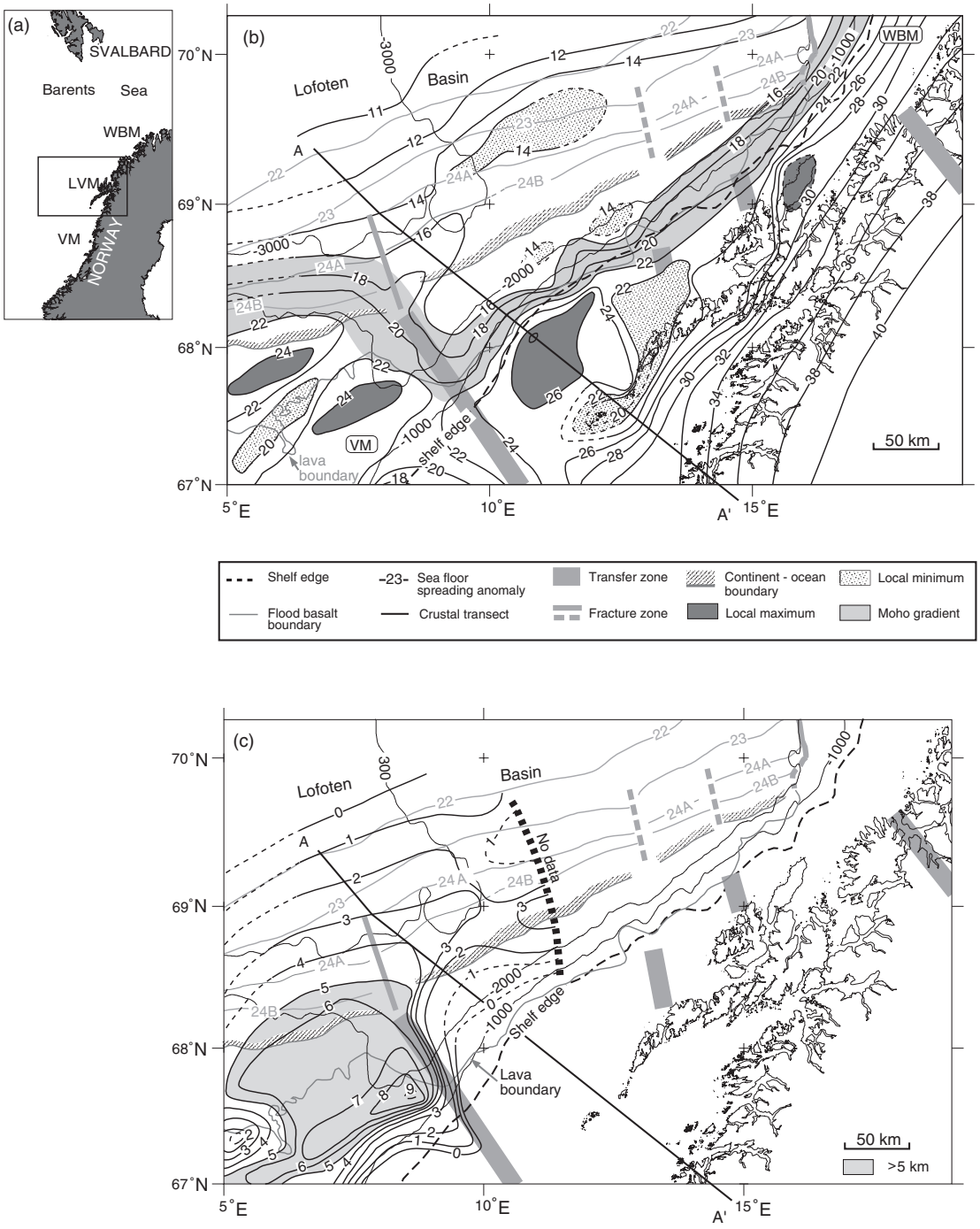

Figure 7.31 *The Lofoten–Vesterålen continental margin. Inset (a) shows Vøring (VM), Lofoten–Vesterålen (LVM), and Western Barents Sea (WBM) margins. (b) Map showing Moho depths with 2 km contour interval. (c) Thickness of high velocity lower crustal body with contour interval of 1 km (images provided by F. Tsikalas and modified from Tsikalas* et al.*, 2005, with permission from Elsevier). A–A' indicates the location of the cross-sections shown in Fig. 7.32.*

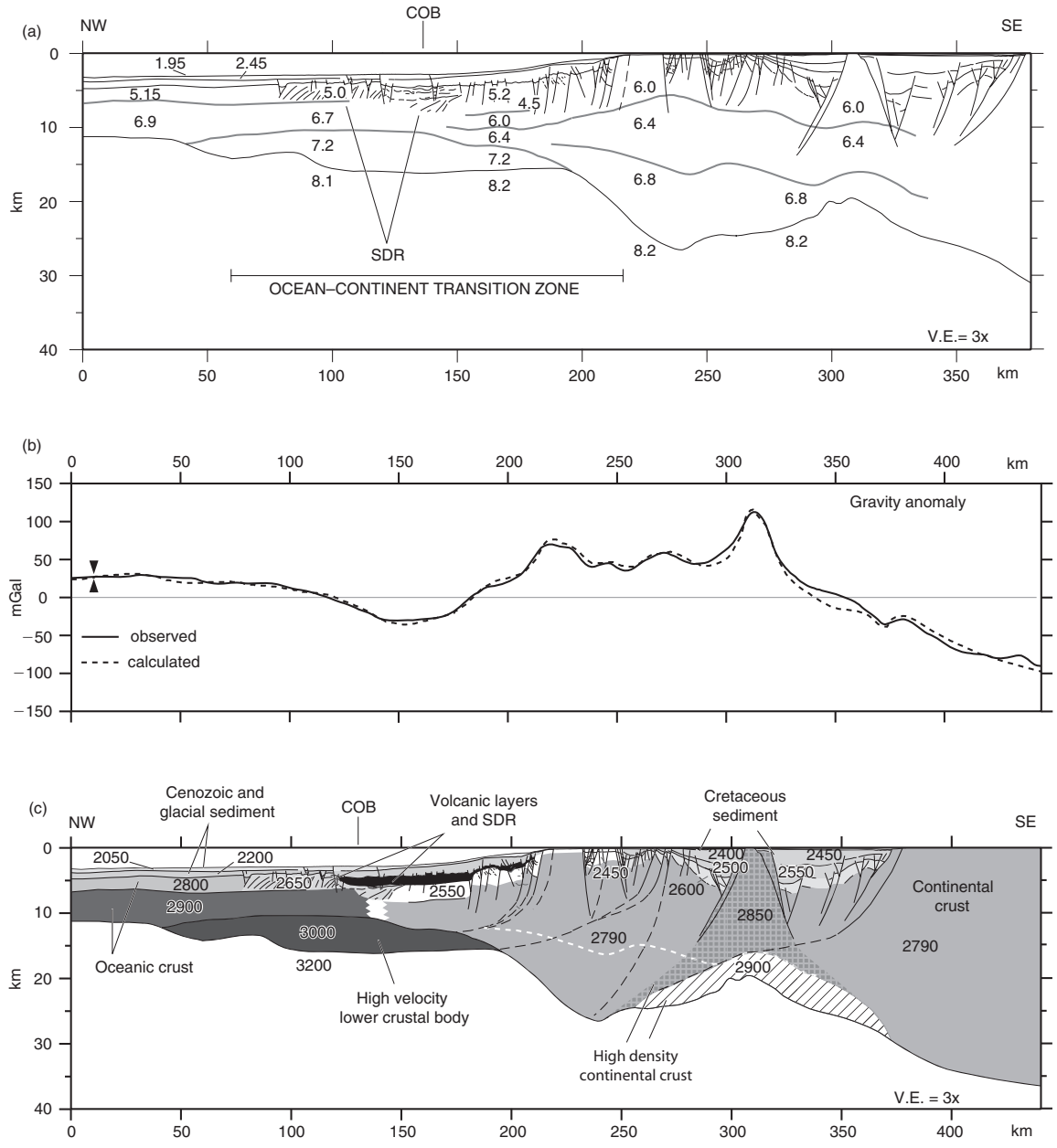

Figure 7.32 *(a) Seismic velocity structure along the southern Lofoten–Vesterålen margin. COB, continent–ocean boundary. (b,c) Gravity modeled transect and interpretation of the geology (images provided by F. Tsikalas and modified from Tsikalas* et al.*, 2005, with permission from Elsevier). Densities in (c) are shown in kilograms per cubic meter. SDR, seaward dipping reflectors. For location of profile see Fig. 7.31.*

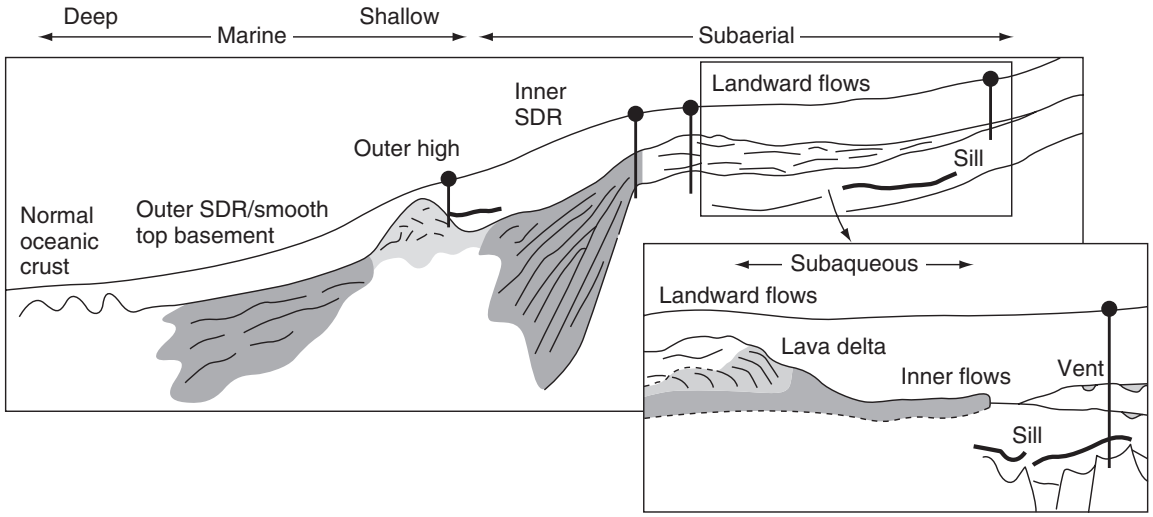

Figure 7.33 *Interpretation of the main seismic facies of extrusive units at volcanic margins (modified from Planke* et al*., 2000, by permission of the American Geophysical Union. Copyright © 2000 American Geophysical Union). Inset shows enlargement of a region of landward subaqueous flows where lava deltas and inner flow units commonly occur. Solid circles with vertical lines show locations of wells where drill holes have penetrated the various units. SDR, seaward dipping reflectors (shaded). Bold black lines, sills.*

landward and, typically, below the lava delta. Lava deltas form as flowing basalt spills outward in front of the growing flood basalts. The emplacement of these features is associated with the establishment of thicker than normal ocean crust within the continent to ocean transition zone (Planke *et al.*, 2000).

The conditions and processes that form volcanic rifted margins are the subject of much debate. In general, the formation of the thick igneous crust appears to require larger amounts of mantle melting compared to that which occurs at normal mid-ocean ridges. The origin of this enhanced igneous activity is uncertain but may be related to asthenospheric temperatures that are higher than those found at mid-ocean ridges or to unusually high rates of upwelling mantle material (Nielson & Hopper, 2002, 2004). Both of these mechanisms could occur in association with mantle plumes (Sections 5.5, 12.10), although this hypothesis requires rigorous testing.

7.7.2 Nonvolcanic margins

The occurrence of nonvolcanic margins (Fig. 7.34a) shows that extreme thinning and stretching of the crust is not necessarily accompanied by large-scale volcanism and melting. Nonvolcanic margins lack the large volume of extrusive and intrusive material that characterizes their volcanic counterparts. Instead, the crust that characterizes this type of margin may include highly faulted and extended continental lithosphere, oceanic lithosphere formed by very slow sea floor spreading, or continental crust intruded by magmatic bodies (Sayers *et al.*, 2001). In addition, these margins may contain areas up to 100 km wide that are composed of exhumed, serpentinized upper mantle (Fig. 7.34b,c) (Pickup *et al.*, 1996; Whitmarsh *et al.*, 2001). Dipping reflectors in seismic profiles also occur within nonvolcanic margins. However, unlike in volcanic varieties, these reflectors may be preferentially tilted continentward and do not represent sequences of volcanic rock (Pickup *et al.*, 1996). Some of these *continentward-dipping* reflectors represent detachment faults (Section 7.3) that formed during rifting (Boillot & Froitzheum, 2001).

Two end-member types of nonvolcanic margins have been identified on the basis of relationships preserved in the North Atlantic region (Louden & Chian, 1999). The first case is derived from the southern Iberia Abyssal Plain, Galicia Bank, and the west Greenland margins. In these margins rifting of the continent

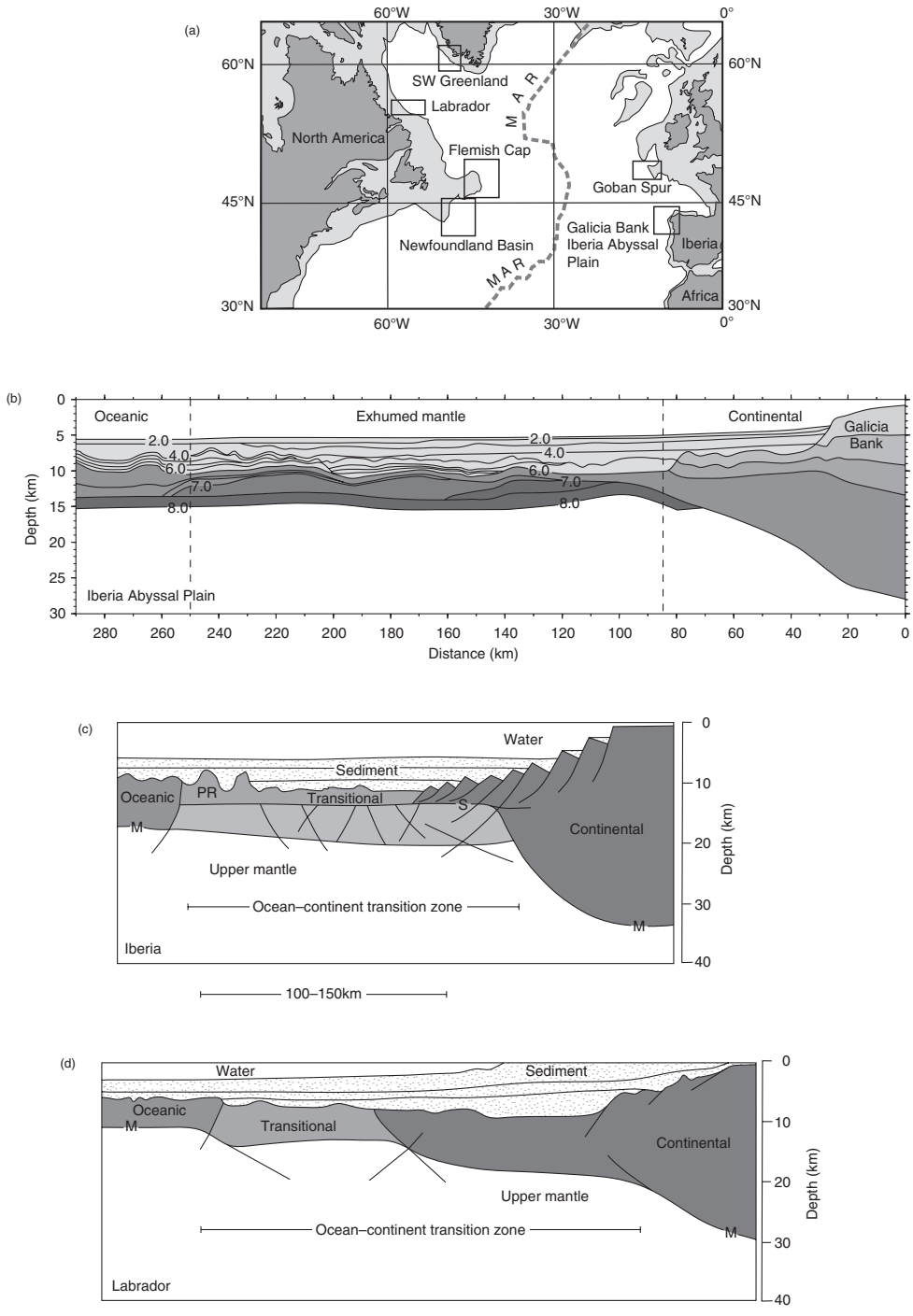

Figure 7.34 *(a) Map of the North Atlantic showing location of selected nonvolcanic margins. MAR, Mid-Atlantic Ridge. (b) Velocity model of the West Iberia margin and the Iberia Abyssal Plain (image provided by T. Minshull and modified from Minshull, 2002 with permission from Royal Society of London). Data are from Dean* et al. *(2000). The dashed lines mark the approximate edges of the ocean–continent transition zone. Velocities in km* s^{-1}*. (c,d) Two end-member types of nonvolcanic margin (images provided by K. Louden and modified from Louden & Chian, 1999, with permission from the Royal Society of London). PR, peridotite ridge; S, reflections interpreted to represent a detachment fault or shear zone; M, Moho reflections.*

produced a zone of extremely thin continental crust. This thin crust is characterized by tilted fault blocks that are underlain by a prominent subhorizontal reflector (*S*) that probably represents a serpentinized shear zone at the crust–mantle boundary (Fig. 7.34c) (Reston *et al.*, 1996). The reflector occurs seaward of stretched continental basement and above a high velocity lower layer of serpentinized mantle. Below the reflector seismic velocities increase gradually with depth and approach normal mantle velocities at depths of 15–20 km. Seaward of the thinned continental crust and landward of the first oceanic crust, a transitional region is characterized by low basement velocities, little reflectivity, and a lower layer of serpentinized mantle showing velocities (V_p > 7.0 km s^{-1}) that are similar to high velocity lower crust. Farther seaward, the basement is characterized by a complex series of peridotite ridges (PR), which contain sea floor spreading magnetic anomalies that approximately parallel the strike of the oceanic spreading center. Although this zone is composed mostly of serpentinized mantle, it may also contain minor intrusions. Thus, basement at these margins consists of faulted continental blocks, a smooth transitional region, and elevated highs. Moho reflections (M) are absent within the ocean–continent transition zone. Instead, this region displays landward and seaward dipping reflectors that extend to depths of 15–20 km.

In the second type of nonvolcanic margin (Fig. 7.34d), based primarily on the Labrador example, only one or two tilted fault blocks of upper continental crust are observed and the S-type horizontal reflection is absent. A zone of thinned mid-lower continental crust occurs beneath a thick sedimentary basin. A transitional region occurs farther seaward in a manner similar to the section shown in Fig. 7.34c. However, dipping reflections within the upper mantle are less prevalent. For Labrador, the region of extended lower continental crust is very wide with a thick sedimentary basin, while for Flemish Cap and the Newfoundland basin, the width of extended lower continental crust is narrow or absent. Moho reflections (M) indicate very thin (~5 km) oceanic crust.

7.7.3 The evolution of rifted margins

The evolution of rifted continental margins is governed by many of the same forces and processes that affect the formation of intracontinental rifts (Section 7.6). Thermal and crustal buoyancy forces, lithospheric flexure, rheological contrasts, and magmatism all may affect margin behavior during continental break-up, although the relative magnitudes and interactions among these factors differ from those of the pre-break-up rifting stage. Two sets of processes that are especially important during the transition from rifting to sea floor spreading include: (i) post-rift subsidence and stretching; and (ii) detachment faulting, mantle exhumation, and ocean crust formation at nonvolcanic margins.

Post-rift subsidence and stretching

As continental rifting progresses to sea floor spreading, the margins of the rift isostatically subside below sea level and eventually become tectonically inactive. This subsidence is governed in part by the mechanical effects of lithospheric stretching (Section 7.6.2) and by a gradual relaxation of the thermal anomaly associated with rifting. Theoretical considerations that incorporate these two effects for the case of uniform stretching predict that subsidence initially will be rapid as the crust is tectonically thinned and eventually slow as the effects of cooling dominate (McKenzie, 1978). However, the amount of subsidence also is influenced by the flexural response of the lithosphere to loads generated by sedimentation and volcanism and by changes in density as magmas intrude and melts crystallize and cool (Section 7.6.7). Subsidence models that include the effects of magmatism and loading predict significant departures from the theoretical thermal subsidence curves.

The amount of subsidence that occurs at rifted margins is related to the magnitude of the stretching factor (β). There are several different ways of estimating the value of this parameter, depending on the scale of observation (Davis & Kusznir, 2004). For the brittle upper crust, the amount of extension typically is derived from summations of the offsets on faults imaged in seismic reflection profiles that are oriented parallel to fault dips. Estimates of the combined upper crustal extension and lower crustal stretching are obtained from variations in crustal thickness measured using wide-angle seismic surveys, gravity studies, and seismic reflection data. This latter approach relies on the assumption that the variations are a consequence of crustal extension and thinning. At the scale of the entire lithosphere, stretching factors are obtained through considerations of the flexural isostatic response to

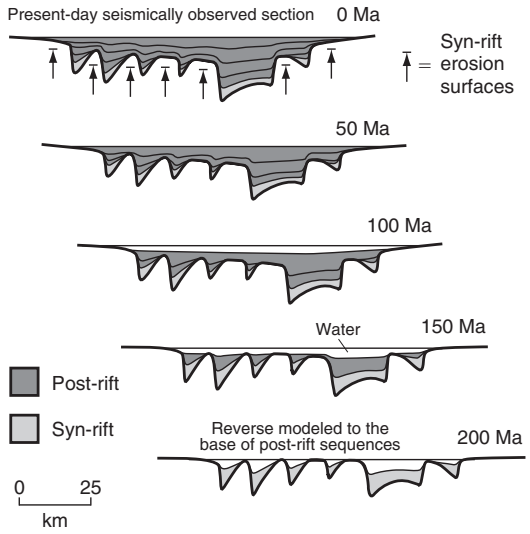

Figure 7.35 *Schematic diagram showing application of flexural backstripping and the modeling of post-rift subsidence to predict sequential restorations of stratigraphy and paleobathymetry. Restored sections are dependent on the* β *stretching factor used to define the magnitude of lithospheric extension and lithospheric flexural strength (after Kusznir* et al.*, 2004, with permission from Blackwell Publishing).*

loading (Section 7.6.4) and thermal subsidence. One of the most commonly used approaches to obtaining lithospheric-scale stretching factors employs a technique known as flexural backstripping.

Flexural backstripping involves reconstructing changes in the depth to basement in an extensional sedimentary basin by taking into account the isostatic effects of loading. The concept behind the method is to exploit the stratigraphic profile of the basin to determine the depth at which basement rock would be in the absence of loads produced by both water and all the overlying layers. This is accomplished by progressively removing, or *backstripping*, the loads produced by each layer and restoring the basement to its depth at the time each layer was deposited (Fig. 7.35). These results combined with knowledge of water depth theoretically allow determination of the stretching factor (β). Nevertheless, as discussed further below, relationships between stretching factor and subsidence curves may be complicated by interactions between the lithosphere and the sublithospheric mantle. In practice, flexural backstripping is carried out by assigning each layer a specific density and elastic thickness (T_e) (Section 7.6.4) and then summing the effects of each layer for successive time intervals. Corrections due to sediment compaction, fluctuations in sea level, and estimates of water depth using fossils or other sedimentary indicators are then applied. This approach generally involves using information derived from post-rift sediments rather than syn-rift units because the latter violate assumptions of a closed system during extension (Kusznir *et al.*, 2004). The results usually show that the depth of rifted margins at successive time intervals depends upon both the magnitude of stretching factor (β) and the flexural strength of the lithosphere. Most applications indicate that the elastic thickness of the lithosphere increases as the thermal anomaly associated with rifting decays.

Investigations of lithospheric-scale stretching factors at both volcanic and nonvolcanic margins have revealed several characteristic relationships. Many margins show more subsidence after an initial tectonic phase due to stretching than is predicted by thermal subsidence curves for uniform stretching. Rifted margins off Norway (Roberts *et al.*, 1997), near northwest Australia (Driscoll & Karner, 1998), and in the Goban Spur and Galicia Bank (Davis & Kusznir, 2004) show significantly more subsidence than is predicted by the magnitude of extension indicated by upper crustal faulting. In addition, many margins show that the magnitude of lithospheric stretching increases with depth within ~150 km of the ocean–continent boundary (Kusznir *et al.*, 2004). Farther toward the continent, stretching and thinning estimates for the upper crust, whole crust, and lithosphere converge as the stretching factor (β) decreases. These observations provide important boundary conditions on the processes that control the transition from rifting to sea floor spreading. However, the causes of the extra subsidence and depth-dependent stretching are uncertain. One possibility is that the extra subsidence results from extra uplift during the initial stage of sea floor spreading, perhaps as a result of upwelling anomalously hot asthenosphere (Hopper *et al.*, 2003; Buck, 2004). Alternatively, greater stretching in the mantle lithosphere than in the crust, or within a zone of mantle lithosphere that is narrow than in the crust, also may result in extra uplift. Once these initial effects decay the ensuing thermal subsidence during cooling would be greater than models of uniform stretching would predict. These hypotheses, although seemingly plausible, require further testing.

Observations of the southeast Greenland volcanic margin support the idea that the flow of low-density mantle during the transition to sea floor spreading strongly influences subsidence and stretching patterns. Hopper *et al.* (2003) found distinctive changes in the morphology of basaltic layers in the crust that indicate significant vertical motions of the ridge system. At the start of spreading, the system was close to sea level for at least 1 Myr when spreading was subaerial. Later subsidence dropped the ridge to shallow water and then deeper water ranging between 900 and 1500 m depth. This history appears to reflect the dynamic support of the ridge system by upwelling of hot mantle material during the initiation of spreading. Exhaustion of this thermal anomaly then led to loss of dynamic support and rapid subsidence of the ridge system over a 2 Ma period. In addition, nearly double the volume of dikes and volcanic material occurred on the Greenland side of the margin compared to the conjugate Hatton Bank margin located south of Iceland on the other side of the North Atlantic ocean. These observations indicate that interactions between hot asthenosphere and the lithosphere continue to influence the tectonic development of rifted margins during the final stages of continental break-up when sea floor spreading centers are established.

The flow of low-density melt-depleted asthenosphere out from under a rift also may help explain the lack of magmatic activity observed at rifted nonvolcanic margins. The absence of large volumes of magma could be linked to the effects of prior melting episodes, convective cooling of hot asthenosphere, and/or the rate of mantle upwelling (Buck, 2004). As sublithospheric mantle wells up beneath a rift it melts and cools. This process could result in shallow mantle convection due to the presence of cool, dense melt-depleted material overlying hotter, less dense mantle. Cooling also restricts further melting by bringing the mantle below its solidus temperature (Section 7.4.2). If some of this previously cooled, melt-depleted asthenosphere is pulled up under the active part of the rift during the transition to sea floor spreading, its presence would suppress further melting, especially if the rate of rifting or sea floor spreading is slow. The slow rates may not allow the deep, undepleted asthenosphere to reach the shallow depths that generate large amounts of melting.

Magma accretion, mantle exhumation, and detachment faulting

The transition from rifting to sea floor spreading at nonvolcanic margins is marked by the exhumation of large sections of upper mantle. Seismic reflection data collected from the Flemish Cap off the Newfoundland margin provide insight into the mechanisms that lead to this exhumation and how they relate to the formation of ocean crust.

The Flemish Cap is an approximately circular shaped block of 30-km-thick continental crust that formed during Mesozoic rifting between Newfoundland and the Galicia Bank margin near Iberia (Fig. 7.36a). The two conjugate margins show a pronounced break-up asymmetry. Seismic images from the Galicia Bank show a transition zone composed of mechanically unroofed continental mantle (Fig. 7.36b) and a strong regional west-dipping S-type reflection (Fig. 7.36b, stages 1 & 2) (Section 7.7.2). The transition zone is several tens of kilometers wide off the Galicia Bank and widens to 130 km to the south off southern Iberia. The S-reflection is interpreted to represent a detachment fault between the lower crust and mantle that underlies a series of fault-bounded blocks. By contrast, the Newfoundland margin lacks a transition zone and shows no evidence of any S-type reflections or detachment faults (Hopper *et al.*, 2004). Instead, this latter margin shows an abrupt boundary between very thin continental crust and a zone of anomalously thin (3 to 4 km thick), highly tectonized oceanic crust (Fig. 7.36b, stages 3, 4, and 5). Seaward of this boundary the oceanic crust thins even further to <1.3 km and exhibits unusual very reflective layering (I).

The five stage model of Hopper *et al.* (2004) explains these structural differences and the evolution of the conjugate margins. In Fig. 7.36b, the top panel shows a reconstruction of the two margins emphasizing their asymmetry at final break-up when the continental crust was thinned to a thickness of only a few kilometers (stage 1). During break-up, displacement within an extensional detachment fault (labeled S in Fig. 7.36b) unroofed a peridotite ridge (PR) above a zone of weak serpentinized upper mantle. Break-up west of the ridge isolated it on the Galicia Bank margin when, during stage 2, mantle melts reached the surface and sea floor spreading was established. Limited magmatism produced the thinner than normal (3–4 km), highly tectonized ocean crust. During stage 3, a

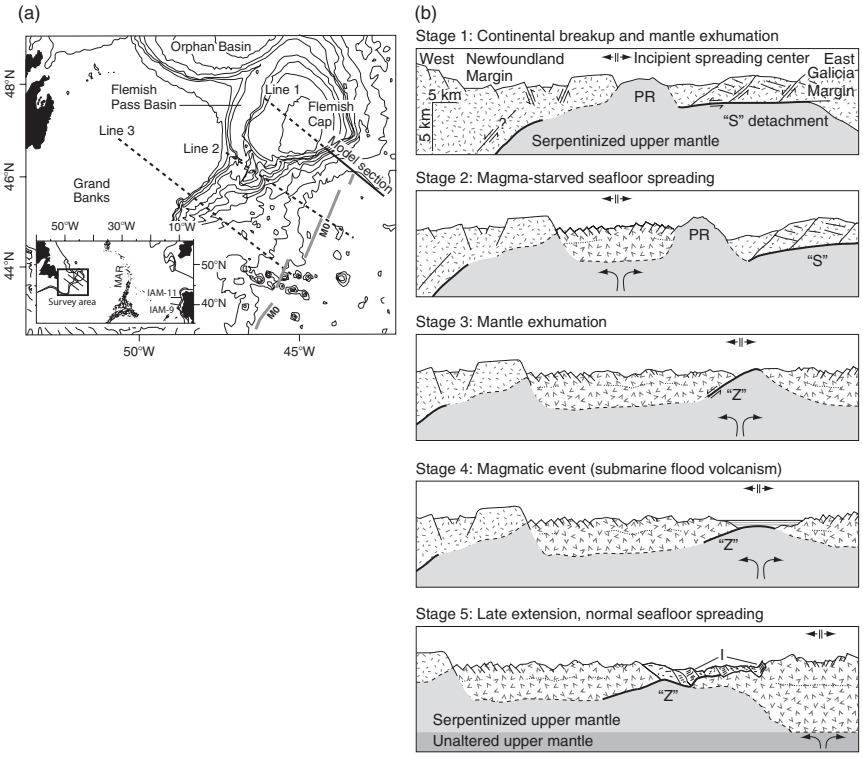

Figure 7.36 *(a) Location of seismic surveys of the Flemish Cap and (b) five stage model of nonvolcanic margins (after Hopper* et al.*, 2004, with permission from the Geological Society of America). MO in (a) is magnetic anomaly. Random-dash pattern, continental crust; v pattern, oceanic crust; light gray shading, serpentinized upper mantle; dark gray shading, unaltered upper mantle; thick lines, strong reflections; dashed lines, inferred crust–mantle boundary; dotted lines, oceanic layers; PR, peridotite ridge; S, reflections interpreted to represent a detachment fault; I, unusual very reflective oceanic crust; Z, reflections interpreted to represent a detachment fault buried by deep marine flood basalts.*

reduction in magma supply led to about 20 km of extension that was accommodated mostly by detachment faulting. The detachment faulting led to the exhumation of the mantle and formed an oceanic core complex that is similar to those found in slow-spreading environments at ridge–transform intersections (Section 6.7). Voluminous but localized magmatism during stage 4 resulted in a 1.5-km-thick layer of deep marine flood basalts that buried the detachment surface (reflection *Z*). The intrusion of gabbroic material may have accompanied this volcanism. This magmatic activity marked the beginning of sea floor spreading that formed normal (6 km) thickness ocean crust (stage 5).

This example shows that, to a first order, the transition from rift to oceanic crust at nonvolcanic margins is fundamentally asymmetric and involves a period of magmatic starvation that leads to the exhumation of the mantle. This type of margin may typify

slow-spreading systems (Section 6.6) where large fluctuations in melt supply occur in transient magma chambers during the early stages of sea floor spreading.

7.8 CASE STUDIES: THE TRANSITION FROM RIFT TO RIFTED MARGIN

7.8.1 The East African Rift system

The East African Rift system (Fig. 7.2) is composed of several discrete rift segments that record different stages in the transition from continental rift to rifted volcanic margin (Ebinger, 2005). The Eastern Rift between northern Tanzania and southern Kenya is an example of a youthful rift that initiated in thick, cold and strong continental lithosphere. Volcanism and sedimentation began by ~5 Ma with the largest fault escarpments forming by ~3 Ma. Strain and magmatism are localized within narrow asymmetric rift basins with no detectable deformation in the broad uplifted plateau adjacent to the rifts (Foster *et al.*, 1997). Earthquake hypocenters occur throughout the entire 35 km thickness of the crust, indicating that crustal heating is at a minimum (Foster & Jackson, 1998). The basins are shallow (~3 km deep) with 100-km-long border faults that accommodate small amounts of extension. The border faults have grown from short fault segments that propagated along their lengths to join with other nearby faults, creating linkages between adjacent basins (Foster *et al.*, 1997). Faults that were oriented unfavorably with respect to the opening direction were abandoned as strain progressively localized onto the border faults (Ebinger, 2005). Geophysical (Green *et al.*, 1991; Birt *et al.*, 1997) and geochemical (Chesley *et al.*, 1999) data show that the mantle lithosphere has been thinned to about 140 km. Elsewhere the lithosphere is at least 200 km and possibly 300–350 km thick (Ritsema *et al.*, 1998). These patterns conform to the predictions of lithospheric stretching models (Section 7.6.2, 7.6.3) in regions of relatively thick lithosphere. They also illustrate that the cross-sectional geometry and the along-axis segmentation in youthful rifts are controlled by the flexural strength of the lithosphere (Section 7.6.4).

The effects of pre-existing weaknesses on the geometry of rifting are also illustrated in the southern segment of the Eastern Rift in Tanzania. Border faults and half graben preferentially formed in a zone of weakness created by a contrast between thick, cool lithosphere of the Archean Tanzanian craton and thin, weak Proterozoic lithosphere located to the east (Foster *et al.*, 1997). From north to south, the axis of the rift diverges from a single ~50 km wide rift to a ~200 km wide zone composed of three narrow segments (Fig. 7.2b). This segmentation and a change in orientation of faults occurs where the rift encounters the Archean Tanzanian craton (Fig. 7.37), indicating that the thick lithosphere has deflected the orientation of the rift. These observations illustrate that lateral heterogeneities at the lithosphere–asthenosphere boundary exert a strong control on the initial location and distribution of strain at the start of rifting (Section 7.4).

An example of a rift that is slightly more evolved than the Tanzanian example occurs in central and northern Kenya where rifting began by 15 Ma. In this rift segment the crust has been thinned by up to 10 km and the thickness of the lithosphere has been reduced to about 90 km (Mechie *et al.*, 1997). A progressive shallowing of the Moho occurs between central and northern Kenya where the rift widens from ~100 km to ~175 km (Fig. 7.2b). In northern Kenya, crustal thickness is about 20 km and the total surface extension is about 35–40 km ($\beta = 1.55$–1.65) (Hendrie *et al.*, 1994). In the south, crustal thickness is 35 km with estimates of total extension ranging from 5 to 10 km (Strecker *et al.*, 1990; Green *et al.*, 1991). As the amount of crustal stretching increases, and the lithosphere–asthenosphere boundary rises beneath a rift, the amount of partial melting resulting from decompression melting also increases (Section 7.4.2). Young lavas exposed in central and northern Kenya indicate source regions that are shallower than those in Tanzania (Furman *et al.*, 2004). High velocity, high density material is present in the upper crust and at the base of the lower crust, suggesting the presence of cooled basaltic intrusions (Mechie *et al.*, 1997; Ibs-von Seht *et al.*, 2001). These relationships indicate that as a continental rift enters maturity magmatic activity increases and a significant component of the extension is accommodated by magmatic intrusion below the rift axis (Ebinger, 2005).

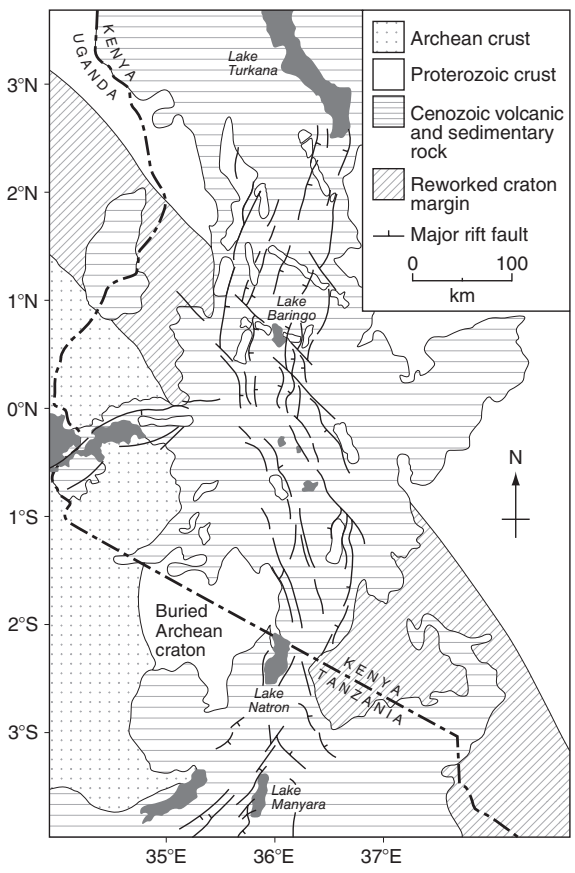

Figure 7.37 *Structural map of the Eastern branch of the East African Rift system in Kenya and northern Tanzania showing the deflection of faults at the boundary of the Archean Tanzanian craton (after Macdonald* et al.*, 2001, with permission from the* Journal of Petrology **42**, *877–900. Copyright © 2001 by permission of Oxford University Press, and Smith & Mosely, 1993, by permission of the American Geophysical Union. Copyright © 1993 American Geophysical Union).*

The increase in magmatic activity that accompanies a shallowing of the asthenosphere–lithosphere boundary beneath the Kenya Rift also results in increased crustal heating and contributes to a decrease in lithospheric strength (Section 7.6.7). This effect is indicated by a progressive decrease in the depth of earthquake hypocenters and in the depth of faulting from 35 km to 27 km (Ibs-von Seht *et al.*, 2001). These patterns suggest a decrease in the effective elastic thickness (T_e) of the lithosphere (Section 7.6.4) compared to the rift in northern Tanzania. Although both the mantle and crust have thinned, the thinning of mantle lithosphere outpaces crustal thinning. This asymmetry occurs because a sufficient amount of magma has accreted to the base of the crust, resulting in a degree of crustal thickening. It also results because the mantle lithosphere is locally weakened by interactions with hot magmatic fluids, which further localizes stretching.

Extension in the central and southern part of the Main Ethiopian Rift began between 18 and 15 Ma and, in the north, after 11 Ma (Wolfenden *et al.*, 2004). The deformation resulted in the formation of a series of high-angle border faults that are marked by chains of volcanic centers (Fig. 7.38a). Since about 1.8 Ma the loci of magmatism and faulting have become progressively more localized, concentrating into ~20-km-wide, 60-km-long magmatic segments (Fig. 7.38b). This localization involved the formation of new, shorter and narrower rift segments that are superimposed on old long border faults in an old broad rift basin. This narrowing of the axis into short segments reflects a plate whose effective elastic thickness is less than it was when the long border faults formed (Ebinger *et al.*, 1999). The extrusion of copious amounts of volcanic rock also has modified both the surface morphology of the rift and its internal structure. Relationships in this rift segment indicate that magma intrusion in the form of vertical dikes first becomes equally and then more important than faulting as rifting approaches sea floor spreading (Kendall *et al.*, 2005). Repeated eruptions create thick piles that load the weakened plate causing older lava flows to bend down toward the rift axis. This process creates the seaward-dipping wedge of lavas (Section 7.7.1) that is typical of rifted volcanic margins (Section 7.7.1).

The rift segments in the Afar Depression illustrate that, as extension increases and the thickness of the lithosphere decreases, the asthenosphere rises and decompresses, and more melt is generated. Eventually all the border faults in the rift are abandoned as magmatism accommodates the extension (Fig. 7.38c). At this stage the rift functions as a slow-spreading mid-ocean ridge that is bordered on both sides by thinned continental lithosphere (Wolfenden *et al.*, 2005). As the melt supply increases and/or strain rate increases, new oceanic lithosphere forms in the magmatic segments and the crust and mantle lithosphere subside below sea level. This transition has occurred in the Gulf of Aden

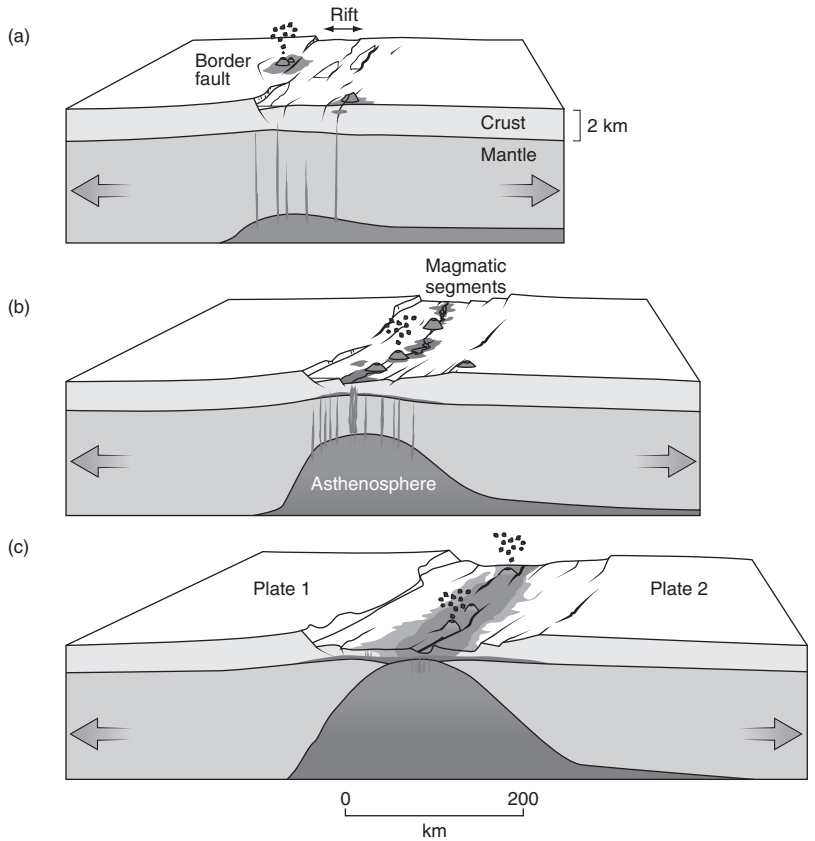

Figure 7.38 *Three-stage model for continental break-up leading to the formation of a volcanic passive margin (after Ebinger, 2005, with permission from Blackwell Publishing).*

(Fig. 7.2b) where conjugate rifted margins have formed recently. The margins on the western side of the Gulf are mostly buried by Oligocene-Miocene lavas from the Afar mantle plume. Those on the eastern side are starved of sediment and volcanic material and preserve 19–35 Ma structures that formed during oblique rifting and the transition to sea floor spreading (d'Acremont *et al.*, 2005). Seismic reflection studies of these latter margins indicate that the southern rifted margin is about twice as wide as the northern one and displays thicker post-rift deposits and greater amounts of subsidence. As rifting gave way to sea floor spreading in this area, deformation localized in a 40-km-wide transition zone where magma intruded into very thin continental crust and, possibly, in the case of the northern side, exhumed mantle. The different widths and structure of the two margins indicate that the transition to sea floor spreading in the Gulf of Aden was an asymmetric process.

7.8.2 The Woodlark Rift

The Woodlark Basin and adjacent Papuan Peninsula (Fig. 7.39a) record a continuum of active extensional processes that vary laterally from continental rifting in the west to sea floor spreading in the east. This example provides an important record of how sea floor spreading segments develop spatially during continental break-up and the formation of nonvolcanic margins. It also illustrates the type of lithospheric conditions that promote the development of metamorphic core complexes during rifting. Continental rifting occurs presently in the Papuan Peninsula where core complexes

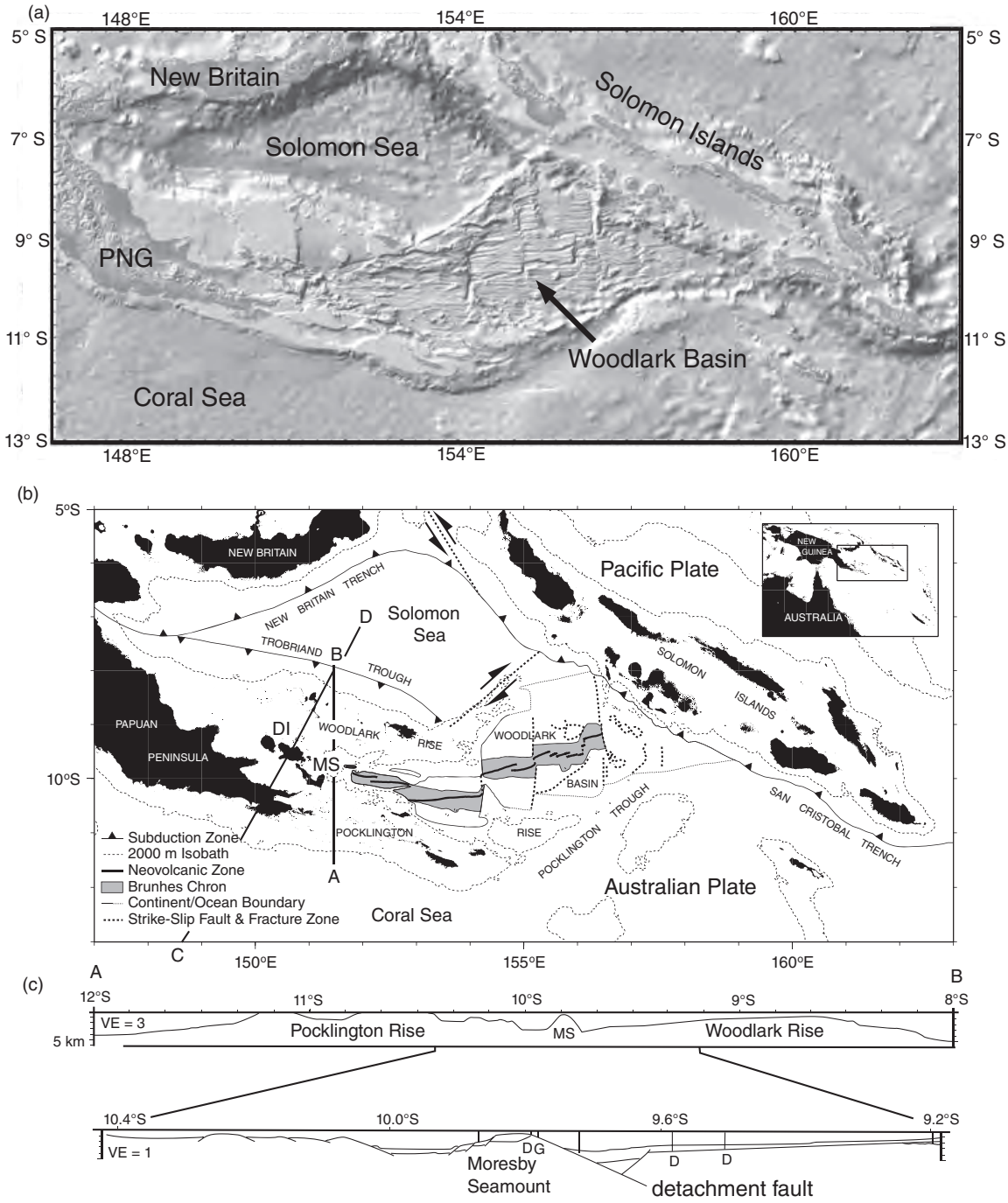

Figure 7.39 *(a) Shaded relief map constructed using same methods and data as Fig. 7.1. (b) Tectonic map of eastern Papua New Guinea (PNG) and the Solomon Islands showing present-day tectonic setting and (c) cross-section (A–B) of western Woodlark Rift showing topography and detachment fault (images in (b) and (c) provided by B. Taylor and modified from Taylor & Huchon, 2002, with permission from the Ocean drilling Program, Texas A & M University). DI, D'Entrecasteaux Islands; MS, Moresby Seamount; D, dolerite; G, gabbro. Line C–D indicates the line of the section shown in Fig. 7.40a.*

and both high-angle (≥45°) and low-angle (<30°) normal faults have formed in the D'Entrecasteaux islands since the Pliocene. Ocean crust in the easternmost and oldest part of the Woodlark Basin is now being consumed to the north beneath the Solomon Islands (Fig. 7.39b).

The pre-rift evolution of the Woodlark region involved subduction, arc volcanism, and arc-continent collision (Section 10.5) along a relic Paleogene convergent plate boundary that now coincides with the Pocklington Rise and southern margin of the Papuan Peninsula (Fig. 7.39b). As the Coral Sea opened from 62 to 56 Ma, fragments of continental crust rifted away from Australia and collided with a Paleogene volcanic arc during north-directed subduction along this plate boundary (Weissel & Watts, 1979). The Trobriand Trough, located to the north of the Woodlark Rise (Fig. 7.39b), is a Neogene subduction zone that accommodates south-directed motion of the Solomon sea floor. This region thus records a history of convergence and crustal thickening that pre-dates the onset of extension during the Pliocene.

Rift initiation in the Pliocene split the rheologically weak continental fragments and volcanic arc of the Woodlark and Pocklington rises. This weak zone lay between two regions of strong oceanic lithosphere in the Coral and Solomon seas and helped to localize strain during rifting (Taylor *et al.*, 1995). Rifting began more or less synchronously along 1000 km of the margin at ~6 Ma. However, strain localization and sea floor spreading developed in a time transgressive fashion from east to west within this large zone. Sea floor spreading began east of about 157° E longitude and was focused there up until ~3.6 Ma. At ~3.6 Ma a spreading ridge abruptly propagated ~300 km westward to ~154°E longitude. Seismic studies (Abers *et al.*, 2002; Ferris *et al.*, 2006) indicate that the crust thickens from <20 km beneath the D'Entrecasteaux islands to 30–35 km beneath the eastern Papuan Peninsula.

Rifting eventually led to the formation of nonvolcanic margins along the northern and southern boundaries of the Woodlark Basin. Currently, continental break-up is focused on an asymmetric rift basin bounded by a low-angle (27°) extensional detachment fault (Fig. 7.39c) that extends though the entire thickness (3–9 km) of the seismogenic layer north of the Moresby Seamount (Abers *et al.*, 1997). Abers & Roecker (1991) identified several possible earthquake events that may indicate active slip on this low-angle detachment. By contrast, break-up at 2 Ma occurred along a symmetric rift basin bounded by high-angle normal faults. Extension and the slip on low-angle shear zones has resulted in the very rapid (>10 mm a^{-1}) exhumation of deep (up to 75 km) Pliocene plutonic and metamorphic rocks that formed during prior subduction (Baldwin *et al.*, 2004). These core complexes formed when thick upper crust was pulled apart by extension. This process was aided by the emplacement of dense ophiolitic material over less dense crust during Paleogene collision (Abers *et al.*, 2002). Focused extension locally raised temperatures in the lithosphere and allowed buoyant lower crust and mantle to flow beneath the core complexes (Fig. 7.40a). Presently, the Moho is elevated beneath the core complexes, indicating that the lower crust maintains some strength and has not yet flowed sufficiently to smooth out these variations.

The Woodlark Rift indicates that continental break-up occurs in a step-wise fashion by successive phases of rift localization, spreading center nucleation, spreading center propagation, and, finally, a jump to the next site of localized rifting (Taylor *et al.*, 1999). Extension within the rifted nonvolcanic margins continued for up to 1 Myr after sea floor spreading initiated. The transition from rifting to sea floor spreading occurred after a uniform degree of continental extension of 200 ± 40 km and some 130–300% strain (Taylor *et al.*, 1999). Spreading segments nucleated in rift basins that were separated from one another by accommodation zones (Fig. 7.40b). The initial spreading segments achieved much of their length at nucleation, and subsequently lengthened further as spreading propagated into rifting continental crust. Offset margins were controlled by the geometry and location of rheological weaknesses in the Papuan Peninsula. The spreading centers nucleated in orientations approximately orthogonal to the opening direction but, because the developing margins were oblique to this direction, nucleation jumps occurred in order to maintain the new spreading centers within rheologically weak zones. Transform faults, which cut across previous rift structures, link spreading segments that had nucleated in, and/or propagated into, offset continental rifts. This relationship indicates that transform faults do not evolve from transfer faults between rift basins. In addition, the Woodlark example shows how rheological weaknesses in the lithosphere continue to control how continents break-up during the final stages of the transition from rifting to sea floor spreading.

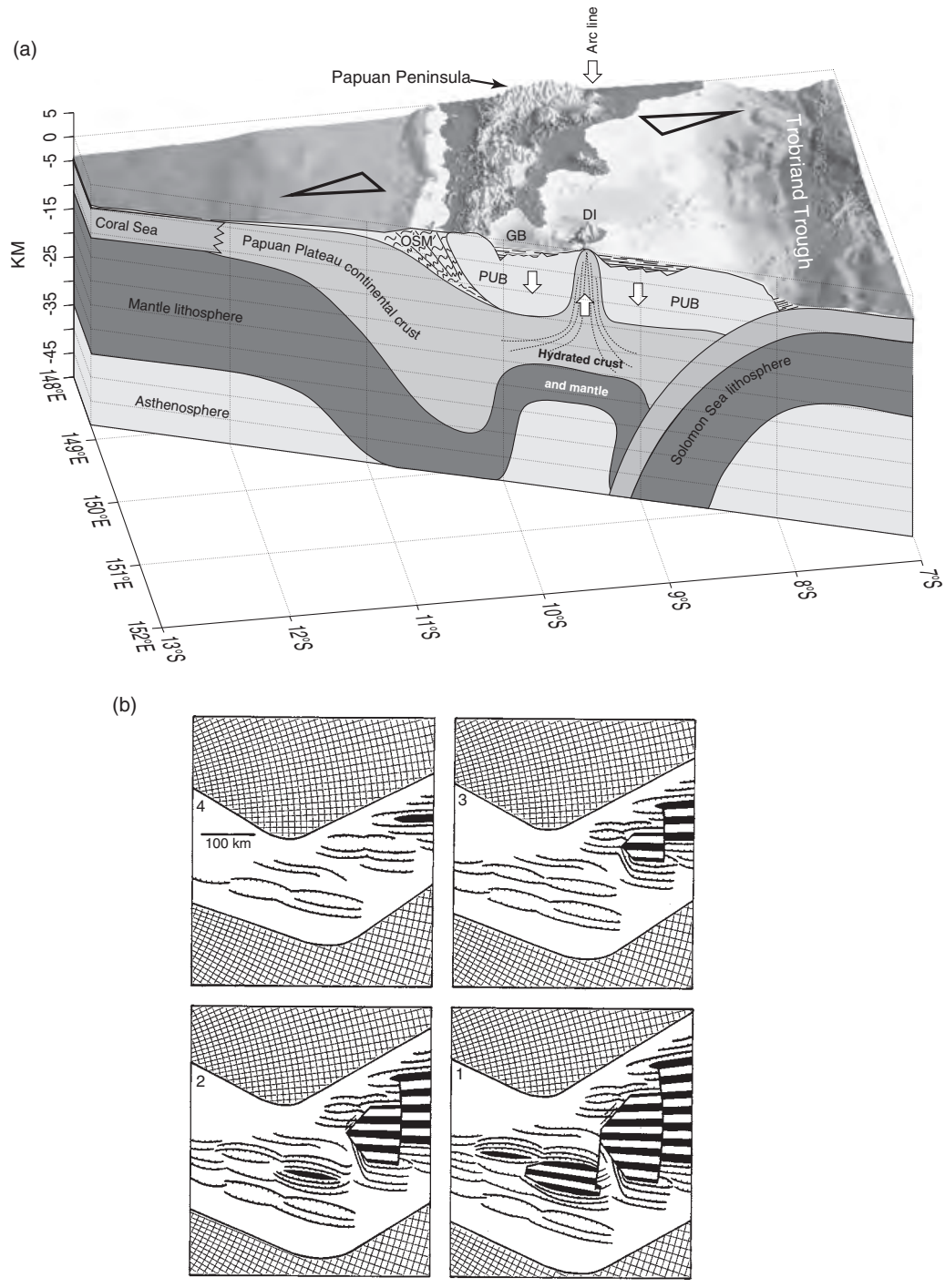

Figure 7.40 *(a) Interpretation of the crustal structure along the profile C–D shown in Fig. 7.39b (image provided by F. Martínez and modified from Martínez* et al.*, 2001, with permission from* Nature ***411***, *930–4. Copyright © 2001 Macmillan Publishers Ltd). DI, D'Entrecasteaux Islands; GB, Goodenough basin; PUB, Papuan ultramafic belt; OSM, Owen Stanley metamorphic belt. (b) Model of continental break-up and ocean formation derived from the Woodlark Basin and Papua New Guinea (modified from Taylor* et al.*, 1999, by permission of the American Geophysical Union. Copyright © 1999 American Geophysical Union). White areas are continental lithosphere. Nonextending regions are represented by a pattern of small and great circles to the pole of opening. Black and white stripes are new oceanic lithosphere. Four stages are shown from 4 Ma to 1 Ma.*

7.9 THE WILSON CYCLE

The transition from intracontinental rift to ocean basin has occurred repeatedly on Earth since at least the Late Archean (Section 11.3.5). The relatively young Mesozoic-Cenozoic age of the current ocean basins implies that there have been many cycles of ocean creation and destruction during the Earth's history. Very little remains of these ancient oceans, although their existence is implied by continental reconstructions (Figs 3.4, 3.5) and by fragments of ancient ocean crust that are preserved as ophiolite assemblages (Section 2.5) in orogenic belts

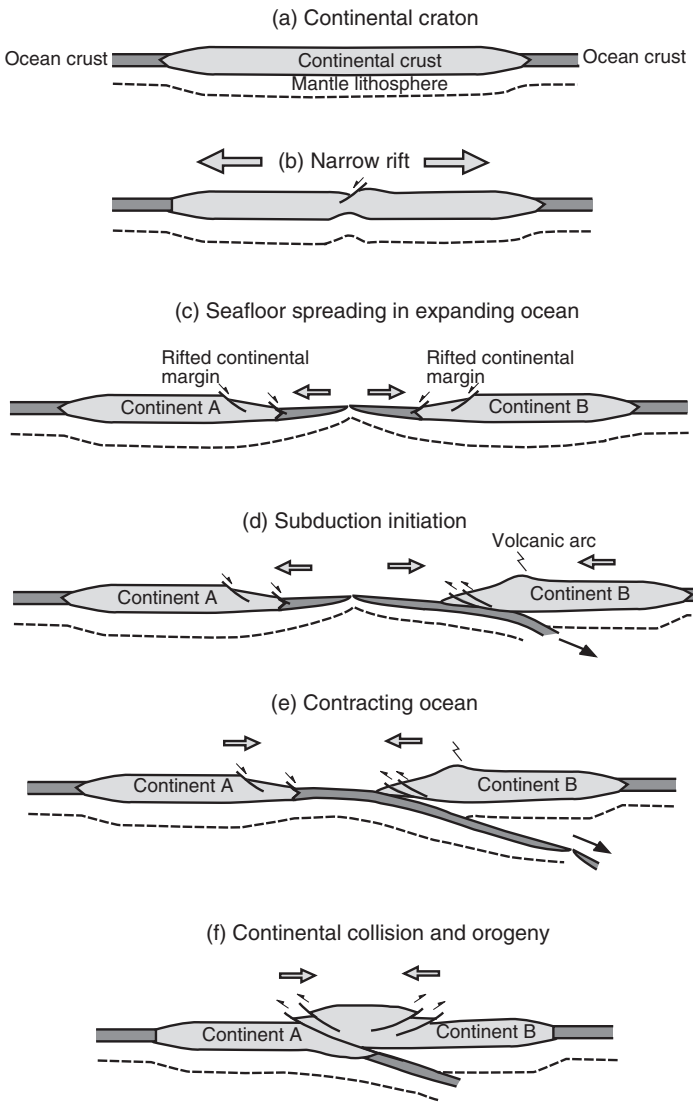

Figure 7.41 *The Wilson cycle showing: (a) continental craton; (b) formation of a narrow rift; (c) initiation of seafloor spreading and formation of rifted continental margins in an expanding ocean basin; (d) initiation of subduction; (e) a closing ocean basin; (f) continental collision and orogeny.*

(Section 10.6.1). This periodicity of ocean formation and closure is known as the *Wilson cycle*, named after J. Tuzo Wilson in recognition of his contributions to the theory of plate tectonics (Dewey & Burke, 1974).

Figure 7.41 shows a schematic illustration of the various stages in the Wilson cycle beginning with the initial break-up of a stable continental craton (Fig. 7.41a) and the thinning of continental lithosphere. Rifting (Fig. 7.41b) is followed by the development of a thinned, rifted continental margin and eventually gives way to sea floor spreading as the two continents separate across an expanding ocean (Fig. 7.41c). The termination of basin opening may occur in response to plate collisions, which could trigger subduction at one or more rifted margins (Fig. 7.41d). Basin closure also may compensate for oceanic lithosphere that is newly formed elsewhere. The contracting ocean is a consequence of subduction at one or both continental margins (Fig. 7.41e). This phase will continue until the two continents collide and the ocean basin closes completely (Fig. 7.41f). Continent–continent collision leads to the formation of a Himalaya-type orogen (Section 10.1) and the exhumation of deep crustal rocks. At this time subduction zones must initiate at other continental margins in order to maintain constant global surface area. The forces associated with these new subduction zones place the continent under tension and, if other conditions are extant (Section 7.5), the rifting process begins again. Present day analogues of the oceans shown in Fig. 7.41 are: Fig. 7.41c (expanding oceans) = the Gulf of Aden, Woodlark Rift, and the Atlantic Ocean; Fig. 7.41d,e (contracting oceans) = the Pacific Ocean. Chapters 9 and 10 provide discussions of the processes that operate during the destructive part of the Wilson cycle as ocean basins close and continents collide.